

Miquéias Jacinto Cirino

**On the role of spatial coherence of optical
beams in one dimensional photonic lattices**

Maceió, AL, Brasil

2024

Miquéias Jacinto Cirino

**On the role of spatial coherence of optical beams in one
dimensional photonic lattices**

Master's thesis presented to the Graduate
Program in Physics of the Federal University
of Alagoas as a partial requirement to obtain
the degree of Master in Physics.

Federal University of Alagoas

Graduate Program in Physics

Supervisor Paulo Cesar Aguiar Brandão Filho

Maceió, AL, Brasil

2024

Catálogo na fonte
Universidade Federal de Alagoas
Biblioteca Central
Divisão de Tratamento Técnico

Bibliotecária: Girlaine da Silva Santos – CRB-4 – 1127

C578o Cirino, Miquéias Jacinto.

On the role of spatial coherence of optical beams in one dimensional photonic lattices / Miquéias Jacinto Cirino. – 2024.

94 f. : il. color.

Orientador: Paulo Cesar Aguiar Brandão Filho.

Dissertação (Mestrado em Física) – Universidade Federal de Alagoas.
Instituto de Física. Programa de Pós-Graduação em Física. Maceió, 2024.

Inclui produto educacional

Inclui bibliografias

Apêndices: f. 76-80.

Anexos: f. 81-94.

1. Óptica. 2. Interferência (Luz). 3. Difração de luz. 3. Coerência Óptica. I.
Título.

CDU: 535



**PARECER DA BANCA EXAMINADORA DE DEFESA DE
DISSERTAÇÃO DE MESTRADO**

***“On the role of spatial coherence of optical beams in one
dimensional photonic lattices”***

por

Miqueias Jacinto Cirino

A Banca Examinadora composta pelos professores Paulo Cesar Aguiar Brandão Filho, como presidente da banca examinadora e orientador, do Instituto de Física da Universidade Federal de Alagoas; Solange Bessa Cavalcanti, do Instituto de Física da Universidade Federal de Alagoas e Alex Emanuel Barros Costa, do Instituto Federal de Alagoas, consideram o **candidato aprovado com conceito “A” - com louvor.**

Maceió, 26 de fevereiro de 2024.

Documento assinado digitalmente
 PAULO CESAR AGUIAR BRANDÃO FILHO
Data: 26/02/2024 14:02:39-0300
Verifique em <https://validar.itl.gov.br>

Prof. Dr. Paulo Cesar Aguiar Brandão Filho

Documento assinado digitalmente
 SOLANGE BESSA CAVALCANTI
Data: 26/02/2024 13:57:12-0300
Verifique em <https://validar.itl.gov.br>

Prof^a. Dr^a. Solange Bessa Cavalcanti

Documento assinado digitalmente
 ALEX EMANUEL BARROS COSTA
Data: 26/02/2024 10:55:47-0300
Verifique em <https://validar.itl.gov.br>

Prof. Dr. Alex Emanuel Barros Costa

STATEMENT OF AUTHORSHIP

I hereby declare that the thesis submitted is my own work. All direct or indirect sources used are acknowledged as references. I further declare that I have not submitted this thesis at any other institution in order to obtain a degree.

Para Rosângela.

Acknowledgements

Há realmente muita gente que eu devo e posso agradecer em relação à minha jornada e principalmente aos últimos dois anos. Que dois últimos anos! Eu vou esquecer alguns nomes, óbvio. Desculpas desde já!

Ao meu orientador do mestrado, Prof. Paulo Brandão. O senhor é um exemplo que eu quero seguir. Agradeço pelo tempo, pela paciência quando as coisas não deram certo ou quando eu compliquei demais, pelas palavras de encorajamento e por confiar em meu potencial. Acima de tudo, obrigado por prover um ambiente enriquecedor para a produção científica e para meu crescimento pessoal e profissional. Obrigado por depositar fé e recursos durante essa jornada.

Aos integrantes do DQNL, grupo que me acolheu durante esta etapa da minha vida acadêmica.

Um agradecimento especial à chefe, Prof. Solange Bessa, que é muito mais jovem do que eu jamais serei! A forma como a senhora estabeleceu um ambiente saudável para discussões sobre Física desde o final de minha graduação foi algo que me fez segurar esta carreira com mais carinho. Obrigado pelos conselhos, pelo esclarecimento em tantos tópicos e pela sala. É claro, obrigado também pela fé.

Ao Zezo, pois você atuou como um grande mentor durante esses dois anos. Obrigado pelo tempo, por quebrar a cabeça comigo, por me escutar falando sobre os problemas de Física e Física Computacional que eu tentei tanto resolver durante esses dois anos. Obrigado pelas sugestões e principalmente pelo apoio humano. Não vou esquecer da sua ajuda, amigo.

Ao Prof. Alex Costa, pelas contribuições em reuniões de grupo e por aceitar fazer parte da minha banca.

Ao Prof. Jonathan Rebouças, você é admirável! Obrigado pelos livros, pelas conversas e pelas aulas.

Um abraço apertado e um obrigado muito caloroso para os meus parceiros favoritos, Igor Beder e Ramsés César. Vê-los crescer durante a graduação foi um presente e espero conseguir acompanhar o ritmo de vocês dois nesta jornada. Obrigado pelos momentos e discussões sobre física no instituto e pelos momentos fora do ambiente de trabalho também! Trabalhar com vocês vai ser um prazer no futuro!

Aos professores Fernanda Selingardi, Sérgio Lira, Guilherme Almeida, Frederico Passos, Maria Tereza de Araujo, Pedro Valentim, Elton Malta e André Moura. Pelas discussões, pelo apoio e por compartilhar momentos bem divertidos vez ou outra. Aos

professores Marcelo Lyra, que admiro profundamente, e Maria Socorro Seixas, que não me deixou de me auxiliar e que serve de inspiração.

Gratidão às minhas amigas que estão do meu lado desde a graduação: Mariana Monteiro, Lavínia Malta e Laís Alves. Às minhas queridas parceirinhas da pós-graduação: Katiele Brito, Helena Bordini e Carolina Costa. Além de contribuírem com minha formação, vocês foram um refúgio muito necessário neste ambiente. E, por fim, ao polonês Pedro Ruyter. Desejo muito sucesso a todos vocês.

Ao Victor e à Rayssa da secretaria da pós-graduação. Vocês fazem tudo ficar mais fácil! Muito muito obrigado!

À Mayra Albuquerque e ao Vinícius Cordeiro, que me encorajaram a tomar decisões que deram ótimos frutos e que me deram suporte em momentos difíceis.

Aos meus graduandos de física favoritos: Eloísa Nicácio, Messias, Julia Bastos. E aos meus graduandos não tão favoritos assim: Rayssa, Badú e Airton. Obrigado por participarem do meu dia a dia, me fazerem muita raiva, mas também trazerem tantos momentos engraçados.

Aos meus físicos experimentais favoritos da pós-graduação, que foram verdadeiros parceiros nestes dois anos: Gilson Melo, Tasso Sales, Rodrigo Ferreira, Célio Vinícius, Pedro Fellype.

Aos amigos que a UFAL me deu e não deixaram de me acompanhar nesta jornada: Luana Júlia Ferreira, Victoria Aquino, Victor Marcel, Júlia Evelynn, Sidna Roberta, Nicolas Tenório, Arthru Santos, Alanne Matias e Juan de Sá.

Ao meu querido amigo, Paulo Daubian-Nosé. Obrigado pelos conselhos, obrigado pela paciência e obrigado pelo carinho. Você é incrível.

Ao Grupo de Gelo e Fogo, vocês são demais! Arieli, Jason, Rodrigo, Mateus, Felipe e até o Andrey. Valeu por participarem.

Ao Grupo do Caos. Um abraço muito especial aos membros Kaio Nabuco, Alice, Louise, Ramon, Victor, Baía, Ste e Mike. Vocês foram e são parte essencial dos meus dias: nos dias de ódio e também nos dias que eu não os odeio tanto assim. A Alice eu nunca deixo de amar, pra ser honesto! Amor é atenção!

À minha psicóloga Alda, que me acompanhou e me ajudou a crescer tanto durante este mestrado. Sem sua ajuda, eu estaria em um lugar muito ruim hoje. Gratidão.

À minha família que não é de sangue: João Pedro e Fuka. O que seria de mim sem vocês dois? O que seriam desses dois últimos anos sem nossa relação? Não consigo conceber. Obrigado pelo amor, pelo tempo, e por compartilhar comigo momentos de tristeza e desespero. Compartilhar coisas boas é muito fácil. Amo muito vocês, espero dar muito orgulho nos próximos capítulos desta jornada.

Ao meu querido amigo, Mário Henrique Werneck (*in memoriam*). Um dia nós iremos nos reencontrar. Obrigado pelo amor, pelo entendimento e pelos momentos.

Aos meus irmãos, Arthur Jacinto e Eliel Júnior. Vocês são parte da força motriz que me mantém vivo.

Ao meu pai, Eliel Cirino, que nunca deixou de acreditar em mim.

À minha mãe, Maria Rosângela. Nem se eu desse minha vida inteira em dedicação à senhora seria o bastante para retribuir tudo que você fez por mim. Eu te amo mais que tudo neste mundo.

"I must not fear. Fear is the mind-killer. Fear is the little-death that brings total obliteration. I will face my fear. I will permit it to pass over me and through me. And when it has gone past I will turn the inner eye to see its path. Where the fear has gone there will be nothing. Only I will remain."

Frank Herbert

Abstract

The propagation of a partially coherent optical field in a periodic photonic lattice with one-dimensional periodicity was investigated using the framework of Floquet-Bloch modes. The deterministic counterpart was explored by using a Gaussian source to establish a solid baseline for how the system responds to parameters: the influence of transverse momentum and lattice amplitude on beam propagation and participation coefficients was discussed. The stochastic aspect of the system was considered, where we described the interplay between lattice properties and field fluctuations by considering the optical beam as a superposition of Floquet-Bloch modes with coefficients being stationary random processes. The second-order theory of coherence was employed to demonstrate that the propagation of partially coherent optical fields depends on the excitation of bands and on the correlations between them. The role of spatial coherence in the system was explored through the cross-correlation participation coefficients, indicating how the power of the beam is distributed in terms of the band structure. In the end, we used the results to describe the dynamics of the beam center.

Keywords: Classical Optics, Interference and Diffraction of Light, Optical Coherence.

Resumo

A propagação de um campo óptico parcialmente coerente em uma rede fotônica periódica com periodicidade unidimensional foi investigada utilizando o formalismo dos modos de Floquet-Bloch. A contraparte determinística foi explorada utilizando uma fonte gaussiana para estabelecer uma linha de base sólida sobre como o sistema responde aos seus parâmetros: a influência do momento transversal e da amplitude da rede na propagação do feixe e nos coeficientes de participação foi extensamente discutida. O aspecto estocástico do sistema foi considerado, onde descrevemos a interação entre as propriedades da rede e as flutuações do campo, considerando o feixe óptico como uma superposição de modos de Floquet-Bloch com coeficientes sendo processos aleatórios estacionários. A teoria de coerência de segunda ordem foi empregada para demonstrar que a propagação de campos ópticos parcialmente coerentes depende da excitação de bandas e das correlações entre elas. O papel da coerência espacial no sistema foi explorado por meio dos coeficientes de participação de correlação cruzada, indicando como o poder do feixe é distribuído em termos da estrutura de banda. No final, utilizamos os resultados para descrever a dinâmica do centro do feixe.

Keywords: Óptica Clássica, Interferência e Difração da Luz, Coerência Óptica.

List of Figures

Figure 1	– Examples of simple photonic crystals: On the left, colors represent different dielectric constants; on the right, a continuous dielectric function is displayed. They're (a) 1D and (b) 2D structures. This illustration is inspired by figure 1 from [8].	21
Figure 2	– (a) Schematic representation of a uniform slab with dielectric function constant in its bulk; (b) orthogonal set formed by the vectors found in the solution: the electromagnetic field, \mathbf{H}_0 and \mathbf{E}_0 , and the wave vector \mathbf{k} ; and (c) band diagram for a uniform dielectric if one plots the frequency $\omega(\mathbf{k})$ in function of a specific direction, depending in the module of its component.	27
Figure 3	– (a) Representation of a photonic crystal formed by dielectric slabs (in blue) alternated with empty space filled. The unit cell of the structure is within the transparent box and the real lattice vector is \mathbf{R}_0 ; (b) band structure for a periodic dielectric structure along one line of the \mathbf{k} space; and (c) a representation of a square lattice and its respective Brillouin zone with its the irreducible part highlighted in blue, the triangle with vertices Γ , X and M	28
Figure 4	– Schematic representation of the fact that natural light is composed by a sum of a large number of light waves, represented by the signals U_j , $j = 1, 2, \dots$, fluctuating as the time goes by. The image was taken by the author and cherished friends during the solar eclipse of 2023 in Maceió, Alagoas.	34
Figure 5	– Examples of the intensity of a realization of an optical field $ U_j(t) ^2$ and its mean intensity $\langle U(t) ^2 \rangle$ for a (a) stationary process and a (b) non stationary process. Inspired by the figure 12.1-1 from [7].	35
Figure 6	– Representation of the Michelson interferometer experiment: σ is the light source; U is the incident optical field; M_j is a mirror, $j = 1, 2$; D is the beam divider; and A is the plane of observation. Inspired by the figure 12.2-2 from [7] and figure 4.1 from [15].	37

Figure 7 – Representation of the Young’s double slit experiment: σ is the thermal light source; Δs is the spatial extent of the source; R is the distance between the source and the double slit plane; S_j are the slits and also the point sources for the secondary wave, $j = 1, 2$; d is the distance between the slits; A is the plane of observation; P_j is any point in the plane A , $j = 1, 2$; U_j is the optical field reaching P_1 from the j th slit, $j = 1, 2$; U'_j is the optical field reaching P_2 from the j th slit, $j = 1, 2$. Inspired by the figures 4.2 and 4.3 from [15].	39
Figure 8 – Free representation of the spectral density as a function of wavelength at three positions in a color image. Adapted from figure 10.1-4 of [7]. In the image, the official album cover for the 2021 album ‘If I could Make It Go Quiet’ by Norwegian musician Girl in Red is utilized to illustrate how the spectral density translates to the perceived color.	42
Figure 9 – (a) Schematic representation of the optical system, featuring the analytical signal profile $U_0(x) = U_0 \exp[-x^2/\sigma^2]e^{iqx}$. Additionally, there’s a purple parallelepiped oriented perpendicular to the transverse direction x , symbolizing a waveguide. Each waveguide has a specific refractive index for each x value, giving rise to the lattice potential $V(x)$. (b) When considering the continuous limit, the lattice potential describing the photonic crystal is depicted as $V(x) = A \cos^2(x)$	45
Figure 10 – Band structure of a $V(x) = A \cos^2 x$, $A = 4$. (a) Band diagram showing the propagation constant $\beta_n(k)$ versus Bloch wave vector k for the first five bands. In the right, the intensity of the Floquet-Bloch function $ u_n(x, k) ^2$ is displayed for x in an unit cell $[-a/2, a/2]$ and for k in the first Brillouin zone $[-\pi/a, \pi/a]$ for the bands (b) $n = 1$ and $n = 2$ in the xk -plane, and (c) fixed values of (n, k) , specifically $(1, 0.0)$, $(2, 1.0)$, and $(3, 0.0)$	48
Figure 11 – (a) Absolute squared Floquet-Bloch participation coefficients $ c_n(k) ^2$ versus wave number k for the potential $V(x) = A \cos^2 x$, $A = 0.01$ with an incident Gaussian beam $U_0(x) = \tilde{U}_0 e^{iqx} e^{-x^2/2\sigma^2}$ with beam width $\sigma = 7\pi$ and transverse momentum (top) $q = 0.0$, (middle) $q = -0.5$ and (bottom) $q = -1.0$; (b) Band diagram showing the propagation constant $\beta_n(k)$ versus Bloch wave vector k for the first five bands.	51

- Figure 12 – (a) Absolute squared Floquet-Bloch participation coefficients $|c_n(k)|^2$ versus wave number k for the potential $V(x) = A \cos^2 x$, $A = 4.0$ with an incident Gaussian beam $U_0(x) = \tilde{U}_0 e^{iqx} e^{-x^2/2\sigma^2}$ with beam width $\sigma = 7\pi$ and transverse momentum (top) $q = 0.0$ (the inset illustrates the contribution of the second and third bands), (middle) $q = -0.5$ and (bottom) $q = -1.0$; (b) Band diagram showing the propagation constant $\beta_n(k)$ versus Bloch wave vector k for the first five bands. 52
- Figure 13 – (a) Absolute squared Floquet-Bloch participation coefficients $|c_n(k)|^2$ versus wave number k for the potential $V(x) = A \cos^2 x$, $A = 10.0$ with an incident Gaussian beam $U_0(x) = \tilde{U}_0 e^{iqx} e^{-x^2/2\sigma^2}$ with beam width $\sigma = 7\pi$ and transverse momentum (top) $q = 0.0$ (the inset illustrates the contribution of the third and fourth bands), (middle) $q = -0.5$ and (bottom) $q = -1.0$; (b) Band diagram showing the propagation constant $\beta_n(k)$ versus Bloch wave vector k for the first five bands. 53
- Figure 14 – (a) Parserval identity terms p_n versus lattice potential amplitude A for and transverse momentum (top) $q = 0.0$, (middle) $q = -0.5$ and (bottom) $q = -1.0$ and (b) versus the transverse momentum q for a specific lattice potential amplitude $A = 4.0$. For both, the input beam is the optical field $U_0(x) = \tilde{U}_0 e^{iqx} e^{-x^2/2\sigma^2}$ with beam width $\sigma = 7\pi$ 54
- Figure 15 – Beam intensity $|U(x, z)|^2$ with the beam center $x_c(z)$ for three input gaussian beam with width $\sigma = 7\pi$ and potential amplitude A and wave number q : (a) $A = 0.01$ and $q = -0.5$; (b) $A = 4$ and $q = 0$; (c) $A = 10$ and $q = -1.0$ 55
- Figure 16 – (a) Absolute value of the cross-spectral density for a Gaussian-Schell source under various coherence parameter δ values. The Gaussian-Schell source has a transverse momentum of $q = 0$, a beam width of $\sigma = 7\pi$, and it is incident on a lattice with an amplitude of $A = 4$. Additionally, the following are displayed: (b) the equivalent deterministic behavior for participation coefficients; (c) the absolute values of cross-correlation coefficients $|C_{nm}(k)|$ for different coherence parameters: $\delta = 0.1\sigma$ (black line), $\delta = \sigma$ (purple line), and $\delta = 50\sigma$ (green line). The panels show results for $n = m = 1$ (top), $n = m = 2$ (middle), and $(n, m) = (1, 2)$ (bottom). 60
- Figure 17 – Spectral degree of coherence $\mu_{12}(k_1, k_2)$ versus the coherence parameter δ for input beam width $\sigma = 7\pi$ and lattice amplitude $A = 4.0$ at various incident angles, correspondent to $q = -1.0$ (solid black line), $q = -0.5$ (dashed line), and $q = 0.0$ (dot-dashed line). Several spectral degrees of coherence between points of the Brillouin zone are displayed: (a) $k_1 = k_2 = -0.3$; (b) $k_1 = -0.2$ and $k_2 = -0.3$; and (c) $k_1 = k_2 = -0.2$. 61

Figure 18 – (a) Beam spectral density $S(x, z)$. (b) Mean beam center oscillation $X_c(z)$ versus propagation distance z . For input wave number $q = -1.0$, width $\sigma = 7\pi$, lattice amplitude $A = 4.0$ and coherence parameter $\delta = \sigma/100$	63
Figure 19 – (a) Beam spectral density $S(x, z)$. (b) Mean beam center oscillation $X_c(z)$ versus propagation distance z . For input wave number $q = -1.0$, width $\sigma = 7\pi$, lattice amplitude $A = 4.0$ and coherence parameter $\delta = \sigma$	64
Figure 20 – (a) Propagation constant $\beta(k)$ versus Bloch wave vector k for the first five Floquet-Bloch modes $u_n(x, k)$; (b) group velocity $d\beta(k)/dk$ versus Bloch wave vector k ; (c) mean beam center oscillation $X_c(z)$ versus propagation distance z for three coherence parameters: σ , 0.1σ and 0.01σ . For input wave number $q = -1.0$, input beam width $\sigma = 7\pi$ and potential amplitude $A = 4.0$, extracted from [93].	67

Contents

1	INTRODUCTION	18
2	PHOTONIC CRYSTALS	20
2.1	Photonic Crystals	20
2.2	General Mathematical Description	22
2.3	Solid-State Physics and Bloch Waves	25
2.4	Paraxial Wave Equation Approximation	30
3	STATISTICAL OPTICS	33
3.1	Stochastic Nature of Light	33
3.2	Coherence, Correlation and the Interference Pattern	36
3.3	Second Order Theory of Scalar Random Light	40
4	SPATIAL COHERENCE OF LIGHT IN PERIODIC LATTICES	44
4.1	General Discussion	44
4.2	Deterministic Case: Gaussian Source	49
4.3	Stochastic Theory	56
4.4	Stochastic Case: Gaussian-Schell Source	58
4.5	Spatial Coherence and the Trembling Motion	64
5	CONCLUSION AND PERSPECTIVES	68
	References	70
	APPENDIX A – ANALYTICAL SIGNALS	78
A.1	Monochromatic Waves	78
A.2	Polychromatic Waves	79
	APPENDIX B – ORTHOGONALITY CONDITION OF FLOQUET- BLOCH MODES IN FINITE AND DISCRETE LATTICES	80
	ANNEX	83
	ANNEX A – PUBLISHED ARTICLES	84
A.1	Spatial coherence effects of stochastic optical beams in periodic potentials	84

A.2	Bragg scattering of stochastic beams in PT-symmetric photonic lattices	92
------------	---	-----------

1 Introduction

Systems with periodic properties are frequently studied in physics, as this characteristic often leads to interesting phenomena. The propagation of waves in such media permeates the interest of areas like electronics [1, 2, 3, 4], acoustics [5, 6], and optics [7, 8, 9, 10, 11, 12]. One strategy to analyze this problem is given by Bloch's theorem, which, in a periodic structure, allows the unfolding of the propagating wave into normal modes with their respective dispersion relations, dictating how the system's vibrations behave. The similarities between quantum mechanics and optics allow band theories and the study of band gaps to gain their deserved place in photonics [13, 14], which holds part of our subject of study. Additionally, every optical field found in nature possesses a stochastic nature, which can be understood through the formalism of Statistical Optics [15, 16], enabling us to study partially coherent light through the propagation of functions associated with signal correlations present in the source.

The main goal of this master's thesis is to present how the Floquet-Bloch theory can be a good strategy for studying the propagation of partially coherent light considering a medium with periodic properties and studying its particularities. In the next paragraphs, the reader will be presented with the structure of this thesis.

In chapter 2, the reader will be briefly introduced to photonic systems, their applications, and the conventional theoretical framework used to study these systems. Analogies with quantum mechanics will be made, specifically with solid-state physics, which will be the terminology for the discussion of the main results.

In chapter 3, the reader will be presented with basic concepts of statistical optics. Basic concepts of scalar wave optics will be necessary, but basic concepts of the theory will be presented in the chapter or in the appendix if it was not mentioned in the previous chapter. The main goal is to settle an intuitive relationship between coherence and correlation, also connecting these concepts to interference phenomena. The important quantities of the theory will be presented, which will be the main characters of the chapter on our results.

In chapter 4, the concepts presented in the previous chapter will be utilized to construct a model describing light in periodic media while considering its spatial coherence effects. The fundamental concepts of our theory will be explored and the connection with concepts and methods from solid-state physics will prove useful. A specific case involving deterministic light will be done for comparative purposes, but the core of the chapter lies in the subsequent investigation of the stochastic case by using the presented framework.

To conclude, chapter 5 provides a summary of the work done, a brief commentary

about the difficulties encountered, and discusses potential future developments.

2 Photonic Crystals

This chapter provides an overview of photonic systems, their applications, and the conventional theoretical framework used to study these systems. Concepts from quantum mechanics and solid-state physics will be mentioned and briefly discussed to draw analogies with quantum mechanics and establish a common language for discussing future topics. Maxwell's equations will be introduced to discuss these materials, delving into the realm of optical systems that this thesis focuses on. Ultimately, the chapter will derive the paraxial wave equation in a medium, which forms the core of this chapter and serves as the foundation of its theoretical framework.

2.1 Photonic Crystals

Humanity's advancement has been intricately tied to our comprehension of the world and its laws. From manipulating iron in the Stone Age to discovering copper, steel, and other materials, our journey has been marked by technological progress. The modern and contemporary ages have seen innovations in ceramics, metallurgy, and plastics. In the last century, breakthroughs in conductivity and transistors have revolutionized the world. Furthermore, the development of new alloys and ceramics has empowered scientists globally to explore high-temperature superconductors, which could lay the groundwork for future technologies [8]. The capacity to manipulate and engineer artificial materials has unveiled frontiers in controlling the optical properties of materials. This advancement holds tremendous potential for technological applications, including the ability to regulate which frequencies of light waves can pass through, the direction of light propagation, and the confinement of light within specific zones of the material. Notably, optical materials such as optical fibers have played a pivotal role in advancing telecommunications [17].

Within the vast array of optical materials, there exists a category where the structure is comparable to the wavelength of the light propagating within it. Some of these materials are known as photonic crystals, distinguished by a periodic refractive index in the macroscopic medium [8, 9].

The most critical information is generally conveyed by the dielectric function $\epsilon(\mathbf{r})$, which, by definition of photonic crystals, is periodic. Figure 1 displays a schematic representation of a photonic crystal formed by different slabs on the left and a graph of a continuous dielectric function on the right. Each color represents a different dielectric constant in the medium, illustrating the discrete case on the left. It is useful to consider a treatment where the periodicity is also continuous (right).

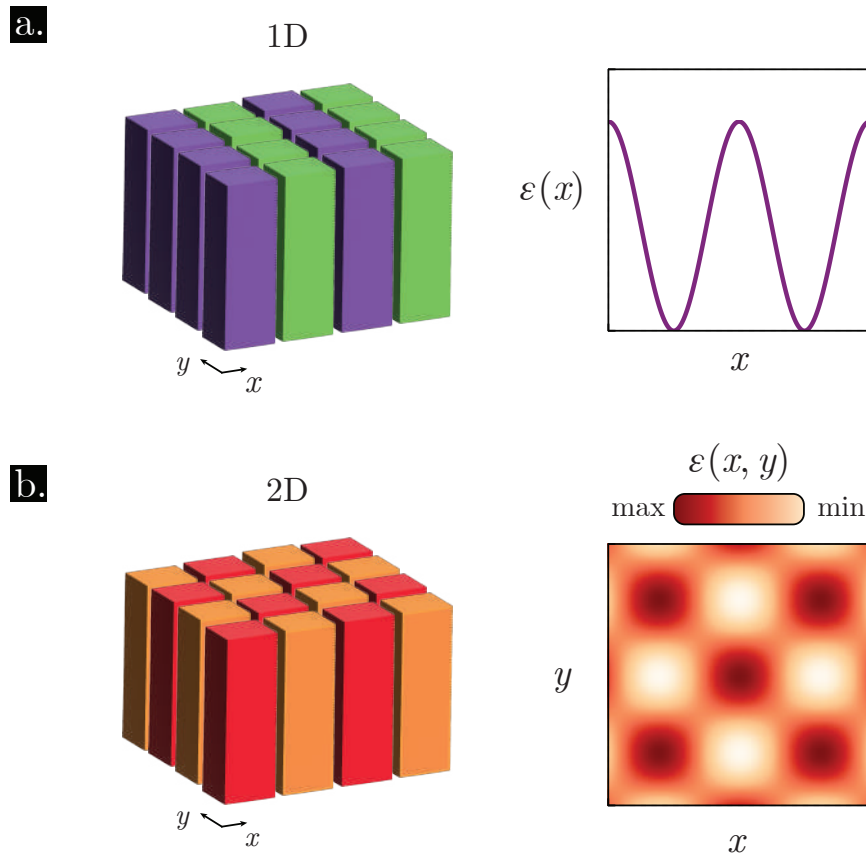


Figure 1 – Examples of simple photonic crystals: On the left, colors represent different dielectric constants; on the right, a continuous dielectric function is displayed. They're (a) 1D and (b) 2D structures. This illustration is inspired by figure 1 from [8].

The primary objective is to study the profile of electromagnetic waves. As is known, electromagnetic waves are generally periodic, and when they interact with a medium with periodicity on the same order as their wavelength, unique phenomena emerge, such as the formation of a photonic band structure and band gaps. All of this enables unprecedented control over light within the medium [7].

Initially, photonic crystals were introduced in the literature as a means to control spontaneous emissions of atoms [18, 19]. It was quickly realized that light propagating in periodic dielectric media behaves analogously to an electron in a solid-state periodic potential [20, 21, 22, 23, 24, 25], giving room to parallels between the theoretical approach between quantum mechanics and photonic crystals [7, 8, 9, 13].

The various phenomena enabled by the complex structure found in photonic crystals have led to a wide range of technological applications and research avenues, such as photonic integrated circuits [26], micro and nanophotonic crystal waveguide circuit boards [27], optical communications [28], wavelength monitors [29], among many others [30, 31, 32, 33]. In the market, silicon nano-photonic integrated circuits are already being commercialized by Luxtera [34], while NKT Photonics offers specialty photonic crystal optical fibers

[35], Lumileds provides photonic crystal light-emitting diodes [36], and OmniGuide offers photonic bandgap fibers for precision surgery and cancer therapy [37, 38]. In addition to artificial materials, photonic crystals can also be found in nature, such as in peacock feathers [39], chameleon colors [40], butterfly scales [41, 42] and other natural sources [43].

In these systems, as mentioned, light exhibits behavior analogous to an electron submitted to periodic atomic potentials, a concept extensively explored in solid-state physics [1, 2, 4]. This resemblance arises because the equations describing light bear similarity to the Schrödinger equation [13]: the study of Bloch modes for optical waves reveals the emergence of bands and forbidden frequencies (band gaps) in photonic lattices [7, 8, 9, 10]. Particularly, in a scalar and paraxial approximation, examining the equation in one dimension, the Floquet-Bloch theorem becomes relevant and one must be aware of the one-dimensional band theory and more profound analysis of the solutions [4, 44, 45, 46, 47, 48].

Research in photonic structures has become an ever-growing subject in physics since their realization and discovery [19, 20]. Several studies explore the electromagnetic wave propagation in periodic structures utilizing Bloch Waves through plane wave expansion techniques [21, 22], as usual. Theoretical and experimental exploration in this has flourished, exploring well-known electronic effects in photonic systems, such as Rabi oscillations [49, 50, 51, 52], Zener tunneling [49, 52, 53, 54, 55], *zitterbewegung* effect [14], Bloch oscillations [54] and the effects of the Bragg resonance in these phenomena [55, 56]. It is important to note that studying Bragg resonance in these lattices or waveguide arrays provides insights into the impact of the incident angle of an initial beam on the optical diffraction and dispersion of optical beams during their propagation [57], which is useful if one aims to study propagation properties of optical beams.

The next sections will provide a brief overview of the theoretical framework used in the study of these systems, drawing connections with solid-state physics and focusing on the theoretical framework that enables one to address the main problem of this thesis. First and foremost, it is important to set the "rules of the game," i.e., the main considerations to develop a good mathematical description for photonic crystals. As always, one must start with Maxwell's equations.

2.2 General Mathematical Description

All problems in the classical electromagnetism can be solved by taking into account the Maxwell's equations. The main characters of the electromagnetic phenomena are the electric field vector $\mathbf{E} = \mathbf{E}(\mathbf{r}, t)$ and the magnetic field vector $\mathbf{B} = \mathbf{B}(\mathbf{r}, t)$. If one needs to consider the interaction with a material medium, one must take into account its properties, given by constitutive relationships between the electric field and the polarization density

field $\mathbf{P} = \mathbf{P}(\mathbf{r}, t)$, that carries the electric response of the media, and between the magnetic field and the magnetization density field $\mathbf{M} = \mathbf{M}(\mathbf{r}, t)$, that holds the information of the magnetic response of the media. One can find a deep discussion about the connection between the microscopic nature and the macroscopic significance of these fields [58]. From them, one can define two auxiliary fields, which are the electric displacement vector $\mathbf{D} = \mathbf{D}(\mathbf{r}, t)$ and the magnetic strength vector $\mathbf{H} = \mathbf{H}(\mathbf{r}, t)$; though their dependence on \mathbf{E} and \mathbf{B} can be really complicated, it can be written as a power series expansion for each component considering all the material's linear and non-linear responses [59, 60].

In the presence of a free charge distribution $\rho = \rho(\mathbf{r}, t)$ and free current density $\mathbf{J} = \mathbf{J}(\mathbf{r}, t)$, Maxwell's equation in the matter is given by the following coupled partial differential equations:

$$\begin{aligned} \nabla \cdot \mathbf{D}(\mathbf{r}, t) &= \rho(\mathbf{r}, t) & \nabla \times \mathbf{E}(\mathbf{r}, t) &= -\frac{\partial \mathbf{B}(\mathbf{r}, t)}{\partial t} \\ \nabla \cdot \mathbf{B}(\mathbf{r}, t) &= 0 & \nabla \times \mathbf{H}(\mathbf{r}, t) &= \frac{\partial \mathbf{D}(\mathbf{r}, t)}{\partial t} + \mathbf{J}(\mathbf{r}, t) \end{aligned} \quad (2.1)$$

These equations are common in any elementary course of electrodynamics, and solving them provides the electromagnetic field at any point in space \mathbf{r} at any time t . In general, when dealing with photonic crystals, certain assumptions can be made to simplify the problem of solving this set of differential equations without losing relevant physics [8, 7]. The dependence of some quantities on the electromagnetic wave frequency ω will be omitted, although it will be present in certain discussions.

Assuming that the electromagnetic field strength is sufficiently small, the material's nonlinear response to the light is negligible, thus only linear responses remain. Furthermore, considering a macroscopic, linear, and isotropic material, the relationship between the fields $\mathbf{E}(\mathbf{r}, t)$ is given by

$$\mathbf{D} = \epsilon_0 \epsilon(\mathbf{r}) \mathbf{E}, \quad (2.2)$$

with $\epsilon(\mathbf{r})$ being the permittivity or dielectric function depending on the spatial position \mathbf{r} and not on the time t . Thus, the material is non-homogeneous and the material's electric properties do not change over time. Another assumption regarding the permittivity is that the material is transparent, i.e., $\epsilon(\mathbf{r})$ is a real and positive function. The real condition $\epsilon(\mathbf{r}) \in \mathbb{R}$ here means that there are no losses in the material and the positive one $\epsilon(\mathbf{r}) > 0$ is to avoid metallic materials, although there are some works on photonic crystals with metals and dielectrics combined [61, 62].

The class of materials that is on the scope of this work does not have a pronunciation magnetic response, thus the relationship between $\mathbf{B}(\mathbf{r}, t)$ and $\mathbf{H}(\mathbf{r}, t)$ is mediated only by the vacuum permeability, for simplicity:

$$\mathbf{B} = \mu_0 \mathbf{H}. \quad (2.3)$$

In the optical regime of the electromagnetic spectrum, the refractive index serves as the universal language. Thus, it will be useful to emphasize the relationship between

the dielectric function $\epsilon(\mathbf{r})$ and the refractive index. Considering what was previously discussed about the material, one can express the refractive index as

$$n(\mathbf{r}) = \sqrt{\epsilon(\mathbf{r})}, \quad (2.4)$$

therefore the permittivity is proportional to the refractive index squared $\epsilon \propto n^2$.

Considering all previous assumptions and that there is no charge or current sources within the material, that is translated to mathematical language as $\rho = 0$ and $\mathbf{J} = 0$, Maxwell's equation can be manipulated from equation 2.1 to:

$$\begin{aligned} \nabla \cdot [\epsilon(\mathbf{r})\mathbf{E}(\mathbf{r}, t)] = 0 & \quad \nabla \times \mathbf{E}(\mathbf{r}, t) = -\mu_0 \frac{\partial \mathbf{H}(\mathbf{r}, t)}{\partial t} \\ \nabla \cdot \mathbf{H}(\mathbf{r}, t) = 0 & \quad \nabla \times \mathbf{H}(\mathbf{r}, t) = \epsilon_0 \epsilon(\mathbf{r}) \frac{\partial \mathbf{E}(\mathbf{r}, t)}{\partial t} \end{aligned} \quad (2.5)$$

This set of equations remains challenging to solve despite the assumptions made, and the time dependence remains problematic. The main concern in exploring light propagation in photonic crystals lies in the spatial content of these equations [7, 8, 9]; thus, to simplify the problem even further, one can utilize the linearity of the differential operators: every physical solution for the electromagnetic field can be thought as the real part of a linear combination of harmonic modes that carry the time dependence with a factor $e^{-i\omega t}$, a monochromatic wave:

$$\begin{aligned} \mathbf{E}(\mathbf{r}, t) &= \mathbf{E}(\mathbf{r})e^{-i\omega t} \\ \mathbf{H}(\mathbf{r}, t) &= \mathbf{H}(\mathbf{r})e^{-i\omega t} \end{aligned} \quad (2.6)$$

that can be inserted into equation 2.5 and the solutions of the resulting equations will be restricted to a given frequency ω :

$$\begin{aligned} \nabla \cdot [\epsilon(\mathbf{r})\mathbf{E}(\mathbf{r})] = 0 & \quad \nabla \times \mathbf{E}(\mathbf{r}) = i\omega\mu_0\mathbf{H}(\mathbf{r}) \\ \nabla \cdot \mathbf{H}(\mathbf{r}) = 0 & \quad \nabla \times \mathbf{H}(\mathbf{r}) = -i\omega\epsilon_0\epsilon(\mathbf{r})\mathbf{E}(\mathbf{r}) \end{aligned} \quad (2.7)$$

these are a set of coupled differential equations with dependence solely on the spatial coordinates. The two divergence equations ensure the transversality of the electromagnetic field within the material, while the curl equations relate the fields \mathbf{H} and \mathbf{E} [8]. To decouple these equations, one must apply the curl operator $\nabla \times$ to the curl equation for the electric field \mathbf{E} , and then divide the curl equation for the field \mathbf{H} and apply the curl operator. The result is as follows:

$$\begin{aligned} \nabla \times [\nabla \times \mathbf{E}(\mathbf{r})] &= k^2\epsilon(\mathbf{r})\mathbf{E}(\mathbf{r}) \\ \nabla \times \left[\frac{1}{\epsilon(\mathbf{r})} \nabla \times \mathbf{H}(\mathbf{r}) \right] &= k^2\mathbf{H}(\mathbf{r}) \end{aligned} \quad (2.8)$$

where the equation for \mathbf{E} is a generalized eigenvalue problem, while the one for \mathbf{H} is standard eigenvalue problem. Due to the complexity of solving for \mathbf{E} , one may prefer to solve the simpler problem for the field \mathbf{H} and then recover the electric field \mathbf{E} through the equation

$$\mathbf{E}(\mathbf{r}) = \frac{i}{\omega\epsilon_0\epsilon(\mathbf{r})} \nabla \times \mathbf{H}(\mathbf{r}); \quad (2.9)$$

or, conversely, solve for \mathbf{E} and recover the field \mathbf{H} through the expression:

$$\mathbf{H}(\mathbf{r}) = -\frac{i}{\omega\mu_0}\nabla \times \mathbf{E}(\mathbf{r}). \quad (2.10)$$

The fact that the general problem can be viewed as an eigenvalue problem is valuable because one can retrieve well-known results from functional analysis and quantum mechanics to handle these equations and interpret the solutions [63, 64, 65, 66]. Define the linear differential operator $\hat{\Xi}$ as follows:

$$\hat{\Xi} \mathbf{H}(\mathbf{r}) := \nabla \times \left[\frac{1}{\epsilon(\mathbf{r})} \nabla \times \mathbf{H}(\mathbf{r}) \right]; \quad (2.11)$$

certainly, it is straightforward to show that this operator is linear and Hermitian. Consequently, the eigenvalues are real, different eigenvalues have orthogonal eigenvectors, and there are symmetries that can be utilized to solve the problem [9, 63, 65].

Given a photonic crystal with dielectric function $\epsilon(\mathbf{r})$ with well-established boundary conditions for the electromagnetic field, the problem can be described by

$$\hat{\Xi} \mathbf{H}(\mathbf{r}) = k^2 \mathbf{H}(\mathbf{r}) \quad (2.12)$$

and one can find a set of **spatial modes** (solutions) that can compose every other solution due to the linearity of the operator $\hat{\Xi}$. With this general formulation, the connection with solid-state physics can be established to discuss the main topic of this thesis. In the next sections, this subject will be discussed in more detail.

Despite the similarity with the quantum mechanical formalism, it is important to emphasize fundamental differences in the treatment of photonic crystals. First, the goal is to find the electromagnetic field, which is a vectorial quantity, in contrast with the scalar wave function in quantum mechanics. Additionally, the problems in photonic crystals are macroscopic and scalable, as the equations do not have a constant establishing the scale, unlike in quantum mechanics where Planck's constant \hbar sets the scale. Furthermore, even if $\epsilon(\mathbf{r})$ is separable, the curl operator couples the spatial coordinates, making analytical solutions with interesting phenomena for photonic crystals rare [9, 8].

2.3 Solid-State Physics and Bloch Waves

Symmetries are foundational to almost everything physicists do. When working theoretically with dielectric structures found in photonic systems, both continuous and discrete symmetries are always present. They influence profoundly the spatial profile of the system's modes (solutions) and the associated spectrum, resembling the results found in the treatment of electronic systems with periodic potentials in quantum mechanics and solid-state physics. Therefore, utilizing these symmetries and adopting terminology from

solid-state physics is highly advantageous for understanding and describing a variety of optical phenomena in these crystals.

Certainly, before dealing with the main results of this work, it is essential to establish a degree of familiarity with the terminology that will be employed. Therefore, this section aims to introduce and briefly discuss the key terms upon which subsequent discussions will be based. This will be done by talking about specific cases. One can read their way through more profound discussions and proofs through the cited literature.

First of all, we will discuss the case of a system with a uniform dielectric function. The permittivity is given by

$$\epsilon(\mathbf{r}) = \epsilon, \quad (2.13)$$

represented by the uniform slab in the figure 2 (a). Thus, finding the harmonic modes (solution) is straightforward and they are given by the set of equations

$$\begin{aligned} \mathbf{H}(\mathbf{r}, t) &= \mathbf{H}_0 e^{i\mathbf{k}\cdot\mathbf{r}} e^{-i\omega t} & \mathbf{E}(\mathbf{r}, t) &= \mathbf{E}_0 e^{i\mathbf{k}\cdot\mathbf{r}} e^{-i\omega t} \\ \mathbf{E}_0 &= \frac{1}{\omega\epsilon_0} \mathbf{H}_0 \times \mathbf{k} & \mathbf{k} \cdot \mathbf{H}_0 &= 0 \end{aligned}, \quad (2.14)$$

in which \mathbf{H}_0 , \mathbf{E}_0 and the wave vector \mathbf{k} are an orthogonal set. Besides, let's discuss the solutions. The dispersion relationship for this system is straightforward:

$$\omega^2 = \epsilon k^2 \quad (2.15)$$

stabilishing k^2 as a conserved quantity of the system associated with the **continuous symmetry** of the dielectric function. Specifically, there is an invariance under a translation operation $\mathbf{r} \rightarrow \mathbf{r} + \mathbf{r}_0$, where \mathbf{r}_0 is any spatial vector. Consequently, this results only in a phase change in the spatial mode upon translation [9, 1]. In another word, a continuous symmetry in a direction implies a plane wave profile to the spatial mode in the specified direction.

Another way to represent the dispersion relationship in equation 2.15 is by considering a **band diagram**. This diagram is defined by a plot that indicates the frequencies of all modes allowed by the dispersion relation $\omega(\mathbf{k})$ depending on some curve in the wave vector \mathbf{k} space. For example, consider some direction β , then the wave vector can be written as $\mathbf{k} = \mathbf{k}_{\parallel} + \mathbf{k}_{\perp}$, \mathbf{k}_{\parallel} is in the β -direction and \mathbf{k}_{\perp} is perpendicular to it, as represented in the figure 2 (b). Considering that $\mathbf{k}_{\parallel}^2 = \beta^2$, the dispersion relationship can be expressed as $\beta^2 + \mathbf{k}_{\perp}^2 = \epsilon\omega^2$. Subsequently, one can construct the band diagram of the system in this particular direction, as shown in figure 2 (c). The possible frequencies, ω , for each spatial mode, distinguished by the *propagation constant* β , are plotted as a function of the propagation number, β . The line $\omega = \beta\epsilon^{-1/2}$ delineates the plane between the region where delocalized modes (plane wave solutions) are possible and where they are not. The region of the band diagram where $\beta < \omega\epsilon^{1/2}$ represents solutions of the plane wave type, possessing a finite value throughout space. Conversely, the region $\beta > \omega\epsilon^{1/2}$ comprises

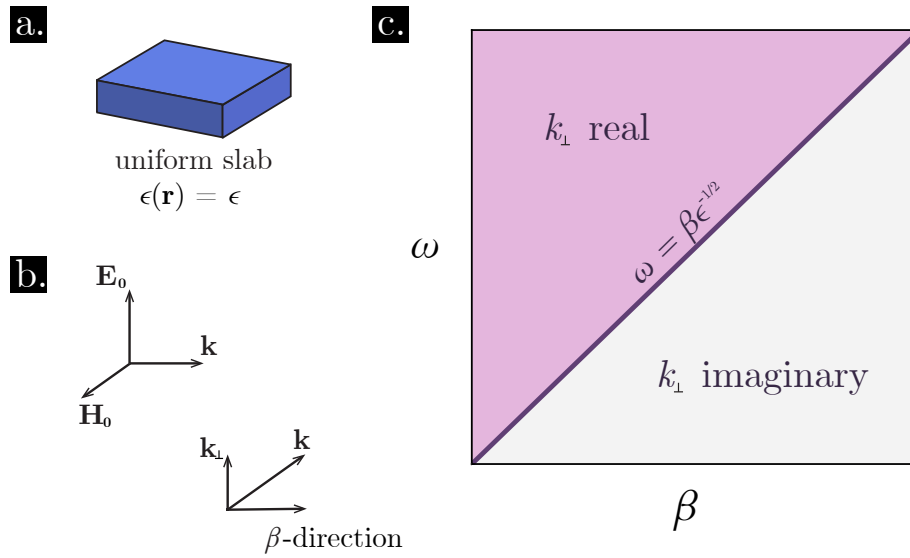


Figure 2 – (a) Schematic representation of a uniform slab with dielectric function constant in its bulk; (b) orthogonal set formed by the vectors found in the solution: the electromagnetic field, \mathbf{H}_0 and \mathbf{E}_0 , and the wave vector \mathbf{k} ; and (c) band diagram for a uniform dielectric if one plots the frequency $\omega(\mathbf{k})$ in function of a specific direction, depending in the module of its component.

solutions that are real exponentials, either growing indefinitely (unphysical solutions) or decaying to zero (evanescent waves). Some of these solutions cannot be observed in nature due to their exponential growth, breaking some conservation of energy principles.

When dealing with photonic crystals, one must consider their **discrete translational symmetry**. This symmetry is associated with the dielectric function, which is not invariant under the translation of any vector \mathbf{r}_0 , but remains invariant under translations \mathbf{R}_0 along certain directions in multiples of fixed lengths, as depicted in figure 3 (a).

If \mathbf{R}_0 represents the vector needed to reach an equivalent point within the crystal, the fixed length $|\mathbf{R}_0| = a$ is termed the **lattice constant**. Moreover, it's evident that this symmetry implies $\epsilon(\mathbf{r}) = \epsilon(\mathbf{r} + N\mathbf{R}_0)$, where N can be any integer. One fact that is very relevant in Spectral Analysis is that if one operator commutes with another, they share the set of eigenvectors. That said, if there is translational symmetries, $\hat{\epsilon}$ commutes with the translation operator $\hat{T}(\mathbf{R})$, that operates in any spatial function as follows:

$$\hat{T}(\mathbf{R})f(\mathbf{r}) = f(\mathbf{r} + \mathbf{R}), \quad (2.16)$$

and, due to the invariance, one can show that $\hat{T}(\mathbf{R})\hat{\epsilon} = \hat{\epsilon}\hat{T}(\mathbf{R})$ holds. Therefore, \hat{T} and $\hat{\epsilon}$ share eigenfunctions, and thus the spatial modes are eigenfunctions with plane waves as eigenvalues in the direction of the translational symmetry. This is discussed in more detail in any solid-state textbook [1, 2, 4] or photonic crystals textbook as well [7, 8, 9].

Consider a two-dimensional photonic crystal like the one presented in the figure 3 (a). The **unit cell** is a yz slab of dielectric material with width a in the x direction,

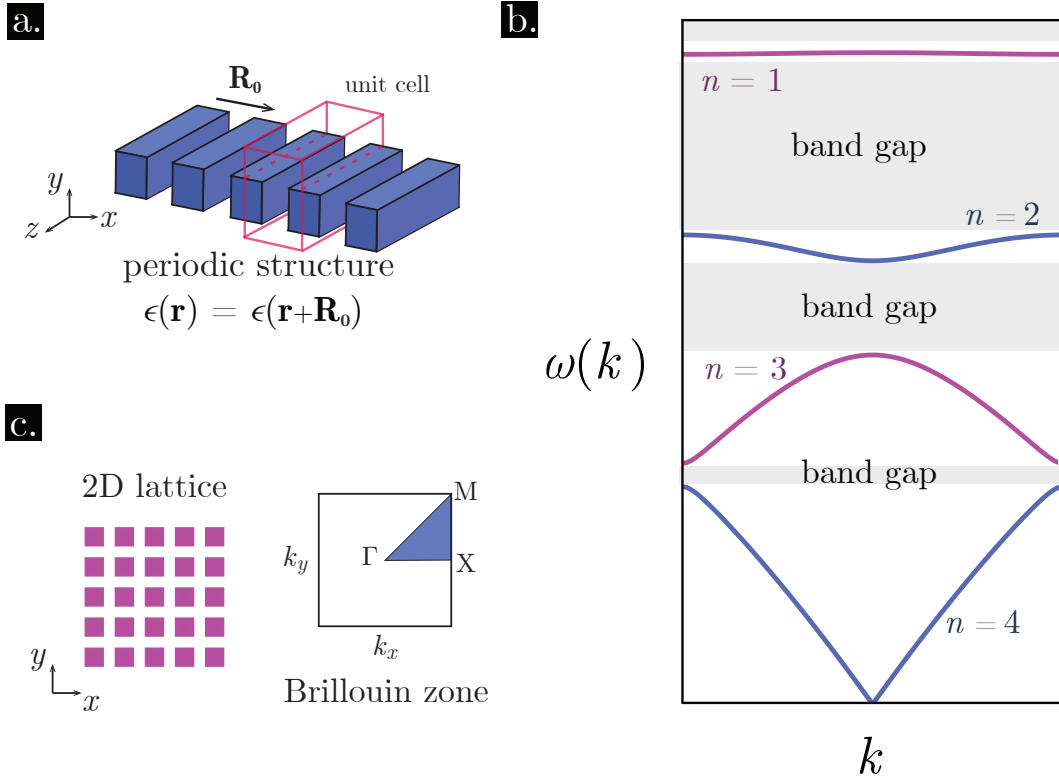


Figure 3 – (a) Representation of a photonic crystal formed by dielectric slabs (in blue) alternated with empty space filled. The unit cell of the structure is within the transparent box and the real lattice vector is \mathbf{R}_0 ; (b) band structure for a periodic dielectric structure along one line of the \mathbf{k} space; and (c) a representation of a square lattice and its respective Brillouin zone with its the irreducible part highlighted in blue, the triangle with vertices Γ , X and M .

as illustrated. The lattice is formed by repeating this unit cell in the x direction with a translation of \mathbf{R}_0 between each one. The lattice vectors for this discrete symmetry are $\mathbf{R}_0 = Na\hat{\mathbf{x}}$, thus

$$\hat{T}(\mathbf{R})e^{ik_x x} = e^{ik_x(x+Na)} \quad (2.17)$$

$$= e^{iNk_x a} e^{ik_x x}, \quad (2.18)$$

from which it is possible to conclude that every mode with wave number $k_x + 2\pi m/a$ has the same eigenvalue, forming a degenerated set of functions. The terms being added to k_x are all multiple of $2\pi/a$, then it is useful to define the **reciprocal lattice vector** $\mathbf{Q} = 2\pi/a\hat{\mathbf{x}}$ that can be thought as the lattice vector for a lattice formed by wave vectors in the \mathbf{k} space. The linear combination of these eigenfunctions are in fact also eigenfunctions of $\hat{\Xi}$ and then the spatial modes, solutions of our problem, and a natural basis to describe any system, can be written as a linear combination:

$$\mathbf{H}_{k_x, k_z}(\mathbf{r}) = e^{ik_z z} \sum_{m=-\infty}^{\infty} \mathbf{c}_{k_x, m}(y) e^{i(k_x + 2\pi m/a)x} \quad (2.19)$$

$$= e^{i(k_x x + k_z z)} \mathbf{u}(x, y, k_x), \quad (2.20)$$

here, $\mathbf{H}_{k_x, k_z}(\mathbf{r})$ represents the spatial mode of the system at position \mathbf{r} with a wave vector in the xz plane given by $\mathbf{k} = k_x \mathbf{Q}_x + k_z \mathbf{Q}_z$. It is straightforward to show that $\mathbf{u}(x, y, k_x) = \mathbf{u}(x + Na, y, k_x)$ holds, indicating the periodicity in the x direction.

As mentioned, there is a degeneracy in the wave number, hence the frequencies are also degenerated in the same way. If one considers only the non-redundant values of k_x , this wave number becomes bounded to the interval $(-\pi/a, \pi/a]$. This specific region of the \mathbf{k} space is called the *first Brillouin zone*.

Each mode has a specific wave vector \mathbf{k} and is associated with an eigenfrequency $\omega_n(\mathbf{k})$. The set of modes with all wave vectors in the first Brillouin zone is called a **band**. The set of all bands is called **band structure** of the material, this one is exemplified in the figure 3 (b). There are regions where there is no allowed spatial mode in the crystal, regardless of the value of k . These regions are called **photonic band gaps** and waves with the forbidden frequencies become evanescent in the medium [7, 8, 9]. The size of the gap is influenced by the difference of values of the refractive index in the medium in relation to the substrate.

This kind of solution, which takes this form due to periodicity in a certain direction, is referred to as a Bloch mode in textbooks on photonics and solid-state physics. Its one-dimensional counterpart is known as a Floquet mode or Floquet-Bloch mode. This result is well-known as Bloch's theorem. The physical interpretation of these Bloch modes $\mathbf{u}_{\mathbf{k}}$ is that as eigenfunctions of the spatial part of the Maxwell equations, they don't scatter through propagation because \mathbf{k} is a conserved quantity in the system.

The three-dimensional generalization of the example is as follows: considering a nonuniform in the three dimensions periodic dielectric function, hence the lattice that represents it is spanned by a linear combination of three primitive lattice vectors \mathbf{R}_1 , \mathbf{R}_2 and \mathbf{R}_3 . Every position of an element of the lattice is given by

$$\mathbf{R} = N_1 \mathbf{R}_1 + N_2 \mathbf{R}_2 + N_3 \mathbf{R}_3 \quad (2.21)$$

considering N_j integer, $j = 1, 2, 3$. It is a consequence that there is also a set of primitive reciprocal wave vectors that span the reciprocal lattice \mathbf{Q}_1 , \mathbf{Q}_2 and \mathbf{Q}_3 and, in analogy with the spatial space, the space of wave vectors also is spanned by them. The primitive reciprocal and the direct lattice vectors obey the following relationship $\mathbf{R}_i \cdot \mathbf{Q}_j = 2\pi \delta_{ij}$; here, $i, j = 1, 2, 3$. The Bloch modes are distinguished by their own **Bloch wave vector**. Each one can reside only in the first Brillouin zone and it's written as

$$\mathbf{k} = k_1 \mathbf{Q}_1 + k_2 \mathbf{Q}_2 + k_3 \mathbf{Q}_3, \quad (2.22)$$

thus the eigenfunction of $\hat{\Xi}$ with eigenfrequency $\omega(\mathbf{k})$ is, by the Bloch's theorem, given by

$$\mathbf{H}_{\mathbf{k}}(\mathbf{r}) = e^{i\mathbf{k} \cdot \mathbf{r}} \mathbf{u}_{\mathbf{k}}(\mathbf{r}), \quad (2.23)$$

here, $\mathbf{u}_{\mathbf{k}}(\mathbf{r})$ is a periodic function with the same periodicity as the lattice, $\mathbf{u}_{\mathbf{k}}(\mathbf{r}) = \mathbf{u}_{\mathbf{k}}(\mathbf{r} + \mathbf{R})$. The band structure of the photonic crystal provides important information about the optical properties of the material. For 2D and 3D materials, the first Brillouin zone can take very convoluted shapes depending on the topography of the real lattice [1, 2, 3], and it is common to plot the band diagram for lines at the boundaries of the first Brillouin zone in the reciprocal lattice. Figure 3 (c), displaying a schematic representation of a square real lattice and the reciprocal lattice. The **irreducible Brillouin zone** forms a triangle with Γ , X , and M as vertices. Like the unit cell, the remaining reciprocal lattice is formed by copies of it.

Before the conclusion of this section, one can ask in which direction the Bloch wave propagates. It is known that \mathbf{k} give this information in homogeneous and isotropic medium, but that is not the case for periodic medium: the velocity in which the energy propagates depends on \mathbf{k} and on the band by the following expression

$$\mathbf{v}_n(\mathbf{k}) := \nabla_{\mathbf{k}}\omega_n, \quad (2.24)$$

here, $\nabla_{\mathbf{k}}$ means that the derivative is with respect to the components of the Bloch wave vector \mathbf{k} . Thus, the spatial mode $\mathbf{u}_n(\mathbf{r}, \mathbf{k})$ has the **group velocity** $\mathbf{v}_n(\mathbf{k})$. One can retrieve a more in-depth discussion from the influence of group velocity on the propagation of these modes and waves from several sources [58, 67].

Now that the fundamental concepts and definitions to deal with photonic crystals have been contemplated, the objective of the last section of this chapter is to present an approximation that will set the stage for the scenario in which the results will be derived, given the complexity of solving Maxwell's equations.

2.4 Paraxial Wave Equation Approximation

A light beam can be thought of as a directional projection of light. It is interesting for many applications that these beams maintain their localization, i.e., remaining spatially confined through propagation, ignoring totally or partially the diffraction of the medium that causes spreading during the propagation. A beam of this kind can be labeled paraxial if the lines normal to the wavefront make small angles with the propagation axis [7, 59]. In the study of optical beams, one regularly resorts to a scalar study of the light, considering all the aspects of the wave propagation, but ignoring the vectorial one [7, 68]. This usually takes into account the solutions of the Helmholtz equation, which can overlap with another field of Optics that is also concerned with the propagation of light, the Fourier Optics [7, 59, 69].

Solving the problem using the set of differential equations exhibited in the equation 2.8 can be an exhausting task, and not always is it a path worth taking. There is interesting

physics to investigate making a smart use of approximations, considering the studied system, and discarding particularities that could make the problem difficult to solve. Here, the common choice to solve this problem is to consider the divergent equation for the electric field \mathbf{E} present in the equation 2.7 and the generalized eigenvalue problem for the same field in the equation 2.8. From the first, one can find the relationship:

$$0 = \nabla \cdot [\epsilon(\mathbf{r})\mathbf{E}(\mathbf{r})] \quad (2.25)$$

$$= \epsilon(\mathbf{r})\nabla \cdot \mathbf{E}(\mathbf{r}) + \nabla\epsilon(\mathbf{r}) \cdot \mathbf{E}(\mathbf{r}) \quad (2.26)$$

$$\therefore \nabla \cdot \mathbf{E}(\mathbf{r}) = -\mathbf{E}(\mathbf{r}) \cdot \nabla (\log \epsilon(\mathbf{r})) \quad (2.27)$$

and, from the generalized eigenvalue problem, making use of the identity $\nabla \times \nabla \times \mathbf{E}(\mathbf{r}) = \nabla(\nabla \cdot \mathbf{E}(\mathbf{r})) - \nabla^2 \mathbf{E}(\mathbf{r})$ and the equation 2.27,

$$k^2 \epsilon(\mathbf{r})\mathbf{E}(\mathbf{r}) = \nabla \times \nabla \times \mathbf{E}(\mathbf{r}) \quad (2.28)$$

$$= \nabla(\nabla \cdot \mathbf{E}(\mathbf{r})) - \nabla^2 \mathbf{E}(\mathbf{r}) \quad (2.29)$$

$$= -\nabla [\mathbf{E}(\mathbf{r}) \cdot \nabla (\log \epsilon(\mathbf{r}))] - \nabla^2 \mathbf{E}(\mathbf{r}) \quad (2.30)$$

$$\therefore \nabla^2 \mathbf{E} + k^2 \epsilon \mathbf{E} = -\nabla [\mathbf{E} \cdot \nabla (\log \epsilon)], \quad (2.31)$$

and it is worth keeping in mind that the spatial dependence will be omitted every time that it can enhance the clarity of the equations. The right side is responsible for the coupling between the different spatial components of the electric field. In problems of beam propagation, one is considerably more interested in the propagation of such beam in one particular direction considering a *very small* deviation from this. Henceforth, this particular direction will be the z -direction and the wave will be thought as a carrier plane wave $e^{i\xi z}$ with large spatial frequency ξ in the propagation direction modulated by a complex envelope $\mathbf{A} = \mathbf{A}(\mathbf{r})$ that must be a *slowly varying* in the z direction [7, 68]:

$$\mathbf{E}(\mathbf{r}) = \mathbf{A}(\mathbf{r})e^{i\xi z}, \quad (2.32)$$

and it will be very useful to decompose the gradient operator ∇ in the transversal gradient operator plus a perpendicular term to apply the assumptions taken in the future steps:

$$\nabla = \nabla_{\perp} + \mathbf{z} \frac{\partial}{\partial z}. \quad (2.33)$$

then, applying this operator in the equation 2.27 assuming that the electric field behaves as in the equation 2.32, one obtain

$$\nabla_{\perp}^2 \mathbf{A} + \partial_z^2 \mathbf{A} + (k^2 \epsilon - \xi^2) \mathbf{A} + 2i\xi \partial_z \mathbf{A} = -\nabla [\mathbf{A} \cdot \nabla (\log \epsilon)] - i\xi \mathbf{A} \cdot \nabla (\log \epsilon), \quad (2.34)$$

in which there are terms that can be neglected considering the assumptions made. As the vector function $\mathbf{A}(\mathbf{r})$ must vary slowly in z , its derivatives are small compared to the transverse ones, so one can neglect the second derivative in the propagation direction $\partial_z^2 \mathbf{A}$.

The first derivative cannot be ignored due to the spatial frequency ξ multiplying it. Then, the expression becomes

$$\nabla_{\perp}^2 \mathbf{A} + (k^2 \epsilon - \xi^2) \mathbf{A} + 2i\xi \partial_z \mathbf{A} = -\nabla [\mathbf{A} \cdot \nabla (\log \epsilon)] - i\xi \mathbf{A} \cdot \nabla (\log \epsilon). \quad (2.35)$$

If the dielectric permittivity $\epsilon(\mathbf{r})$ has a smooth derivative, one can neglect the term $\nabla \log \epsilon$ [68], then the components of \mathbf{A} are decoupled and thus the propagating wave will not carry any information about the polarization. If the medium changes the polarization of the propagating wave, it cannot be described in large distances by this approximation, because errors will accumulate. Thus,

$$\nabla_{\perp}^2 \mathbf{A} + (k^2 \epsilon - \xi^2) \mathbf{A} + 2i\xi \partial_z \mathbf{A} = 0 \quad (2.36)$$

and, as the polarization will not change through propagation, one can take the component of \mathbf{A}

$$\mathbf{A}(\mathbf{r}) = U(\mathbf{r}) \hat{\mathbf{u}} \quad (2.37)$$

and reduce the problem to a scalar one. Additionally, if one takes $\xi = k$ considering the one equivalent to the one found in the homogeneous solution, the equation becomes

$$\nabla_{\perp}^2 U(\mathbf{r}) + \Delta n^2(\mathbf{r}) U(\mathbf{r}) + 2ki \partial_z U(\mathbf{r}) = 0 \quad (2.38)$$

that is the usual paraxial wave equation approximation. As we know from wave physics and quantum mechanics, the term ∇_{\perp}^2 describes the diffraction effects, and the one with $\Delta n^2(\mathbf{r}) = n^2(\mathbf{r}) - 1 = \epsilon - 1$ describes scattering and refraction. Of course, here the similarity with the non-relativistic quantum mechanics is very clear: the difference between the refractive index of the material and the vacuum gives us the potential and $2k$ is the energy of the system. As mentioned before, k is indeed a conserved quantity and here this holds. There are fundamental differences: there are only two spatial components in the one that would be the laplacian operator and the role of the time is given to the propagation direction's coordinate.

The techniques utilized to solve problems of quantum mechanics can be applied in equation 2.38 to solve for optical systems and one can discuss in optics condensed matter analogs [13]. For instance, the formalism presented in the previous section can be utilized to derive Bloch modes for the paraxial wave equation and then one can discuss the results for a particular initial optical beam utilizing the terminology of solid-state physics.

3 Statistical Optics

The chosen approach in this thesis to solve optical problems aims to embrace a more realistic scenario by acknowledging that all light sources are inherently stochastic. This stochastic nature arises from the general uncertainty and fluctuations present in the light source, the medium through which it propagates, and the measurement device. To properly account for these occurrences, it is essential to describe light within a statistical framework [7, 15, 59, 70, 71], which gives rise to the optical concept of coherence. In particular, when considering applications such as imaging [72], tomography [73, 74], beam propagation [75], information storage [76], and many others [77], it becomes evident that a statistical framework is crucial. Therefore, taking spatial coherence into account when dealing with light propagating in periodic structures is imperative for achieving our goals.

In this chapter, the reader will be presented with basic concepts of statistical optics. First of all, a digression about scalar wave optics will be made and basic concepts of the theory will be presented, such as the definition of spatial coherence and time coherence. Every step is made using analytical signals (see Appendix A). Major quantities of the theory will be presented like the spectral density function and the cross spectral density function, all in the context of the second-order stochastic theory of light.

3.1 Stochastic Nature of Light

Statistical optics is the branch of optics that considers the stochastic properties of light. Absolutely all electromagnetic wave found in nature has fluctuations, even though one can not observe them directly. This intrinsic stochastic behavior can only be observed when one pays attention to the light in two or more space-time points (\mathbf{r}, ct) due to how fast they occur [15, 70]. One can ask where these fluctuations come from and it will be an excellent inquiring because almost all encounters with Optics take place in a deterministic framework in basic physics courses. The answer lies in the source and in the medium in which the light propagates: even when several light waves within a light beam come from the same source, they can be pretty different in the very instant they leave the source [16]. For example, light irradiated by a hot object is random and is formed by an Avogadro number of atoms emitting light independently, causing differences in frequencies and phases. If one considers the medium, one must consider all the scattering, diffuse transmission, turbulence, and other phenomena that create irregularities in the wavefront. You can not escape from these field fluctuations in the real world. As in the last chapter, the discussion presented here will take into account the optical region of the electromagnetic spectrum.

The common description of light is one where everything related to it is deterministic

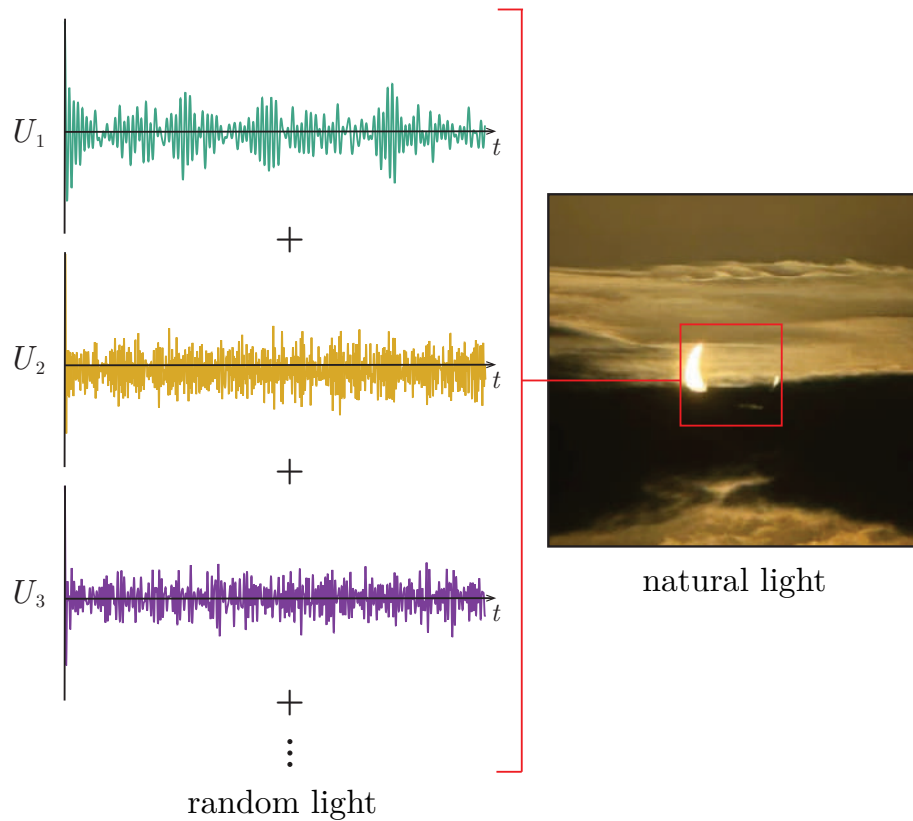


Figure 4 – Schematic representation of the fact that natural light is composed by a sum of a large number of light waves, represented by the signals U_j , $j = 1, 2, \dots$, fluctuating as the time goes by.

The image was taken by the author and cherished friends during the solar eclipse of 2023 in Maceió, Alagoas.

or **coherent**. If one is interested in natural light, one considers completely **incoherent** or completely random description. These extreme limits are the easiest way to deal with some physical systems analytically, of course. The general case lies in the **partial coherence** regime, which constitutes the "in-between"[7, 59]. But how one can describe light? One usually recurs into averages and statistics. Natural light, for example, is composed of a large number of individual light waves with different phases, frequencies, and polarizations. A scalar representation of this random characteristic of this kind of light is depicted in the figure 4, where the light of a solar eclipse is decomposed in a sum of several wave functions $U_j(t)$. One must stabilize a cohesive way to treat these **optical fields** taking into account the stochasticity of the light.

First, each optical field $U(t)$ can be thought of as a **random process**. As a random process, a specific form of it is called a sample or realization. For simplicity, the discussion will consider only its dependence on time, but the spatial dependence is not hard to include. A beam of light is formed by a large number of realizations of this optical field, thus every physical quantity will be an average of them. The set of all countable possible samples of this field is known as the **ensemble** of $U(t)$: $\{U_1(t), U_2(t), U_3(t), \dots, U_j(t), \dots\}$.

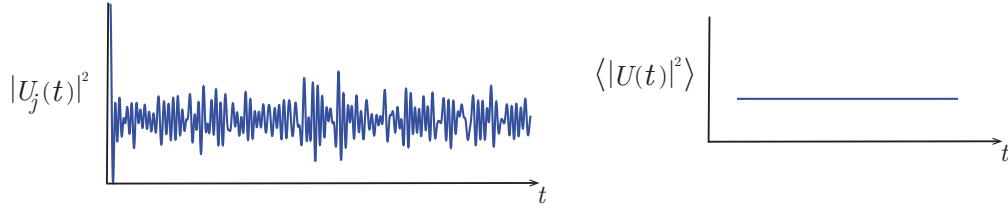
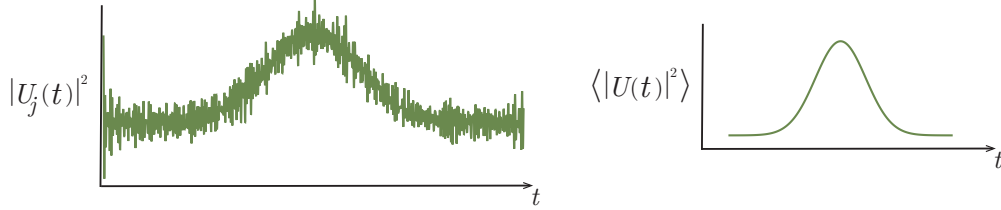
a. stationary process**b.** nonstationary process

Figure 5 – Examples of the intensity of a realization of an optical field $|U_j(t)|^2$ and its mean intensity $\langle |U(t)|^2$ for a (a) stationary process and a (b) non stationary process. Inspired by the figure 12.1-1 from [7].

An **ensemble average** of this optical field is defined by the following expression

$$\langle U(t) \rangle = \lim_{N \rightarrow \infty} \sum_{j=1}^N U_j(t), \quad (3.1)$$

and the generalization for physical quantities that can be written as functions of the optical field like the field intensity can be written straightforwardly.

Besides, it will be shown in the next sections that several quantities important to the field of statistical optics depend on correlation functions, that explain various phenomena and are the usual way to verify experimentally how the theory and results predicted by statistical optics hold in reality [7, 16, 59]. The correlation function $\Gamma(t_1, t_2)$ of the optical field $U(t)$ in two different instants is written as

$$\Gamma(t_1, t_2) = \langle U^*(t_1)U(t_2) \rangle, \quad (3.2)$$

also known as the autocorrelation function. It is clear that one can compute correlations of higher orders with respect to other variables. Exemplifying, $\langle U(t) \rangle$ is a first order mean value and $\langle U^*(t_1)U(t_2) \rangle$ is a second order correlation.

An infinite variety of random processes can be considered, but only a few have physical significance: the stationary ones [16]. But what does one mean by stationary? An optical field has realizations $U_j(t)$ that can fluctuate continually in time, but if these fluctuations have a character that does not change with time, i.e., the probability densities associated with the random process remain the same, they're referred to as a statistically **stationary** process and the mean values does not change with time (see figure 5 (a)).

This condition is strong and thus this classification is also called stationary in the *strictly sense* stationary process. If the mean value $\langle U(t) \rangle$ is independent of t and the correlation $\Gamma(t_1, t_2)$ depends on $t_2 - t_1$, the process is called stationary in the *wide sense*. If none of these conditions are met, the process is called **nonstationary** (see figure 5 (b)). A more profound discussion and elucidation can be found in some statistical optics textbooks [15, 16]. Considering a stationary optical field, one can define a **time average** of a realization:

$$\overline{U_j(t)} = \lim_{T \rightarrow \infty} \frac{1}{T} \int_{t-T/2}^{t+T/2} U_j(t') dt'. \quad (3.3)$$

In practice, one single realization of the ensemble $U_j(t)$ carries the statistical information about the whole stationary process [15]. Usually, one can safely assume the **ergodic hypothesis**: the time average of one realization $\overline{U_j(t)}$ is equivalent to the ensemble average $\langle U(t) \rangle$.

With these brief introductions to some important concepts and intuitive knowledge about statistical optics, one is prepared to understand how correlations reign upon optical fields and how concepts like coherence arise from them [15, 59]. For this, the next section will discuss coherence through the lenses of interference effects.

3.2 Coherence, Correlation and the Interference Pattern

The previous mentions of the term coherence did not carry out the physical meaning of this concept. Here, coherence is a quantity that translates the ability of one to observe (or not) interference of waves. Usually, this concept is associated with the visibility or contrast measured from interference patterns [78].

Coherence is intrinsically related to correlations and it is usually divided into two categories: spatial coherence and temporal coherence. These two classes of coherence are faces of the same coin, showing the impact of the stochasticity of the light. To discuss this classification and understand the connection between coherence and correlation, the traditional way is two systems that present interference of light: the Michelson interferometer and the Young's double slit experiment.

With the Michelson interferometer (see figure 6) the goal is to elucidate the temporal coherence of light. Hence, consider a light beam from a sufficiently small source σ that does not fluctuate in a macroscopic time scale. The assumption of a small source is picked to ignore some spatial coherence effects, as one will see in the next example. Also, assume a quasi-monochromatic so its bandwidth $\delta\nu$ is very small if compared with the mean frequency ν_0 . Follow the image in the figure 6 to understand the experiment: the beam propagates until it is divided into two different beams by the beam divider D : one branch makes a path of distance d_1 and the other branch a distance of d_2 ; thus, when they reflect in the mirrors M_1 and M_2 and join together again in the beam divider D , one deal with a

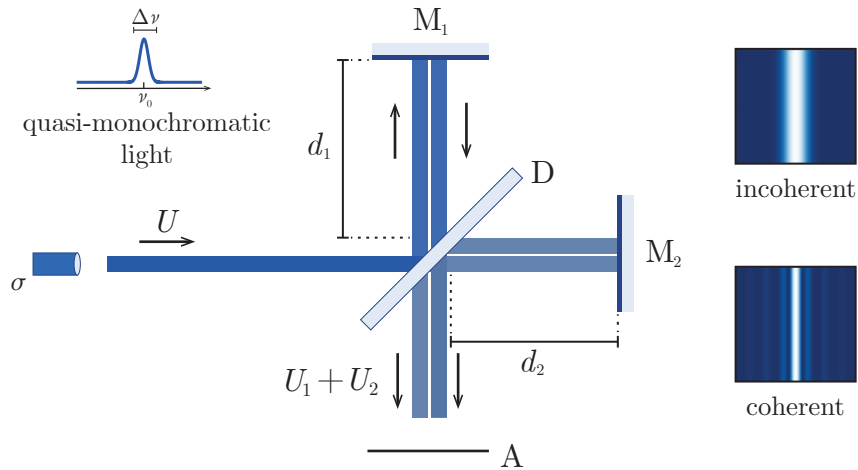


Figure 6 – Representation of the Michelson interferometer experiment: σ is the light source; U is the incident optical field; M_j is a mirror, $j = 1, 2$; D is the beam divider; and A is the plane of observation. Inspired by the figure 12.2-2 from [7] and figure 4.1 from [15].

beam composed of two different beams with path difference $\Delta l = 2|d_2 - d_1| = c\Delta t$. As expected, if Δl is small enough, interference fringes appear in the plane of observation A [15].

The rise of the interference pattern is conditioned to the time delay Δt by one beam submitted in relation to another. This phenomenon can be understood as follows: the interference pattern in A arises from the superposition of the spatial profile of light, each one with a frequency from the spectrum. Of course, spatial profiles with different frequencies have different spatial periodicities. Consequently, if one takes from a coherent standpoint where the interference pattern appears and begins to increase Δt , the interference pattern will become less and less well defined in A : the contributions of each frequency of the spectrum will get out of step in relation to the others, forming an incoherent beam of light. One representation of this is given by the intensity spatial profile on the right side of the figure 6.

In fact, it is an experimental fact that the fringes will appear only if $\Delta t\Delta\nu \lesssim 1$. Hence, one can find an order for the time delay $\Delta t \sim 1/\Delta\nu$ and take this as the coherence time of the light. This is a manifestation of **temporal coherence**, arising from the finite bandwidth of the source [59].

One may ask the following question: how coherence is related to correlations in this case? To answer this, consider an optical field $U(t)$ in a point of the plane of observation A . As this point is fixed, omitting the spatial dependence of the field will cause no harm. This field is a stochastic process composed of other two stochastic processes $U = U_1 + U_2$, $U_j(t)$ refers to the optical field coming from the beam of the j th branch, $j = 1, 2$. As discussed, there is a time delay between these fields, so a realization of the optical field in

the observation plane is given by:

$$U(t) = U_1(t) + U_2(t + \Delta t), \quad (3.4)$$

so one can easily compute the measured quantity in the plane of observation. Of course, this corresponds to a mean intensity of the field realizations $I(t) = \langle |U(t)|^2 \rangle$:

$$I(t) = \langle |U(t)|^2 \rangle \quad (3.5)$$

$$= \langle U^*(t)U(t) \rangle \quad (3.6)$$

$$= \langle [(U_1^*(t) + U_2^*(t)) \cdot (U_1(t) + U_2(t))] \rangle \quad (3.7)$$

$$= \langle |U_1(t)|^2 \rangle + \langle |U_2(t)|^2 \rangle + 2\text{Re} \{ \langle U_1^*(t)U_2(t) \rangle \}, \quad (3.8)$$

hence, the intensity measured is equal to the intensity of each beam as if the other did not exist plus a term that depends on the correlation between the fields. One can utilize the concepts mentioned in the last section to rewrite this expression:

$$I(t) = \Gamma_1(t, t) + \Gamma_2(\Delta t, \Delta t) + 2\text{Re} [\Gamma_{12}(t, t + \Delta t)] \quad (3.9)$$

and if the optical field is a stationary process in the wide sense, assuming that the mean intensity of each beam is the same for simplicity $\Gamma_1(t, t) = \Gamma_2(\Delta t, \Delta t) = \Gamma(0) = I_0$, one obtains

$$I(t) = \Gamma(0) \left[1 + 2\text{Re} \frac{\Gamma(\Delta t)}{\Gamma(0)} \right], \quad (3.10)$$

that reinforces the discussion: interference fringes will appear if the correlation of the field allows it [79]. One important quantity can be defined from this expression, the **complex coherence degree**:

$$\gamma(\Delta t) := \frac{\Gamma(\Delta t)}{\Gamma(0)}, \quad (3.11)$$

giving a quantitative metric to how correlated these fields are, therefore also giving information about how coherent this light is. The absolute value of this function is bounded: $0 \leq |\gamma(\Delta t)| \leq 1$. The limit $\gamma \rightarrow 0$ means that the fields are not correlated at all, thus the light is incoherent; the limit $\gamma \rightarrow 1$ means that the fields are completely correlated, so the light is coherent. The intermediary region implies that the fields are partially correlated, so the light is partially coherent. This allows one to take a glimpse into how correlation *is* coherence [15, 79].

On the other side, there is the spatial coherence and Young's double-slit interference experiment. Consider again a quasi-monochromatic light from a thermal source σ with a considerable spatial extent Δs . The light propagates through a distance R until it includes in two pinholes S_j , $j = 1, 2$, separated from each other in a distance d . The pinholes act like secondary sources and the light resulting from the superposition of the light coming from each one is measured in the plane of observation A . As d decreases, the interference pattern becomes more and more visible in A . Experimentally results show that the interference

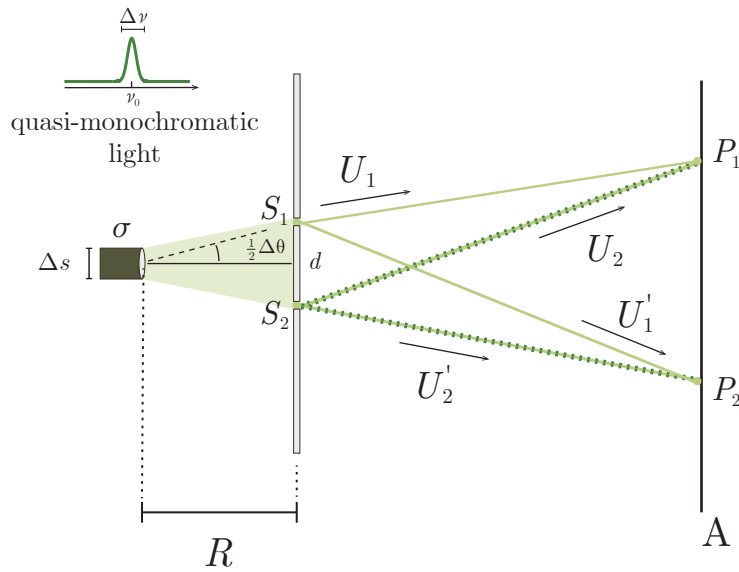


Figure 7 – Representation of the Young's double slit experiment: σ is the thermal light source; Δs is the spatial extent of the source; R is the distance between the source and the double slit plane; S_j are the slits and also the point sources for the secondary wave, $j = 1, 2$; d is the distance between the slits; A is the plane of observation; P_j is any point in the plane A , $j = 1, 2$; U_j is the optical field reaching P_1 from the j th slit, $j = 1, 2$; U'_j is the optical field reaching P_2 from the j th slit, $j = 1, 2$. Inspired by the figures 4.2 and 4.3 from [15].

pattern will appear only if $\delta\theta\delta s \lesssim \lambda_0 = c/\nu_0$. The area in the plane of the slit in which the pinholes can be positioned and one can observe the interference pattern is called coherence area and is given by $\Delta A \sim (R\delta\theta)^2$ [15].

One may ask: how does an interference pattern arise if one of the assumptions of the system is that there is a thermal light? The reasoning for this doubt is that light from different points of the source is independent of others, thus no fixed phase relationship between the different points of the beam can be stabilized. How can correlations arise and enable the interference pattern?

Consider S_1 and S_2 like the secondary light sources they are: thus, it is straightforward to assume that these sources are also quasi-monochromatic and there are no correlations between the light fields emitted by them. Though it may be true, the disturbances in two different points of A and fluctuations suffered by these emitted fields are very similar when they propagate. In the point P_1 , one will measure the intensity of the superposition $U_1 + U_2$ while in the point P_2 , $U'_1 + U'_2$ will contribute to the intensity pattern measured in A . Considering that the distance of the path propagated by each optical field is small in comparison to the coherence length, the individual fields will not have a correlation, but the sum of them will. Furthermore, these correlations are generated through propagation and superposition [15, 59, 79]. The **spatial coherence** here arises from the finite spatial extent of the light source [59].

Aiming to see the correlations in the field arise from a mathematical description of the system, some quantities must be defined. First, take a point P in the plane of observation A . The distance between the j th pinhole and this point is $r_j = \overline{S_j P}$, then the time interval taken by the optical field to reach P from S_j is $\Delta t_j = r_j/c$, thus the optical field $U(t)$ in P is:

$$U(t) = K_1 U_1(t - t_1) + K_2 U_2(t - t_2), \quad (3.12)$$

in which K_j , $j = 1, 2$, is an imaginary number that arises when one solves the Fresnel's diffraction integral [7, 78, 79]. Hence, the intensity measured in P is given by

$$I(t) = \langle |U(t)|^2 \rangle \quad (3.13)$$

$$= \langle U^*(t)U(t) \rangle \quad (3.14)$$

$$= \langle [K_1^* U_1^*(t - t_1) + K_2^* U_2^*(t - t_2)] \cdot [K_1 U_1(t - t_1) + K_2 U_2(t - t_2)] \rangle \quad (3.15)$$

$$= |K_1|^2 \langle |U_1(t - t_1)|^2 \rangle + |K_2|^2 \langle |U_2(t - t_2)|^2 \rangle \quad (3.16)$$

$$+ 2|K_1||K_2|\text{Re} \{ \langle U_1^*(t - t_1)U_2(t - t_2) \rangle \}, \quad (3.17)$$

from which one can write using the optical fields correlations,

$$I(t) = I_1 + I_2 + 2\sqrt{I_1 I_2} \text{Re} [\gamma_{12}(t_2 - t_1)], \quad (3.18)$$

in which one considered the following substitutions: $I_j = |K_j|^2 \langle |U_j(t - t_j)|^2 \rangle$, $j = 1, 2$, and one utilized the definition of the complex degree of coherence:

$$\gamma_{12}(\Delta t) := \frac{\Gamma_{12}(t_2 - t_1)}{\sqrt{\Gamma_1(0)\Gamma_2(0)}}, \quad (3.19)$$

where the index in the cross-correlation function Γ_{12} indicates that it considers the correlations coming from two different points and, of course, the wide sense stationary condition was considered. Again, the interference pattern is contained in the term where the coherence has a role and the coherence between two points of the optical field became relevant. In the next section, the general theoretical framework to deal with these systems will be established and one can make the connection with our current rudimental approach.

3.3 Second Order Theory of Scalar Random Light

In the previous section, one was concerned with stationary fields. Furthermore, an assumption utilized was that these fields are ergodic, then the ensemble averages and the time averages are and stay the same. The optical field was commonly treated as an analytical signal (see appendix A). This section will stabilize the second-order scalar theory of random light, it is the framework utilized in the remaining chapters of this thesis.

The fundamental quantity of the previous examples and of the theory of optical coherence is the **mutual correlation function** $\Gamma(\mathbf{r}_1, \mathbf{r}_2, \tau)$ [15], that carries the correlation

between two analytical signals in two different positions with the time difference τ between them:

$$\Gamma(\mathbf{r}_1, \mathbf{r}_2, \tau) := \langle U^*(\mathbf{r}_1, t)U(\mathbf{r}_2, t + \tau) \rangle \quad (3.20)$$

that is not a bounded function; it is useful to normalize this function by defining another quantity, the **complex degree of coherence** of the light in two points \mathbf{r}_1 and \mathbf{r}_2 :

$$\gamma(\mathbf{r}_1, \mathbf{r}_2, \tau) := \frac{\Gamma(\mathbf{r}_1, \mathbf{r}_2, \tau)}{[\Gamma(\mathbf{r}_1, \mathbf{r}_1, 0)\Gamma(\mathbf{r}_2, \mathbf{r}_2, 0)]^{1/2}}, \quad (3.21)$$

that by the properties of stationary random processes [15, 16, 71], satisfies the inequality:

$$0 \leq |\gamma(\mathbf{r}_1, \mathbf{r}_2, \tau)| \leq 1 \quad (3.22)$$

and the limits, as discussed, determine in which regime the system is: coherent, partially coherent, or incoherent. All these quantities depend on the time, but it is useful for many applications and also for measurements to treat these correlations in the space-frequency domain. As these quantities depend on two random processes at two different points, it is said that this theory is of second order.

Consider an analytic signal $U(\mathbf{r}, t)$ representing an ergodic and stationary (at least in the wide sense) optical field fluctuating at (\mathbf{r}, t) . This function can be thought of as a Fourier integral:

$$U(\mathbf{r}, t) = \int_0^\infty \tilde{U}(\mathbf{r}, \nu)e^{-2\pi i\nu t} d\nu, \quad (3.23)$$

with $\tilde{U}(\mathbf{r}, \nu)$ being its Fourier transform with dependence on the frequency ν instead of time t : this can be useful if one is interested in investigating the spectrum of the system. Additionally, optical waves vary very rapidly, so it is really more experimentally approachable to think about the frequency in the measurements. Thus, considering the ensemble of the analytical signal in the frequency domain, one can define the **cross-spectral density function** of these fluctuations:

$$W(\mathbf{r}_1, \mathbf{r}_2, \nu) := \langle \tilde{U}^*(\mathbf{r}_1, \nu)\tilde{U}(\mathbf{r}_2, \nu) \rangle, \quad (3.24)$$

that is interpreted as a measure of the correlation between two points in the optical field fluctuations with dependence on a frequency of the spectrum. If one considers the Wiener-Khintchine theorem [15, 16, 70], the mutual coherence function and the cross-spectral density function form a pair of Fourier transform, thus satisfying the definition of analytical signals:

$$\Gamma(\mathbf{r}_1, \mathbf{r}_2, \tau) = \int_0^\infty W(\mathbf{r}_1, \mathbf{r}_2, \nu)e^{-2\pi i\nu\tau} d\nu, \quad (3.25)$$

$$W(\mathbf{r}_1, \mathbf{r}_2, \nu) = \int_{-\infty}^\infty \Gamma(\mathbf{r}_1, \mathbf{r}_2, \nu)e^{2\pi i\nu\tau} d\tau. \quad (3.26)$$

The cross-spectral density gives us all the information about the correlation to every pair of points of the space. One experimentally important quantity is retrieved if



Figure 8 – Free representation of the spectral density as a function of wavelength at three positions in a color image. Adapted from figure 10.1-4 of [7]. In the image, the official album cover for the 2021 album 'If I could Make It Go Quiet' by Norwegian musician Girl in Red is utilized to illustrate how the spectral density translates to the perceived color.

one considers $\mathbf{r}_1 = \mathbf{r}_2 = \mathbf{r}$, this density function depends on only one position of the space and the resulting function is the **spectral density** of light:

$$S(\mathbf{r}, \nu) = W(\mathbf{r}, \mathbf{r}\nu) \quad (3.27)$$

$$= \langle |\tilde{U}(\mathbf{r}, \nu)|^2 \rangle, \quad (3.28)$$

that represents the power per unit area of light in the position \mathbf{r} for the frequency ν of the spectrum [7]. Figure 8 shows an illustration in which one can observe how the average power per unit area from $S(\nu)$ in a specific position translates to a perceived color.

There are properties that can be mentioned about the cross-spectral density function and the spectral density. First, the spectral density is strictly positive $S(\mathbf{r}, \nu)$ and also composes a Fourier pair with the the autocorrelation function, this being is a direct consequence of the equations 3.25 and 3.26:

$$\Gamma(\mathbf{r}, \mathbf{r}, \tau) = \int_0^\infty S(\mathbf{r}, \nu) e^{-2\pi i \nu \tau} d\nu, \quad (3.29)$$

$$S(\mathbf{r}, \nu) = \int_{-\infty}^\infty \Gamma(\mathbf{r}, \mathbf{r}, \nu) e^{2\pi i \nu \tau} d\tau. \quad (3.30)$$

Furthermore, one can normalize the cross-spectral density as in the mutual correlation and define the **spectral degree of coherence** at frequency ν :

$$\mu(\mathbf{r}_1, \mathbf{r}_2, \nu) := \frac{W(\mathbf{r}_1, \mathbf{r}_2, \nu)}{[S(\mathbf{r}_1, \nu)]^{1/2} [S(\mathbf{r}_2, \nu)]^{1/2}}, \quad (3.31)$$

and, as before [15, 71, 16], satisfies the inequality:

$$0 \leq |\mu(\mathbf{r}_1, \mathbf{r}_2, \nu)| \leq 1, \quad (3.32)$$

but, differing from the other quantities, μ and γ do not make a Fourier pair.

With these concepts established, one can utilize the theory of coherence to study physical systems considering the statistical nature of light. Further discussion about the historic development of the field can be found in optics textbooks [7, 59, 78], and more mathematical descriptions and proofs of all results exposed here can be found in statistical optics textbooks [15, 16, 70, 71, 79].

4 Spatial Coherence of Light in Periodic Lattices

In this chapter, we will employ the concepts presented in the previous chapter to construct a model describing light in periodic media while considering its spatial coherence effects. Initially, we will explore the fundamental concepts of our theory: we will introduce the system under study and establish a subtle connection with well-known concepts and methods from solid-state physics. We will also study a specific case involving deterministic light for comparative purposes. Subsequently, we will investigate the stochastic case by using our framework to explore the physics of the system.

4.1 General Discussion

Let us consider a 2D material system with a refractive index that is periodic in the transverse direction x and constant in the propagation direction z . Our issue involves propagation, and therefore, we will assume that everything occurs within the bulk of the material, as if it fills the entire xz -plane. As discussed in chapter 2, the information about the change in the refractive index concerning a base value n_0 is provided by the lattice potential $V(x)$, which governs the matter-light interaction in the system. As previously described, the lattice potential V satisfies:

$$V(x) = V(x + a), \quad (4.1)$$

here, a represents the lattice constant. Since the periodicity is one-dimensional, our lattice-related quantities will also be 1D. Our primary objective in achieving the chapter's goal is to analyze the propagation of a light beam, represented by an analytical signal, through this periodic lattice. This beam's profile at $z = 0$ is denoted as $U(x, z = 0) = U_0(x)$. To begin, we need to establish an approach for propagation of the signal $U(x, z)$ within the lattice. To do so, we will utilize the framework derived from the wave equation in the paraxial approximation:

$$i\partial_z U(x, z) + \partial_x^2 U(x, z) + V(x)U(x, z) = 0, \quad (4.2)$$

that closely resembles Schrödinger's equation, enabling us to employ similar solution methods used in optical systems. In figure 9, a schematic representation for the system is displayed, exhibiting one particular case for the real and imaginary part of U_0 in $z = 0$, a gaussian beam times a plane wave, and a 1D harmonic periodic lattice, a cosine squared profile.

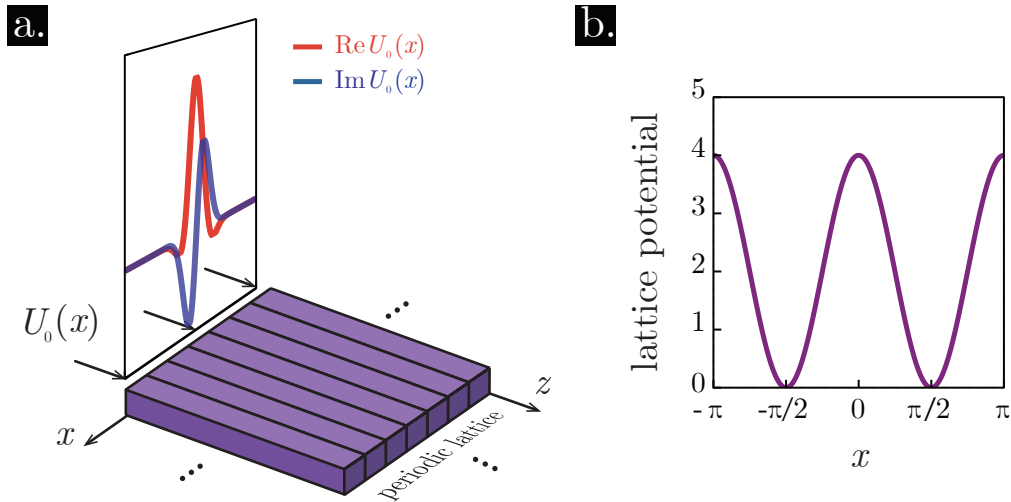


Figure 9 – (a) Schematic representation of the optical system, featuring the analytical signal profile $U_0(x) = U_0 \exp[-x^2/\sigma^2]e^{iqx}$. Additionally, there's a purple parallelepiped oriented perpendicular to the transverse direction x , symbolizing a waveguide. Each waveguide has a specific refractive index for each x value, giving rise to the lattice potential $V(x)$. (b) When considering the continuous limit, the lattice potential describing the photonic crystal is depicted as $V(x) = A \cos^2(x)$.

During the study of photonic systems, our initial focus is on identifying the spatial modes of the system and its band structure. These modes exhibit a unique property within the periodic media of the system: they resist diffraction or spreading out during propagation. Given that the lattice potential remains independent of the propagation direction, z , we can separate the x -dependence from the z -dependence. Consider a solution $U_n(x, z)$ to equation 4.2:

$$U_n(x, z) = u_n(x, k)e^{i\beta_n(k)z}, \quad (4.3)$$

Here, k denotes the wavenumber, and $\beta_n(k)$ represents the propagation number associated with the n th eigenfunction $u_n(x, k)$. Through this substitution, our paraxial wave equation transforms into an eigenvalue problem. This transformation prompts a discussion of the parallels between non-relativistic quantum mechanics and optical systems under the paraxial approximation. This comparison allows us to do a deep dive into the physics underlying light propagation using insights from quantum mechanics.

$$D_x^2 u_n(x, k) + V(x)u_n(x, k) = \beta_n(k)u_n(x, k). \quad (4.4)$$

It is essential to note, however, that while we draw from quantum mechanics' findings, we must consider that light operates under distinct constraints compared to electrons. Specifically, in quantum theory of solid state physics, a fundamental aspect of the study of periodic systems involves computing the energy levels and wave functions of electrons using the Bloch theory. Henceforth, we will draw upon this theoretical framework and its results to enhance our understanding of the physics governing our optical system.

From Bloch's theorem, we know that $V(x)$ being a periodic function, the solution of the eigenvalue equation is the product between a periodic function $v_n(x, k)$ — with the same periodicity of the potential [1, 4] — and a plane wave e^{ikx} with k being its respective Bloch wavenumber:

$$u_n(x, k) = v_n(x, k)e^{ikx}, \quad (4.5)$$

which can lead us to the following equation:

$$D_x^2 v_n(x, k) + 2ikD_x v_n(x, k) + [V(x) - k^2]v_n(x, k) = \beta_n(k)v_n(x, k). \quad (4.6)$$

In the study of photonic lattices, the central task typically revolves around the band structure and finding the allowable frequencies $\omega(k)$ within the material. Frequencies lying outside the allowed zones of the band structure tend to be evanescent waves in the medium. It is important to underscore that our attention is directed not towards temporal frequencies associated with the wave's temporal aspect, but rather towards the propagation number connected to the spatial characteristics of light. Consequently, the band structure in the following discussion focuses specifically to this spatial aspect of light.

Several methods exist for solving equations 4.2, 4.4, and 4.6 [9, 80, 81, 82]. Our selected method involves employing the plane wave expansion technique. This choice is driven by the Fourier series expansion of both $v_n(x, k)$ and $V(x)$ due to their periodicity. Considering a as the lattice constant,

$$v_n(x, k) = \frac{1}{\sqrt{2\pi}} \sum_{m=-\infty}^{\infty} b_n^m(k) e^{\frac{2i\pi m}{a}x} = \frac{1}{\sqrt{2\pi}} \sum_m b_n^m(k) e^{iK_m x}, \quad (4.7)$$

noting that $K_m = 2\pi m/a$ is the reciprocal lattice number. Let us take a moment for a digression: $b_n^m(k)$ serves as a Fourier expansion coefficient reliant on the Bloch wavenumber, k , and the reciprocal lattice number K_m . Hence, an alternate representation for this coefficient, observed in certain literature, is as $b_n(k + K_m)$. This format is frequently utilized across a variety of literary sources. For the lattice potential, we do the same procedure:

$$V(x) = \sum_{m=-\infty}^{\infty} V_m e^{\frac{2i\pi m}{a}x} = \sum_m V_m e^{iK_m x}. \quad (4.8)$$

Upon substituting equations 4.7 and 4.8 into 4.6, we arrive at the subsequent linear system governing the coefficients $b_n^m(k)$ for each Bloch wavenumber, k :

$$-(K_m + k)^2 b_n^m(k) + \sum_p V_p b_n^{m-p}(k) = \beta_n(k) b_n^m(k), \quad (4.9)$$

with one equation for each value of m , the problem is an eigenvalue problem. To guarantee a good visualization to the reader, we can express it in a matrix form. The matrix $\hat{\Lambda} =$

$\hat{\Lambda}(k)$ for the Fourier coefficients is structured as follows:

$$\hat{\Lambda}(k) = \begin{bmatrix} \ddots & \vdots & \vdots & \vdots & \ddots \\ \dots & V_0 - (k - K_{-1})^2 & V_{-1} & V_{-2} & \dots \\ \dots & V_1 & V_0 - k^2 & V_{-1} & \dots \\ \dots & V_2 & V_1 & V_0 - (k + K_1)^2 & \dots \\ \ddots & \vdots & \vdots & \vdots & \ddots \end{bmatrix}_{M \times M}. \quad (4.10)$$

This square matrix has dimensions $M \times M$, where M signifies the number of terms considered in the plane wave expansion for the Floquet-Bloch modes. It is worth noting that as we truncate the series, we assume that M will always be an odd number. If b is the column vector formed by the coefficients of the Fourier expansion, we have

$$b(k) = \begin{bmatrix} \vdots \\ b_n^{-1}(k) \\ b_n^0(k) \\ b_n^1(k) \\ \vdots \end{bmatrix} \quad (4.11)$$

and our problem is essentially to find the eigenvectors and eigenvalues of the operator $\hat{\Lambda}(k)$. We can rewrite the problem as

$$\hat{\Lambda}(k)b(k) = \beta_n(k)b(k) \quad (4.12)$$

and the outcome of this process yields the N Fourier coefficients for the desired Floquet-Bloch solutions, along with their respective propagation numbers. Accomplishing this task is straightforward with matrix diagonalization algorithms. Specifically, we employed the LinearAlgebra package in Julia for this purpose. Then, by using equations 4.7 and 4.5, we construct the basis necessary for solving any initial value problem. First, let us discuss some properties of the band structure.

Analogous to their role in a homogeneous medium, the Floquet-Bloch modes assume a position akin to plane waves, wherein each beam can be envisioned as a composite assembly of several plane waves. These modes distinctly bear the lattice structure's fingerprint. Like the temporal counterpart, they remain inert until stimulated by an incident wave, and its propagation is entirely dictated by the band structure.

We can analyze the band structure by using the symmetry of our potential (see equation 4.1). Initially, let us explore the band diagram: the potential exhibits translational discrete symmetry, thus one know that the band structure presents a discrete number of bands. Figure 10 showcases the first five bands for the potential represented by the expansion 4.8 for the potential $V(x) = A \cos^2$, given by:

$$V(x) = \frac{A}{4}e^{-2ix} + \frac{A}{2} + \frac{A}{4}e^{2ix}, \quad (4.13)$$

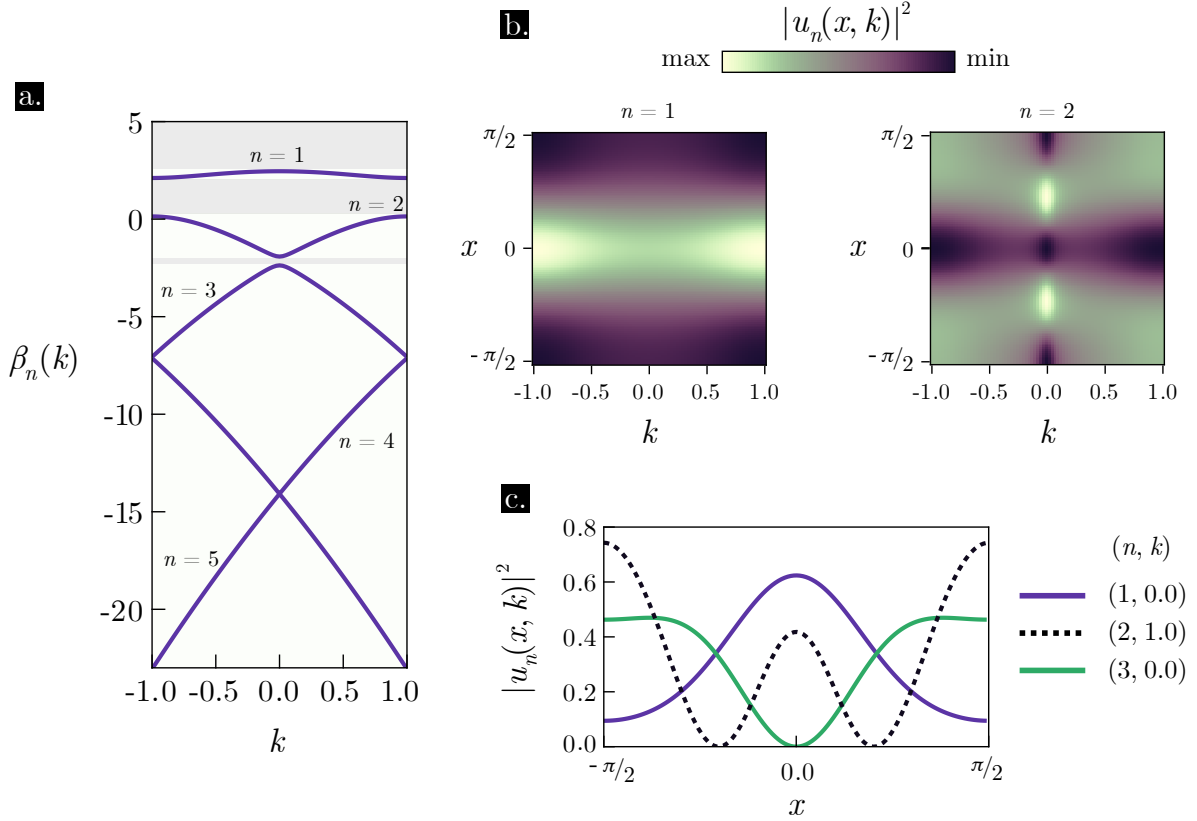


Figure 10 – Band structure of a $V(x) = A \cos^2 x$, $A = 4$. (a) Band diagram showing the propagation constant $\beta_n(k)$ versus Bloch wave vector k for the first five bands. In the right, the intensity of the Floquet-Bloch function $|u_n(x, k)|^2$ is displayed for x in a unit cell $[-a/2, a/2]$ and for k in the first Brillouin zone $[-\pi/a, \pi/a]$ for the bands (b) $n = 1$ and $n = 2$ in the xk -plane, and (c) fixed values of (n, k) , specifically $(1, 0.0)$, $(2, 1.0)$, and $(3, 0.0)$.

In this case, only the terms with $m = 0, \pm 1$ are non-zero. The band structure for $A = 4$ displays two band gaps between the first three bands and a semi-infinite one above the first band. Alongside the band structure, the intensity distributions of the first and second Floquet-Bloch solutions are displayed in the xk plane and the transverse x direction, considering fixed values for k . Here, x represents the unit cell while k is confined within the first Brillouin zone. This presentation effectively showcases the periodic nature of these modes in both the k and x directions, as expected.

Any analytical signal propagating in this periodic media can be written as the following general solution for the equation 4.2:

$$U(x, z) = \sum_{n=1}^{\infty} \int_{-\pi/a}^{\pi/a} c_n(k) u_n(x, k) e^{i\beta_n(k)z} dk, \quad (4.14)$$

i.e., a superposition of Floquet-Bloch modes considering the entire band structure. These solutions satisfy an orthogonal condition concerning k and x . This condition can be proved in both the continuous and discrete cases, the last offering significant utility in addressing computational challenges associated with these modes. For details of derivation

see appendix B. The orthogonality relationship is given by

$$\int_{-\infty}^{\infty} u_n^*(x, k) u_m(x, q) dx = \delta_{nm} \delta(k - q). \quad (4.15)$$

Combining the equation 4.15 with the general solution displayed in equation 4.14 in $z = 0$,

$$U(x, 0) = U_0(x) = \sum_{n=1}^{\infty} \int_{-\pi/a}^{\pi/a} c_n(k) u_n(x, k) dk, \quad (4.16)$$

the participation coefficients $c_n(k)$ that carries the contribution of each Floquet-Bloch function for each mode k within the first Brillouin zone in the initial beam. Multiplying both sides by $u_m^*(x, q)$ and integrating in the entire x direction,

$$c_n(k) = \int_{-\infty}^{\infty} u_n^*(x, k) U_0(x) dx. \quad (4.17)$$

Thus, we have all the information necessary to describe the propagation of any given beam in our system. Moreover, we can make use of a conserved quantity (in real systems) through the Parserval's identity [45], with each term quantifying the total contribution to the beam from each band:

$$P = \sum_{n=1}^{\infty} \int_{\text{B.Z.}} |c_n(k)|^2 dk = \sum_{n=1}^{\infty} p_n \quad (4.18)$$

that is also valuable in determining in which n to truncate the band sum depending on the model's parameters for the computational treatment of the system. In the following section, the theory developed thus far is used to stabilish a baseline for comparison with the stochastic discussion that will be presented in subsequent sections.

4.2 Deterministic Case: Gaussian Source

Let us apply the theory to the deterministic case involving a Gaussian source. Among various common source types like Hermite-Gaussian, Laguerre-Gaussian and even Bessel beams that could be implemented (if one take into account this theory for $(2+1)D$), the Gaussian beams holds a prominent position in beam optics; also, choosing this as our fully coherent source allows for a straightforward comparison with the Gaussian-Schell source to be presented in the stochastic description of the problem. We will describe the initial optical field $U_0(x)$ as:

$$U_0(x) = \tilde{U}_0 e^{-x^2/2\sigma^2} e^{-iqx}, \quad (4.19)$$

representing a gaussian intensity distribution around $x = 0$ and width of $\sqrt{2}\sigma$ with complex exponential carrying a transverse momentum q . Here, \tilde{U}_0 denotes the field amplitude.

The band structure governs the propagation of a beam within the periodic lattice. One advantage of using the Floquet-Bloch framework is to get some physical insight about

the system through its particularities. Hence, it is relevant to know which modes are excited as the beam travels through the lattice. This computation can be done using equation 4.17:

$$\begin{aligned}
c_n(k) &= \int_{-\infty}^{\infty} u_n^*(x, k) U_0(x) dx \\
&= \int_{-\infty}^{\infty} \sum_{m=-\infty}^{\infty} \frac{[b_n^m(k)]^*}{\sqrt{2\pi}} e^{-i(2m+k)x} \cdot \tilde{U}_0 e^{iqx} e^{-x^2/2\sigma^2} dx \\
&= \frac{\tilde{U}_0}{\sqrt{2\pi}} \sum_{m=-\infty}^{\infty} [b_n^m(k)]^* e^{-(2m+k-q)^2\sigma^2/2} \int_{-\infty}^{\infty} dx e^{-x^2/2\sigma^2} \\
&= \sigma U_0 \sum_{m=-\infty}^{\infty} [b_n^m(k)]^* e^{-(2m+k-q)^2\sigma^2/2},
\end{aligned} \tag{4.20}$$

where the integral in the second line was solved by completing the square to obtain $[x + i(2m + k - q)\sigma^2]^2$, taking the substitution $x = x' + i(2m + k - q)\sigma^2$ and writing the result for a simple Gaussian integral. Note that, for a gaussian beam, the participation coefficient can be viewed as a weighted arithmetic mean value for Gaussian functions of k centered in $k = q - 2m$ with the weight being the functions $[b_n^m(k)]^*$, varying across the first Brillouin zone. For the parameters values of interest (n, A, k) , $b_n^m(k)$ are nonzero for few values for m ; then it is useful to truncate the series in a specific value M , so the computations can be more efficient.

We will investigate the behavior of the participation coefficient using equation 4.20 with Gaussian sources characterized by variable parameters, mainly the transverse momentum, being related to the angle of excitation and controls diffraction properties of the incident beam [57]. Hence, let us examine the terms derived from Parseval's identity across different lattice potential amplitudes A and the transverse momentums q . Afterwards, we will discuss details concerning the deterministic propagation of the Gaussian beam in the periodic lattice.

In figure 11, we display the shallow-lattice regime, where the lattice potential amplitude satisfies the condition $A \ll 1$. The figure exhibits the first two non-zero participation coefficients (normalized by $\sigma\tilde{U}_0$) for Gaussian waves with transverse momentum values $q = 0.0, -0.5$ and -1.0 . In this scenario, the lattice's influence on the beam is weak, resulting in a band diagram that resembles one in the absence of a lattice potential (see figure 11 (b)) with $\beta = -k^2$ periodically folded inside the first Brillouin zone. For $q = 0$ in figure 11 (a) top, corresponding to the normal incidence, the "energy" contribution comes majority from the first band, then one band is sufficient for describing the beam propagation, the same occurs for $q = -0.5$ in (a) middle, where the largest contribution comes from the first band for modes around the Bloch wavenumber $k = -0.5$. At the edge of the Brillouin zone, $q = -1$, we expect that the first two bands exhibit similar contributions to the overall beam evolution, as displayed in figure 11 (a) bottom.

In figure 12, the influence of the potential is prominent, resulting in the appearance

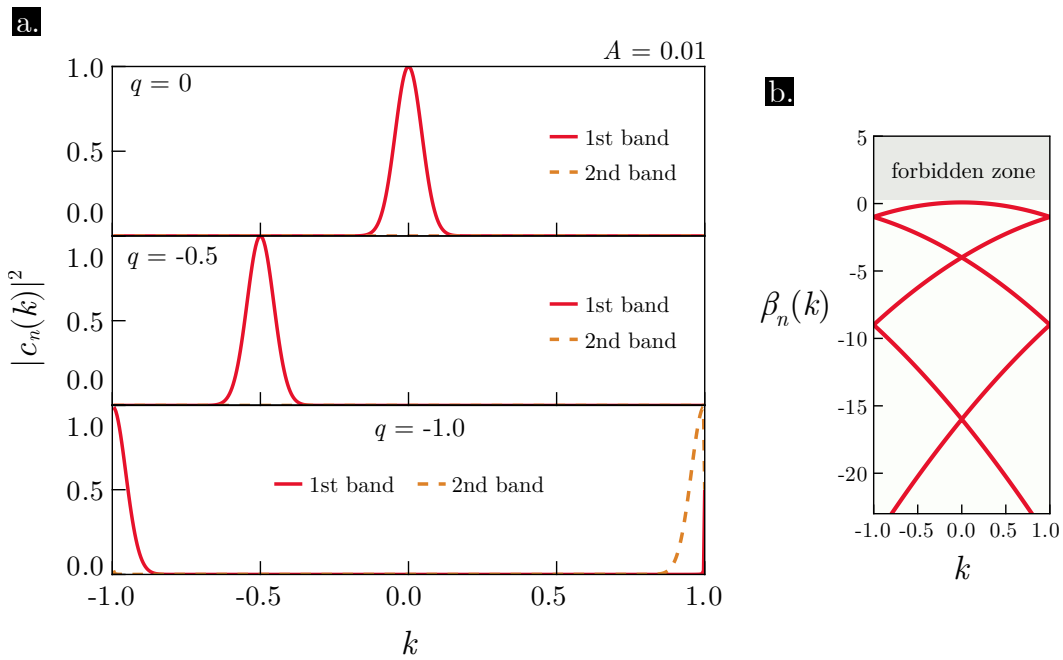


Figure 11 – (a) Absolute squared Floquet-Bloch participation coefficients $|c_n(k)|^2$ versus wave number k for the potential $V(x) = A \cos^2 x$, $A = 0.01$ with an incident Gaussian beam $U_0(x) = \tilde{U}_0 e^{iqx} e^{-x^2/2\sigma^2}$ with beam width $\sigma = 7\pi$ and transverse momentum (top) $q = 0.0$, (middle) $q = -0.5$ and (bottom) $q = -1.0$; (b) Band diagram showing the propagation constant $\beta_n(k)$ versus Bloch wave vector k for the first five bands.

of band gaps between the first and second band, and between the second and third, as depicted in the band diagram in figure 12 (b). Of course, above the first band, there is a semi-infinite bandgap. The figure 12 displays the first three non-zero participation coefficients (normalized by $\sigma \tilde{U}_0$) for Gaussian waves with transverse momentum values $q = 0.0$, $q = -0.5$ and $q = -1.0$. For the normal incidence, $q = 0$, shown in (a) top panel, the "energy" contribution arises predominantly from the first band, akin to the shallow-lattice case. Interestingly, the "energy" contribution from the third band surpasses that of the second band. Conversely, for $q = -0.5$ (middle panel (a)), the contribution from the second band exceeds that of the third band, although the first band remains the most significant. Lastly, for $q = -1.0$ (bottom panel (a)), we observe a similar contribution from the first two bands.

In figure 13, the potential's impact is notably stronger, leading to an additional band gap between the third and fourth bands, as depicted in Figure 13(b). In contrast to the previous case, we witness non-zero contributions from the fourth band for normal incidence ($q = 0$), showed in the top panel (a). Additionally, there is almost an equivalent contribution between the second and third bands in the $q = -0.5$ case, showcased in the middle panel (a). In the case of $q = -1.0$, both the second and third band contributions are non-zero, altering the previously observed similarity in the contributions of the first two bands.

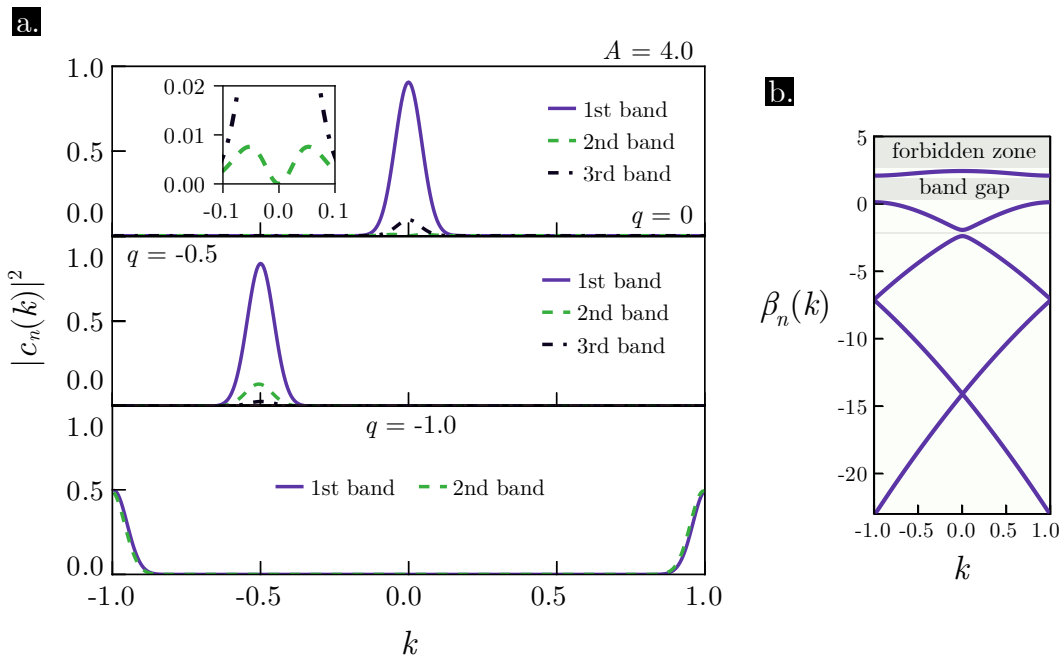


Figure 12 – (a) Absolute squared Floquet-Bloch participation coefficients $|c_n(k)|^2$ versus wave number k for the potential $V(x) = A \cos^2 x$, $A = 4.0$ with an incident Gaussian beam $U_0(x) = \tilde{U}_0 e^{iqx} e^{-x^2/2\sigma^2}$ with beam width $\sigma = 7\pi$ and transverse momentum (top) $q = 0.0$ (the inset illustrates the contribution of the second and third bands), (middle) $q = -0.5$ and (bottom) $q = -1.0$; (b) Band diagram showing the propagation constant $\beta_n(k)$ versus Bloch wave vector k for the first five bands.

For this system, we can make some statements: the significant contribution for the modes of each band is centered around the incident wave transverse momentum q , but the energy distribution does not follow a Gaussian profile, not necessarily symmetric around the Bloch wave number, that strongly affects the propagation dynamics. Furthermore, as the lattice potential becomes more intense, more bands become relevant to the system and more band gaps arise. These statements can be verified by investigating the contribution of each band, the Parseval's identity and the band structure for several sets of parameters.

The Parseval's identity shown in equation 4.18 is a conserved quantity and can be viewed as the sum of contributions of each band for the beam p_n in the first Brillouin zone. Each term gives us information on how much each band contributes to the beam depending on the parameters of the lattice and the incident beam. This will be particularly useful for the stochastic case, but here it helps to understand the behavior of the contribution coefficients.

In figure 14, the normalized Parseval identity ($P = \sum p_n = 1$) terms p_n are depicted versus (a) the lattice potential amplitude and (b) the transverse momentum. In (a), the range of the lattice potential amplitude varies from the shallow lattice regime ($A \ll 1$) to a very strong potential $A = 10$; the top panel corresponds to normal incidence ($q = 0$) and

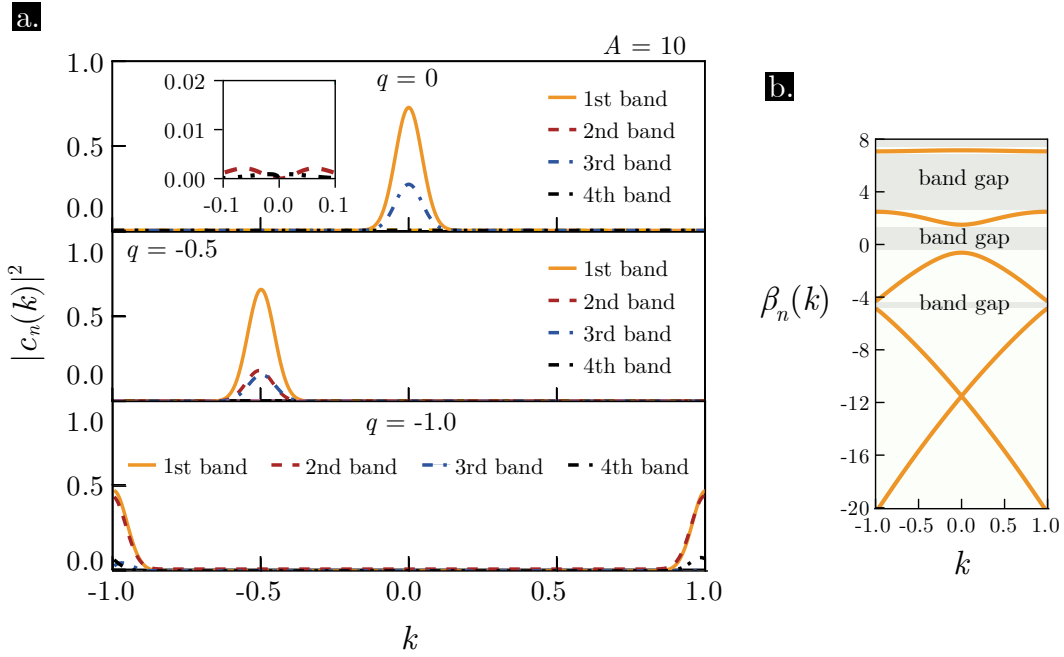


Figure 13 – (a) Absolute squared Floquet-Bloch participation coefficients $|c_n(k)|^2$ versus wave number k for the potential $V(x) = A \cos^2 x$, $A = 10.0$ with an incident Gaussian beam $U_0(x) = \tilde{U}_0 e^{iqx} e^{-x^2/2\sigma^2}$ with beam width $\sigma = 7\pi$ and transverse momentum (top) $q = 0.0$ (the inset illustrates the contribution of the third and fourth bands), (middle) $q = -0.5$ and (bottom) $q = -1.0$; (b) Band diagram showing the propagation constant $\beta_n(k)$ versus Bloch wave vector k for the first five bands.

we can see that the major contribution is due to the first and third bands only, similar to the case in the Bragg condition $q = -1$, where only two bands contribute to the beam so far as $A = 5$. In this case, a two-wave model can give reliable results considering the Bragg resonant modes [50, 83]. Moreover, as the lattice potential amplitude increases, the contribution for the reminiscent bands increases, decreasing the contribution of the first two, as expected because P is a conserved quantity. For $q = -0.5$ (see figure 14 (a) middle panel), we see the contribution of the second and third bands becoming equal. As expected, the contribution for the first one decays as the others increase. In the right of the figure, in (b), we see the dependence of the transverse momentum for a fixed $A = 4$: we see that the p_n are even in q .

Let us now analyze the influence of the lattice on the beam's evolution. The input beam's transverse momentum q controls significantly its diffraction [57]. Specifically, the beam direction is strongly influenced by the group velocity's direction $\nabla_k \beta_n(k)$: the direction aligns perpendicular to the transmission band. The precise relationship with propagation will be explored further in the last section of this chapter.

One can ask how the potential amplitude A affects the propagation and the intensity pattern of the propagating beam. This analysis is straightforwardly conducted by plotting

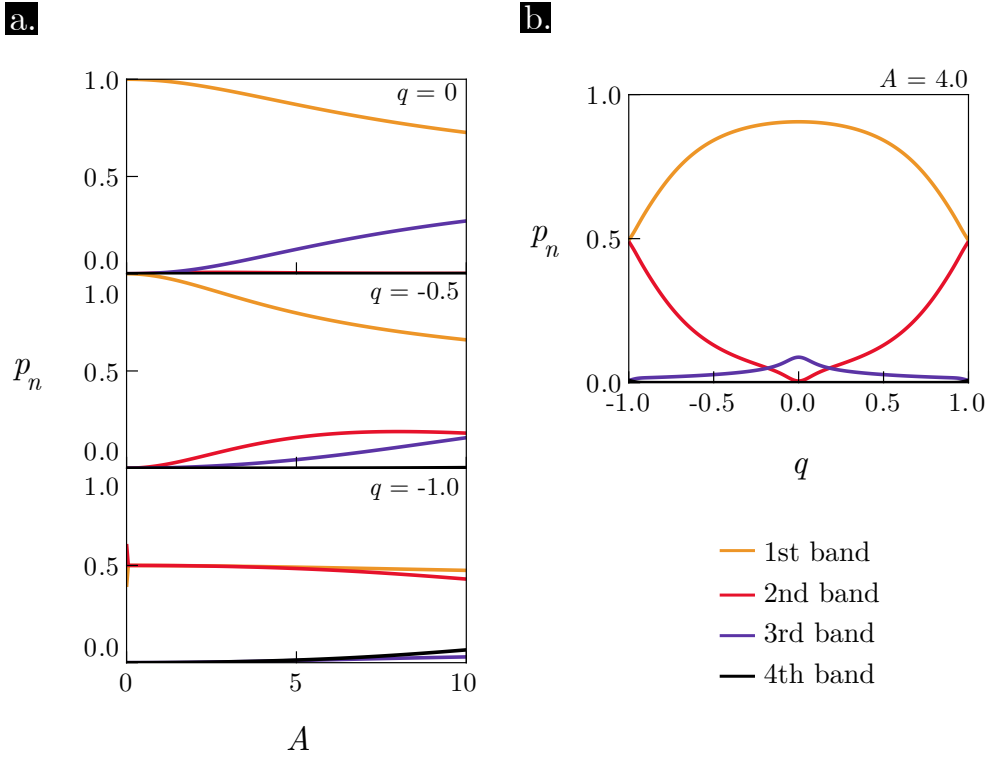


Figure 14 – (a) Parserval identity terms p_n versus lattice potential amplitude A for and transverse momentum (top) $q = 0.0$, (middle) $q = -0.5$ and (bottom) $q = -1.0$ and (b) versus the transverse momentum q for a specific lattice potential amplitude $A = 4.0$. For both, the input beam is the optical field $U_0(x) = \tilde{U}_0 e^{iqx} e^{-x^2/2\sigma^2}$ with beam width $\sigma = 7\pi$.

the beam intensity $|U(x, z)|^2$, displayed in figure 15 for several initial conditions along with the beam center $x_c(z)$ defined by

$$x_c(z) = \frac{\int x |U(x, z)|^2 dx}{\int |U(x, z)|^2 dx}, \quad (4.21)$$

which delineates the beam's center overall movement. It is important to note that these visualizations were computed by employing equations 4.14 and 4.20, and the accuracy of the results was verified using Split-Step Methods. We consider three regimes to illustrate the lattice's role in beam propagation. First, for a shallow lattice potential amplitude $A = 0.01$, where the variation in the photonic crystal's refractive index is minimal, and a transverse momentum $q = -0.5$ (figure 15 (a)), the beam propagates without considerable spreading, tilted to the negative x direction due to the lattice excitation by the transverse momentum. As we discussed and showed, the Parserval identity term p_1 is the more prominent, so the significant contribution comes from the first band that has its participation coefficient $c_n(k)$ centered around the wave number $k = -0.5$. The group velocity $\nabla_k \beta_1(k)$ around this Bloch wave number is tilted to the negative x , aligning with the tilt seen in the beam propagation. This inclination is highlighted through the beam center $x_c(z)$ (dashed black line).

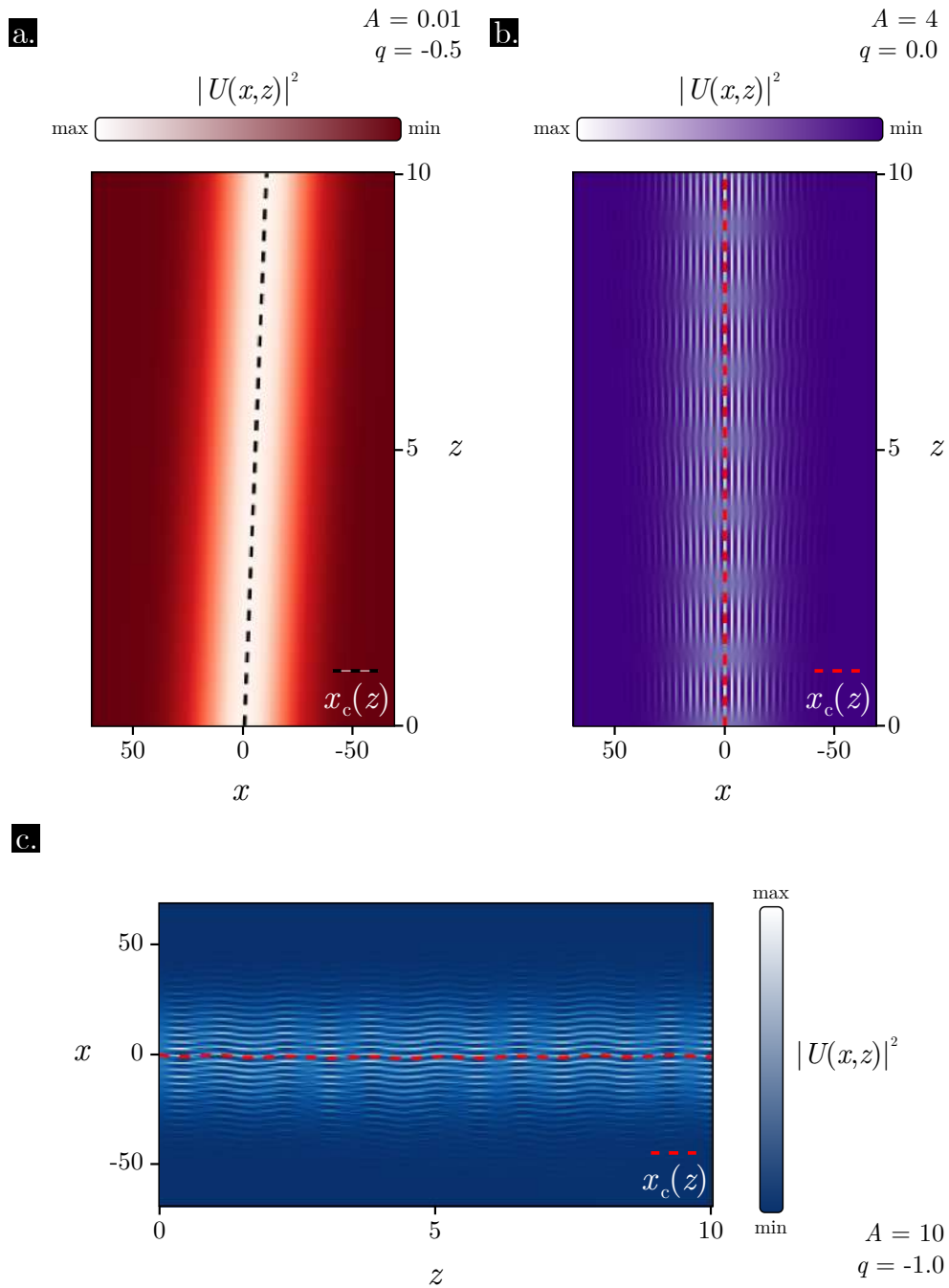


Figure 15 – Beam intensity $|U(x,z)|^2$ with the beam center $x_c(z)$ for three input gaussian beam with width $\sigma = 7\pi$ and potential amplitude A and wave number q : (a) $A = 0.01$ and $q = -0.5$; (b) $A = 4$ and $q = 0$; (c) $A = 10$ and $q = -1.0$.

Considering the potential amplitude $A = 4$ and transverse momentum $q = 0$, one observes significant contributions primarily from the first three bands: the first being the most pronounced, the second non-negligible, and the third nearly absent, evident in the Parseval's term p_n . Their participation coefficient $c_n(k)$ is centered around the Bloch wave number $k = 0$. From the band diagram's analysis of $\nabla_k \beta_n(k)$, we anticipate that the beam will propagate along the z direction. In figure 15 (b), we observe that while the beam remains relatively free from diffraction effects, its interaction with the lattice induces oscillations along the x direction. Additionally, the intensity distribution exhibits oscillations along the z direction. Remarkably, the beam center x_c (dashed red line) remains a straight line $x = 0$.

Increasing the potential amplitude to $A = 10$, more excited bands contribute to the beam dynamics. By choosing $q = -1.0$, we ensure that the Bragg condition is satisfied, where the first two bands exhibit almost identical contributions to the overall beam evolution, as reflected in Parseval's coefficient p_n . Notably, the contributions from the third and fourth bands are not negligible. By inspecting the participation coefficients $c_n(k)$, we observe an asymmetry around $k = 0$. Some modes around $k = -1$ are more excited than those at $k = 1$ for certain bands, and vice versa. Consequently, analyzing the beam direction via $\nabla_k \beta_n(k)$ requires more nuanced attention. Furthermore, through the beam propagation exhibited in figure 15 (b), we also observe that the beam remains diffractionless, but with even more oscillations. The beam exhibits oscillatory behavior around $x = 0$, evident in the beam center x_c , resembling the Zitterbewegung effect (more details will be discussed in the last section of this chapter).

In the next section, we reach the main results of our model through the consideration of the random fluctuations in the optical fields. This discussion of a gaussian source will serve as a limiting case and a baseline for our future discussions about the beam dynamics in periodic potentials considering the stochastic nature of optical beams in nature.

4.3 Stochastic Theory

The objective of this section is to incorporate the inherent random fluctuations of optical fields, irrespective of their physical origin — spontaneous emission, temperature fluctuations, mechanical vibrations, or others. To achieve this, we employ statistical concepts, particularly the formalism of second-order classical statistical optics. Here, we consider correlations between two spatial points through the cross-spectral density function, defined as:

$$W(x_1, x_2, z) = \langle U^*(x_1, z)U(x_2, z) \rangle_\omega, \quad (4.22)$$

that represents the correlation between two spatial points of the optical field, (x_1, z) and (x_2, z) , averaged over an ensemble of monochromatic (fixed ω) realizations of the

optical field U . Considering a periodic medium, each field realization is essentially a linear combination of the Floquet-Bloch modes previously discussed. By using equation 4.14 in the definition of the cross-spectral density function, we obtain:

$$\begin{aligned}
W(x_1, x_2, z) &= \langle U^*(x_1, z)U(x_2, z) \rangle_\omega \\
&= \left\langle \sum_{n,m=1}^{\infty} \int_{-\pi/a}^{\pi/a} dk_1 \int_{-\pi/a}^{\pi/a} dk_2 c_n^*(k_1)c_m(k_2) \right. \\
&\quad \times u_n^*(x_1, k_1)u_m(x_2, k_2)e^{i[\beta_n(k_2)-\beta_n(k_1)]z} \left. \right\rangle_\omega \\
&= \sum_{n,m=1}^{\infty} \int_{-\pi/a}^{\pi/a} dk_1 \int_{-\pi/a}^{\pi/a} dk_2 \langle c_n^*(k_1)c_m(k_2) \rangle_\omega \\
&\quad \times u_n^*(x_1, k_1)u_m(x_2, k_2)e^{i\Delta\beta_{nm}z} \\
&= \sum_{n,m=1}^{\infty} \int_{-\pi/a}^{\pi/a} dk_1 \int_{-\pi/a}^{\pi/a} dk_2 C_{nm}(k_1, k_2) \\
&\quad \times u_n^*(x_1, k_1)u_m(x_2, k_2)e^{i\Delta\beta_{nm}z}.
\end{aligned} \tag{4.23}$$

As the propagation of each random optical field $U(x, z)$ relies on the participation coefficient of each band $c_n(k)$, the propagation of the cross-spectral density function depends on the correlations existent between the bands. These correlations are described by the cross-correlation coefficients $C_{nm}(k_1, k_2) = \langle c_n^*(k_1)c_m(k_2) \rangle_\omega$. This quantity characterizes the spatial coherence of the beam, as the Floquet-Bloch functions and the exponentials with each propagation number are deterministic by nature. The propagation of the correlations can be approached similarly to the deterministic case, but one must analyze the cross-correlation coefficients, which can be determined from any initial cross-spectral density function $W_0(x_1, x_2) = W(x_1, x_2, 0)$ as follows:

$$\begin{aligned}
C_{nm}(k_1, k_2) &= \langle c_n^*(k_1)c_m(k_2) \rangle_\omega \\
&= \iint dx_1 dx_2 u_n(x_1, k_1)u_m^*(x_2, k_2)W_0(x_1, x_2),
\end{aligned} \tag{4.24}$$

representing a correlation measure between the n th and m th bands for the Floquet-Bloch wave numbers k_1 and k_2 . By using the definition from equation 4.22, the average beam intensity at a position (x, z) can be obtained by assuming $x_1 = x_2 = x$, which results in the spectral density $S(x, z)$:

$$\begin{aligned}
S(x, z) &= \langle |U(x, z)|^2 \rangle_\omega \\
&= \iint_{\text{B.Z.}} dk_1 dk_2 C_{nm}(k_1, k_2)u_n(x, k_1)u_m^*(x, k_2)e^{i\Delta\beta_{nm}z},
\end{aligned} \tag{4.25}$$

a quantity measurable in laboratory experiments.

It is evident that the spatial correlation introduced by the cross-correlation coefficients can notably influence the beam intensity. However, a pertinent question arises: to what extent does the beam behavior deviate from the deterministic case? The quantity that

measures the impact of these correlations is the spectral degree of coherence $\mu_{nm}(k_1, k_2)$:

$$\mu_{nm}(k_1, k_2) = \frac{\langle c_n^*(k_1)c_m(k_2) \rangle_\omega}{\sqrt{\langle |c_n(k_1)|^2 \rangle_\omega \langle |c_m(k_2)|^2 \rangle_\omega}}, \quad (4.26)$$

which represents the overall correlation between two bands for a point within the $k_1 k_2$ plane within the first Brillouin Zone. By definition, it is a bounded quantity, and its squared magnitude adheres to the following condition:

$$0 \leq |\mu_{nm}(k_1, k_2)| \leq 1 \quad (4.27)$$

and it is equal to unity when the optical field is fully coherent, as observed in the deterministic case discussed earlier, and it vanishes when the field is incoherent. Between these extremes lies the domain of partial spatial coherence, which is the main point of this work. To compute quantities from the deterministic case in this stochastic context, we consider averaged values through ensemble averaging. Considering the contribution to the beam from each band, we introduce the Parseval's term in Stochastic Theory:

$$P_n = \int_{\text{B.Z.}} \langle |c_n(k)|^2 \rangle_\omega dk, \quad (4.28)$$

that aids in deciding in which band to truncate equation 4.23 within computational programs and to understand the role of spatial coherence in exciting the lattice bands.

4.4 Stochastic Case: Gaussian-Schell Source

In the domain of partially coherent beams, one notory correlation distribution model is the Gaussian-Schell model [84, 85, 86, 87, 88]. This model provides insight into the distinction between coherent and incoherent sources. One key characteristic of such a beam is that, between two points, say x_1 and x_2 , the spectral degree of coherence solely relies on their separation distance, denoted as $|x_2 - x_1|$. In the context of a stationary process, following the notation used in the section on deterministic Gaussian sources, we can describe field fluctuations through the cross-spectral density function at the input ($z = 0$) as:

$$W_0(x_1, x_2) = S_0 e^{-(x_1^2 + x_2^2)/2\sigma^2} e^{-(x_1 - x_2)^2/2\delta^2} e^{-iq(x_1 - x_2)}, \quad (4.29)$$

showing the optical beam correlation between points x_1 and x_2 in a Gaussian intensity distribution centered around $x = 0$, having a width of $\sqrt{2}\sigma$. Note that $S_0 = |\tilde{U}_0|^2 = \tilde{U}_0^* \tilde{U}_0$ represents the field intensity amplitude. The coherence parameter δ plays a crucial role here: as δ tends to infinity, the source approaches a fully spatially coherent beam, while a decrease of δ approaches a spatially incoherent beam. Our next steps aim to establish the foundational discussions regarding cross-spectral density, average beam intensity, and the influence of spatial correlation within the system. Initially, we will investigate the behavior

of cross-correlation coefficients and, subsequently, analyze Parseval's identity terms P_n and discuss our main results.

By using equation 4.24, the Floquet-Bloch cross-correlation coefficients can be determined from the correlations of the optical field at the incident plane $z = 0$. The resulting integral is a multidimensional Gaussian integral that can be easily solved [89, 90]. The calculation is intricate and it does not add any physical insight. It is given by

$$\begin{aligned}
C_{nm}(k_1, k_2) &= \frac{2\pi S_0 \delta \sigma^2}{\sqrt{\delta^2 + 2\sigma^2}} \sum_{r,s=-\infty}^{\infty} b_r^n(k_1) [b_s^m(k_2)]^* \\
&\times \exp \left[-\frac{\delta^2 \sigma^2 (k_1 + \frac{2\pi}{a} r - q)^2}{2(\delta^2 + 2\sigma^2)} \right] \\
&\times \exp \left[-\frac{\delta^2 \sigma^2 (k_2 + \frac{2\pi}{a} s - q)^2}{2(\delta^2 + 2\sigma^2)} \right] \\
&\times \exp \left[-\frac{\sigma^4 [k_1 - k_2 + \frac{2\pi}{a} (r - s)]^2}{2(\delta^2 + 2\sigma^2)} \right].
\end{aligned} \tag{4.30}$$

This is a general expression for the participation coefficient of a Gaussian-Schell source and can lead to the deterministic one found previously. To confirm this, one can verify its consistency by taking the limit as δ approaches infinity. In this limit, imposing the conditions $k_1 = k_2 = k$ and $n = m$, one can recover the expression for $\langle |c_n(k)|^2 \rangle$, where $c_n(k)$ is given by equation 4.20. Even without these constraints, while still considering the same limit, an expression for $C_{nm}(k_1, k_2)$ is derived as a product of two factors, one depending on (n, k_1) and the other on (m, k_2) , corresponding to a regime of complete spatial coherence, as expected.

First, let us understand the role of the coherence parameter δ and stabilize the terms that will be used to discuss our results. The Gaussian-Schell source expressed in equation 4.29 has an exponential term containing the distance between two points in the lattice $|x_1 - x_2|$ with the same z . In figure 16 (a), we present the initial absolute value of the cross-spectral density $|W_0(x_1, x_2)|$ for a Gaussian-Schell source with a transverse momentum $q = 0$ and a beam width of $\sigma = 7\pi$. For high coherence values ($\delta \gg \sigma$), the cross-spectral density spreads out in the $x_1 x_2$ plane with circular symmetry and we can expect a regime similar to the deterministic Gaussian source. As the coherence parameter decreases, for intermediary values ($\delta \sim \sigma$), the distribution becomes skewed. In a low coherence regime ($\delta \ll \sigma$), the third factor in the expression of W_0 localizes the distribution to the line $x_1 = x_2$, with the other regions of the plane being negligible.

When a Gaussian-Schell source propagates in a periodic lattice, one can ask for the role of the coherence in the Floquet-Bloch modes excitations. Consider the constraint $k_1 = k_2 = k$. It is worth mentioning that if one plots the cross-correlation participation in the $k_1 k_2$ plane, the coherence parameter δ exhibits a similar effect on its profile to the one observed in the Gaussian-Schell cross-spectral density W_0 : in high coherence,

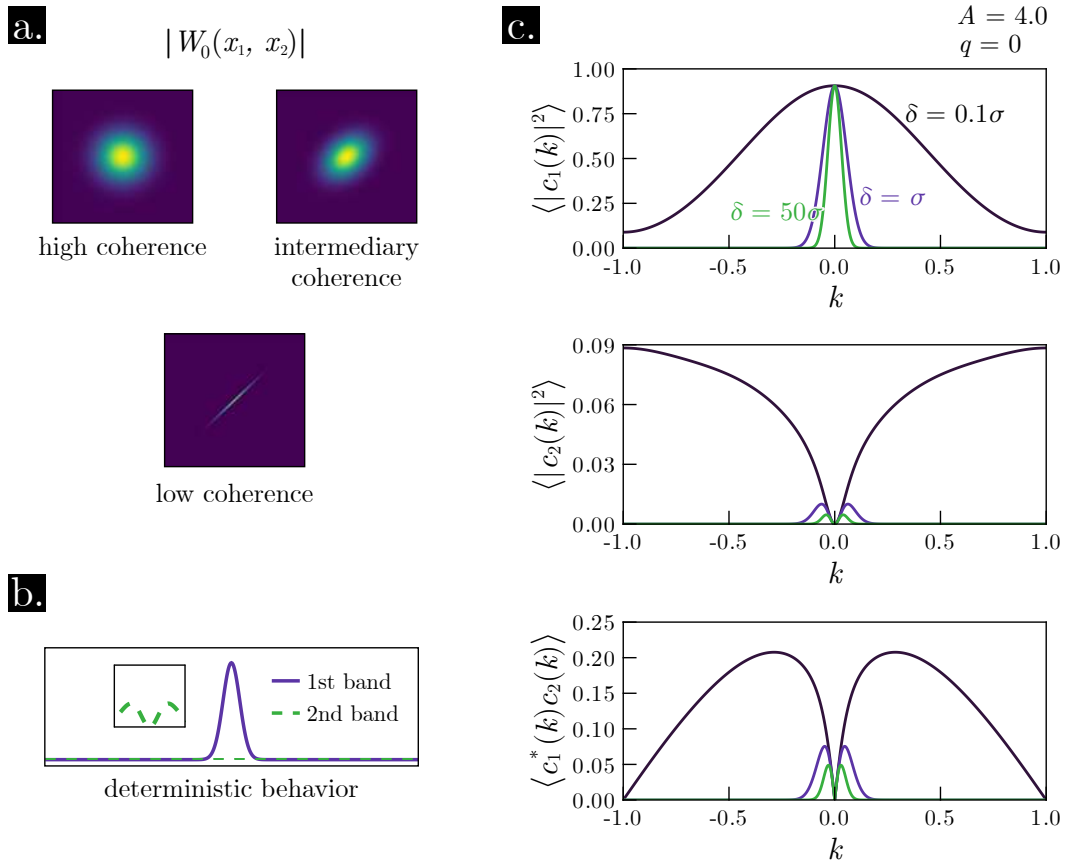


Figure 16 – (a) Absolute value of the cross-spectral density for a Gaussian-Schell source under various coherence parameter δ values. The Gaussian-Schell source has a transverse momentum of $q = 0$, a beam width of $\sigma = 7\pi$, and it is incident on a lattice with an amplitude of $A = 4$. Additionally, the following are displayed: (b) the equivalent deterministic behavior for participation coefficients; (c) the absolute values of cross-correlation coefficients $|C_{nm}(k)|$ for different coherence parameters: $\delta = 0.1\sigma$ (black line), $\delta = \sigma$ (purple line), and $\delta = 50\sigma$ (green line). The panels show results for $n = m = 1$ (top), $n = m = 2$ (middle), and $(n, m) = (1, 2)$ (bottom).

the profile is gaussian-like while in low coherence, the profile gets skewed. Figure 16 (b) displays the expected participation coefficients profile for the first two bands with a lattice amplitude $A = 4$ and a deterministic Gaussian beam source. This deterministic profile will serve as a reference for comparison with the results of cross-correlation coefficients presented in figure 16 (c). The coefficients are normalized by the constant previous to the summations in equation 4.30. As the coherence parameter δ increases, the results approach the deterministic case. The figure shows the averaged values of the participation coefficients $c_n(k)$ for $n = 1, 2$ (top and middle panel, respectively) and the cross-correlation coefficient $C_{12}(k, k)$ (bottom panel).

In a low coherence regime, a large number of Floquet-Bloch modes are excited, with non-zero values of the coefficients covering almost the entire Brillouin zone. This suggests that the stochastic nature of the beam induces the excitation of more modes

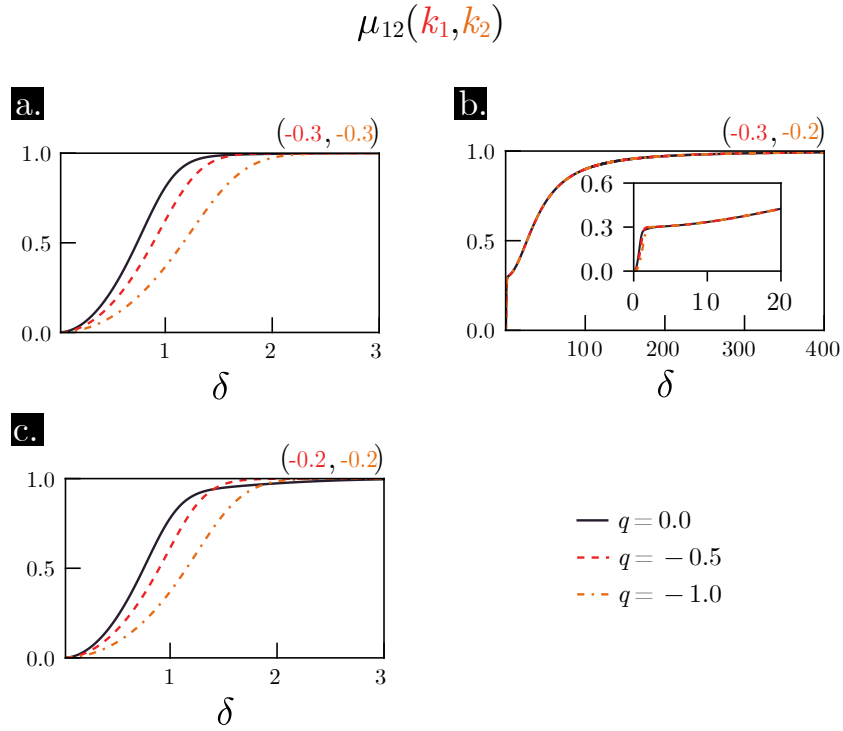


Figure 17 – Spectral degree of coherence $\mu_{12}(k_1, k_2)$ versus the coherence parameter δ for input beam width $\sigma = 7\pi$ and lattice amplitude $A = 4.0$ at various incident angles, correspondent to $q = -1.0$ (solid black line), $q = -0.5$ (dashed line), and $q = 0.0$ (dot-dashed line). Several spectral degrees of coherence between points of the Brillouin zone are displayed: (a) $k_1 = k_2 = -0.3$; (b) $k_1 = -0.2$ and $k_2 = -0.3$; and (c) $k_1 = k_2 = -0.2$.

in the lattice. As we increase the coherence parameter, such as for $\delta = \sigma$, there is a slight recovery in the profile found in the deterministic case: the excitation becomes more localized around $k = 0$. As we approach high coherence, the spatial coherence effect causes the excitation spectrum to decay, resembling the deterministic case. Moreover, as the correlation becomes more accentuated, $\langle c_1^*(k_1)c_2(k_2) \rangle = c_1^*c_2$. We observe the same pattern when changing the transverse momentum q and the lattice constant A . Thus, we conclude that the broadening of the Floquet-Bloch modes excitation can be controlled by the degree of coherence. This result differs drastically from the deterministic one: if one remembers the previous discussion, the only way to excite more modes in this case is by changing the profile of the incident beam or its incidence angle. The spatial coherence adds another degree of freedom to control the Floquet-Bloch modes.

As mentioned earlier, a quantity that can be used to visualize the correlations arising from the spatial coherence of the beam is the spectral degree of coherence, denoted as $\mu_{nm}(k_1, k_2)$ (see equation 4.26). This parameter measures the normalized degree of coherence between two modes from two different bands. By fixing the Floquet-Bloch wavenumbers and focusing only on the first and second bands (i.e., $n = 1$ and $n = 2$), we can examine $\mu_{12}(k_1, k_2)$ as a function of the coherence parameter δ , as shown in Figure 17

for some values in the Brillouin zone. Let us define a pair of points as "direct" if $k_1 = k_2 = k$ and "indirect" if $k_1 \neq k_2$. The figure presents the results for a Gaussian-Schell source with a width of $\sigma = 7\pi$ and lattice amplitude $A = 4$ at various incident angles. The general behavior, as expected, is that $\mu \rightarrow 1$ as $\delta \rightarrow \infty$, and $\mu \rightarrow 0$ as $\delta \rightarrow 0$. This sheds light on the relationship between the coherence parameter δ and the actual spectral degree of coherence.

Figures 17 (a) and (b) show the coherence degree for a direct point $(-0.3, -0.3)$ and $(-0.2, -0.2)$, respectively: for $q = -1$ (solid black line), in the Bragg condition, the contribution and distribution in the Brillouin Zone from both bands are very similar, thus it is expected that their coherence degree increases to unity as the cross-correlation coefficients resemble more and more their deterministic counterparts; the curves for $q = -0.5$ (dashed red line) and $q = 0.0$ (dot-dashed line), as the distribution and contribution are not very similar, we see that they approach unity in a larger value of δ in comparison to the $q = -1.0$. In the indirect point $(-0.3, -0.2)$, the rate at which the coherence degree approaches unity is even larger values for δ than the direct ones.

Now, let us discuss the effects of spatial coherence on beam propagation. Similar to the deterministic case, the beam direction is strongly influenced by the group's velocity direction $\nabla_k \beta_n(k)$ and has some influence from the cross-correlation coefficients as well. As before, our goal is to study the beam evolution also considering the beam center $X_c(z)$, defined in terms of the spectral density $S(x, z)$ in the stochastic case:

$$X_c(z) = \frac{\int x S(x, z); dx}{\int S(x, z); dx}. \quad (4.31)$$

First, let us consider a scenario with low coherence, where the coherence parameter δ is considerably smaller than the beam width σ . In the previous sections, we observed that $A = 4$ is a lattice parameter sufficiently strong to exhibit considerable effects from the lattice on the beam evolution. By taking this value for A , beam width to $\sigma = 7\pi$, incident angle with transverse momentum $q = -1.0$, and the coherence parameter to $\delta = \sigma/100$. Figure 18 illustrates this case.

As expected from coherence theory, the influence of a very low coherence parameter on the propagation causes the beam to spread more significantly through the lattice: the lack of spatial coherence makes the beam behavior similar to one propagating in a medium without periodic lattice. The stochastic nature of our source causes the beam propagation to ignore the lattice even in a relatively high lattice amplitude, resulting in a wider spreading compared to a beam propagating in the shallow lattice regime (see figure 15 (a)) for the same low value of the propagation distance z . Also, note that the beam center is tilted to the negative x-axis, as observed in the deterministic cases (see figure 15 (a) and (c)), and presents oscillations. One can ask how this occurs even in low coherence and even in the Bragg condition, where we can expect the tilt to be very small and what

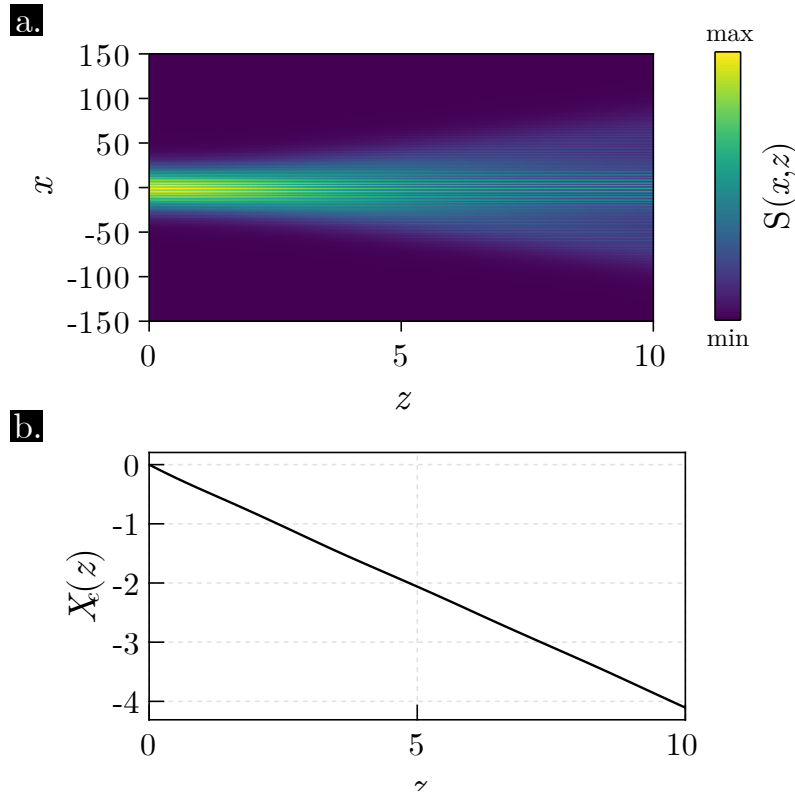


Figure 18 – (a) Beam spectral density $S(x, z)$. (b) Mean beam center oscillation $X_c(z)$ versus propagation distance z . For input wave number $q = -1.0$, width $\sigma = 7\pi$, lattice amplitude $A = 4.0$ and coherence parameter $\delta = \sigma/100$.

can be inferred from these oscillations.

For comparison purposes, it is interesting to consider an intermediate coherence case, where the coherence parameter δ is of the same order of magnitude as the beam width σ . As discussed in the section about cross-correlation participation coefficients $C_{nm}(k_1, k_2)$ and the role of spatial coherence, let us assume $\delta = \sigma$ with the other parameters the same as in the low-coherence case discussed above. This case is displayed in figure 19. We observe that the coherence is close enough to the deterministic case to reduce the tilt and restore oscillations to the beam center, along with a more well-defined intensity pattern. The spreading of the beam also becomes negligible, occurring because the cross-correlation participation coefficients become closer to the deterministic ones, exciting many fewer modes in the Brillouin zone compared to a low-coherence scenario.

The general form of the beam center is given by an expression of the form $X_c(z) = X_c(0) + Vz + P(z)$, where $p(z)$ is a periodic function of z that depends on the correlation between different bands, and v is the linear inclination which depends mainly on the mean participation coefficients values $\langle |c_n(k)|^2 \rangle$ for all the bands and the group velocity. As δ approaches smaller values, the oscillations from the beam vanish and only the rectilinear movement is left. Absolutely, how much the beam is spatially localized, tilt, and beam oscillations are all influenced by the coherence degree as the beam propagates over the

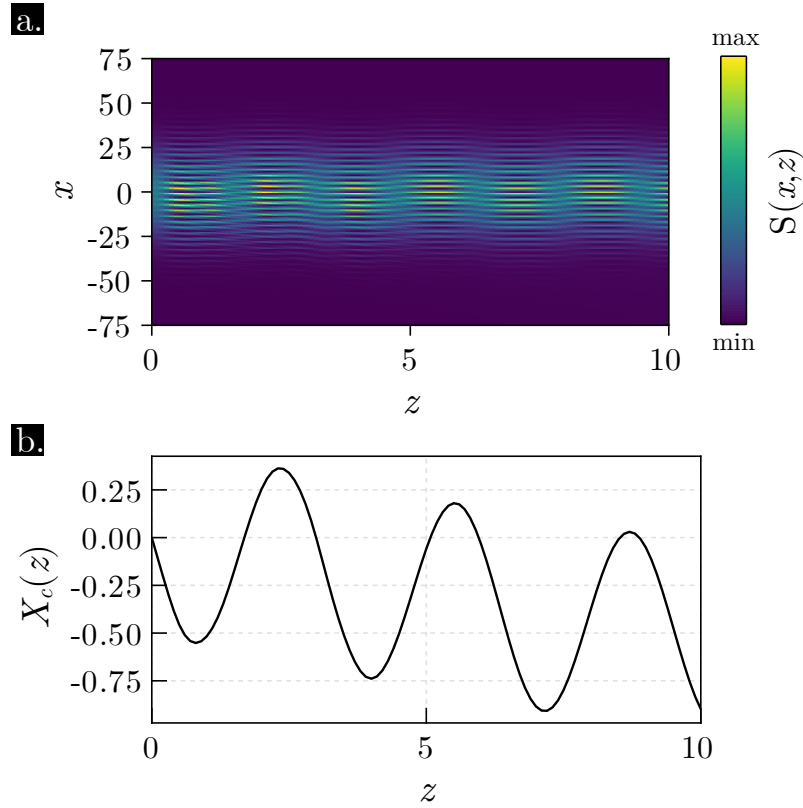


Figure 19 – (a) Beam spectral density $S(x, z)$. (b) Mean beam center oscillation $X_c(z)$ versus propagation distance z . For input wave number $q = -1.0$, width $\sigma = 7\pi$, lattice amplitude $A = 4.0$ and coherence parameter $\delta = \sigma$.

distance z . This interplay can have implications and applications in experimental setups, making it an interesting aspect to investigate and control for specific purposes.

4.5 Spatial Coherence and the Trembling Motion

In the previous sections, we observed that the motion of the beam center undergoes a trembling motion as it propagates in the periodic lattice. Let us investigate the physics behind this motion. The calculations are extensive and several steps will be omitted (see [4] for more details), we only will talk about the outline. First, consider the deterministic case. Overlooking the normalization constant present on equation 4.21,

$$x_c(z) = \int_{-\infty}^{\infty} x |U(x, z)|^2 dx, \quad (4.32)$$

and, if we insert in this equation the expression for the beam in equation 4.14, we obtain

$$x_c(z) = \sum_{n,m=1}^{\infty} dk dk' c_n^*(k) c_m(k') e^{-i\Delta\beta_{nm}(k,k')z} \int_{-\infty}^{\infty} x u_n^*(x, k) u_m(x, k') dx \quad (4.33)$$

where $\Delta\beta_{nm}(k, k') = \beta_n(k) - \beta_m(k')$. The term integral in the transversal direction x on the right side can be expanded as

$$\int_{-\infty}^{\infty} x u_n^*(x, k) u_m(x, k') dx = i \int_{-\infty}^{\infty} e^{-i(k-k')x} v_n^*(x, k) \frac{\partial}{\partial k'} v_m(x, k') dx \quad (4.34)$$

$$- i \frac{\partial}{\partial k'} \int_{-\infty}^{\infty} u_n^*(x, k) u_m(x, k') dx \quad (4.35)$$

$$= \delta(k - k') X_{nm}(k, k') - i \delta_{nm} \frac{d}{dk'} \delta(k - k'), \quad (4.36)$$

where X_{nm} is a integral in the unit cell of the lattice:

$$X_{nm}(k, k') = \frac{2\pi i}{a} \int_{-a/2}^{a/2} v_n^*(x, k) \frac{\partial}{\partial k'} v_m(x, k') dx \quad (4.37)$$

and, if we do the substitution in the original integral, one can obtain the following expression for the beam center:

$$x_c(z) = x_c(0) + vz + p(z) \quad (4.38)$$

where $x_c(0)$ is the initial position, v is the angular coefficient of its linear motion in the propagation direction z , and $p(z)$ is a periodic multifrequency function. This expression is condensed for clarity. The initial position is $x_c(0)$ given by

$$x_c(0) = i \sum_{n=1}^{\infty} \int_{\text{B.Z.}} c_n^*(k) \frac{d}{dk} c_n(k) dk + \sum_{n=1}^{\infty} \int_{\text{B.Z.}} X_{nn}(k) |c_n(k)|^2 dk, \quad (4.39)$$

where each term depends only on the participation of individual bands. The angular coefficient v is

$$v = - \sum_{n=1}^{\infty} \int_{\text{B.Z.}} |c_n(k)|^2 \frac{d}{dk} \beta_n(k) dk, \quad (4.40)$$

that is given by the sum of contributions of each band. The direction of the beam is partially controlled by this term. The group velocity plays an important role here. Due to its odd parity, the absolute participation coefficient squared $|c_n(k)|^2$ has to be asymmetric in the first Brillouin zone for each integral to be non-zero, which explains the tilt of the beam for some initial beams. Finally, the oscillations came from the third term term $p(z)$,

$$p(z) = \sum_{n=1}^{\infty} \sum_{m \neq n} \int_{\text{B.Z.}} X_{nm}(k) c_n^*(k) c_m(k) e^{-i\Delta\beta_{nm}(k)z} dk, \quad (4.41)$$

that clearly has in each term k -dependent periods $\omega_{nm} = 2\pi/\Delta\beta_{nm}(k)$. The medium contributes to the oscillations through the interference between bands: the counts only terms where $n \neq m$ and we have also a factor with a phase mismatch coming from the difference between propagation numbers of two bands $\beta_{nm}(k)$. This is the origin of the trembling motion of the system [91]. One can do the same for the stochastic case, obtaining an expression very similar to the equation 4.38:

$$X_c(z) = X_c(0) + Vz + P(z), \quad (4.42)$$

where the initial position $X_c(0)$ is

$$X_c(0) = i \sum_{n=1}^{\infty} \int_{\text{B.Z.}} \frac{d}{dk} C_{nn}(k, k) dk + \sum_{n=1}^{\infty} \int_{\text{B.Z.}} X_{nn}(k) |C_{nn}(k, k)|^2 dk, \quad (4.43)$$

the angular coefficient V is

$$V = - \sum_{n=1}^{\infty} \int_{\text{B.Z.}} C_{nn}(k, k) \frac{d}{dk} \beta_n(k) dk, \quad (4.44)$$

and the oscillation term $P(z)$ is

$$P(z) = \sum_{n=1}^{\infty} \sum_{m \neq n} \int_{\text{B.Z.}} X_{nm}(k) C_{nm}(k, k) e^{-i\Delta\beta_{nm}(k)z} dk. \quad (4.45)$$

The terms from the stochastic case are very similar to the deterministic ones due to the fact that they are ensemble averages of each realization that can be thought of as deterministic. If the coherence parameter grows indefinitely, one can observe that $v \rightarrow V$ and $p \rightarrow P$ whenever $c_n(k)$ and $c_m(k)$ become statistically independent random processes, meaning, $\langle c_m^*(k_1) c_n(k_2) \rangle = \langle c_m^*(k_1) \rangle \langle c_n(k_2) \rangle$. The main difference between the deterministic and random cases is that the oscillations $A(z)$ may disappear gradually down to zero, even when the coefficients $c_n(k)$ are non-zero, as long as the bands become weakly correlated, to the point of no correlation at all, when $C_{nm}(k, k) = 0$.

This trembling motion is well-known in several areas of physics and it is called the *zitterbewegung* effect. This effect originates from the results obtained for free electrons using the Dirac equation. These results predict the presence of fast, small oscillations in addition to the expected rectilinear classical motion, giving rise to a trembling motion. Since its initial prediction, researchers have explored analogs of this effect in various systems, including photonic lattices [14] and semiconductors [91, 92].

In figure 20 (a), we have the propagation numbers $\beta_n(k)$ that characterize the band structure and in (b) its respective group velocity. Note that as there is the parity symmetry $\beta_n(k) = \beta_n(-k)$ within the first Brillouin zone, the group velocity profile is formed by odd functions. Furthermore, its values grow as n increases; however, as discussed before, the contribution of each band decreases with n for the deterministic case. As the coherence parameter δ decreases, the contributions become more evenly distributed among the bands. The integrals in v and V are far from trivial when considering the dependence on the model parameters.

Furthermore, in figure 20 (c), one can observe how spatial coherence affects the trembling motion of the system: for $\delta = \sigma$, oscillations are seen alongside those expected for the deterministic case. In low coherence ($\delta = 0.1\sigma$), the beam center becomes more tilted due to the skewness of the participation profiles (see Figure 16) and the tilt's dependence on the autocorrelation participation coefficients and group velocity. Additionally, the oscillations experience some damping effect. If δ decreases even further ($\delta = 0.01\sigma$), the tilt is smaller, and the damping effect is stronger, attenuating the oscillations even further.

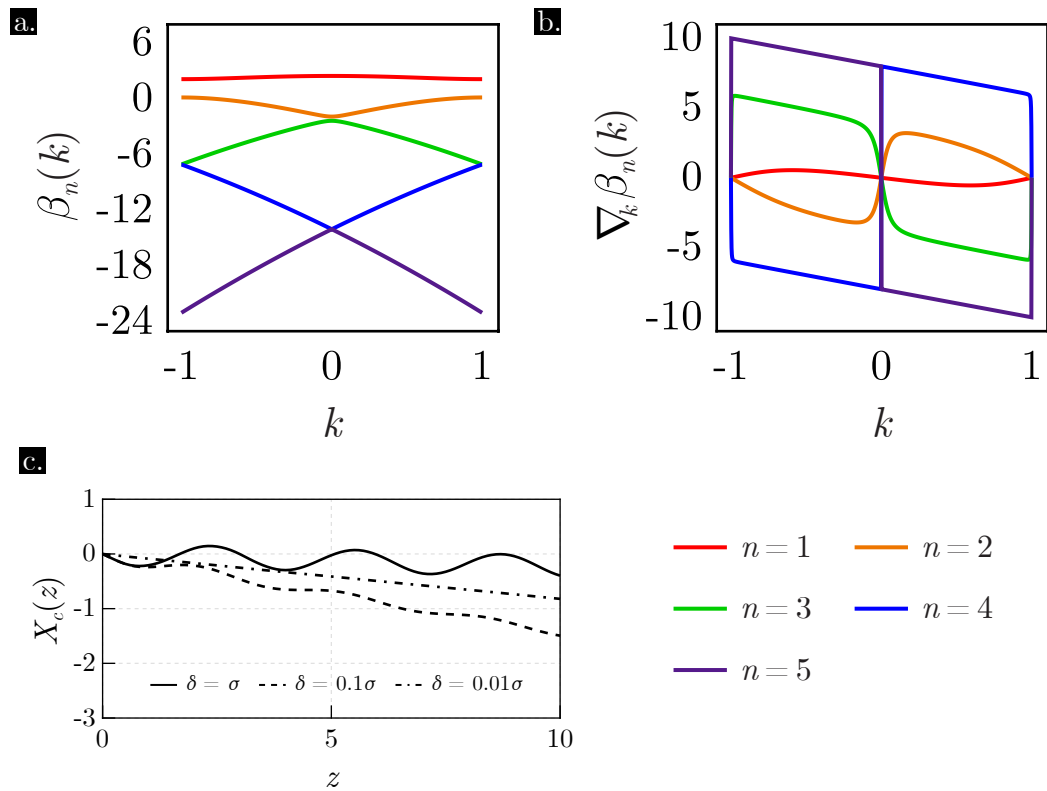


Figure 20 – (a) Propagation constant $\beta(k)$ versus Bloch wave vector k for the first five Floquet-Bloch modes $u_n(x, k)$; (b) group velocity $d\beta(k)/dk$ versus Bloch wave vector k ; (c) mean beam center oscillation $X_c(z)$ versus propagation distance z for three coherence parameters: σ , 0.1σ and 0.01σ . For input wave number $q = -1.0$, input beam width $\sigma = 7\pi$ and potential amplitude $A = 4.0$, extracted from [93].

5 Conclusion and Perspectives

In our research, we presented a model aiming to analyze the propagation of partially coherent beams in periodic media. The framework utilized was the one of Floquet-Bloch waves, that enables a detailed examination of the influence of the material on the light propagation. The model presented here considered a $2D$ system with a refractive index exhibiting $1D$ periodicity. The refractive index governs the matter-light interaction and plays a central role in the dynamics alongside the input beam. The potential considered was harmonic, but the theory allows for the consideration of other $1D$ periodic potentials.

The results were primarily obtained using the plane-wave expansion method and applying diagonalization routines in the Julia programming language. In contrast to free space, when considering a periodic medium, one encounters a band structure that significantly influences and alters light propagation. To illustrate these results, we applied the theory to a deterministic case: the Gaussian source. With this source, we computed the participation coefficients and we found a general solution for the beam profile in any point (x, z) of the space during propagation. The band structure was discussed with details: we showed that how the contribution of each band to the beam propagation was influenced by the lattice through changing the lattice amplitude A and studying the Parseval's terms p_n , and also how the transverse momentum changes the excitation of Floquet-Bloch modes in the first Brillouin zone. The propagation for the deterministic case was analyzed, outlining how the lattice contributes to its dynamics. We explored both the shallow-lattice regime and lattices with very strong influences to better understand the system and its dependence on its parameters.

With the particularities of the Floquet-Bloch framework in mind, we then utilized the second-order theory of coherence to describe light through the cross-spectral density $W(x_1, x_2, z)$, where the light was described as a linear combination of several Floquet-Bloch modes with participation coefficients that fluctuate in the space subject to some correlation between them. This correlation is conveyed by the initial cross-spectral density. We chose the Gaussian-Schell beam as the input and extracted the results.

We demonstrated that even weak correlations can drastically change the power distribution of Floquet-Bloch modes through the cross-correlation coefficients $C_{nm}(k_1, k_2)$. The influence of spatial coherence was shown to spread or narrow down the contribution of wavenumbers in the first Brillouin zone. The spatial coherence adds another degree of freedom to control the Floquet-Bloch modes, differing drastically from the deterministic case. Additionally, the stochastic description introduces interbands correlations into play, as we showed that the cross-spectral density significantly depends on cross terms.

In conclusion, we demonstrated that spatial coherence influences the intensity profile of the propagating beam. If the coherence is low enough, the beam passes through the material as if it is not there: the interactions between the light and the lattice can hardly be noticed. The beam center was one of the objects of study, and we also showed that it propagates as the sum of a linear plus oscillatory term, resembling the trembling motion found in electronic systems known as the *zitterbewegung* effect.

One may be interested in utilizing this framework to explore stochastic systems in a variety of scenarios or combinations thereof: the *zitterbewegung* effect can be further discussed; an extension to $(2+1)D$ enables the investigation of other interesting beams such as Hermite-Gaussian, Laguerre-Gaussian, and even Bessel beams. Theoretical developments were carried out by us in both z -dependent potentials and \mathcal{PT} -symmetric lattices. The latter even resulted in a publication not discussed in this thesis but is indeed related [94].

References

- [1] N.W. Ashcroft e N.D. Mermin. *Solid State Physics*. Cengage Learning, 2011. ISBN: 9788131500521.
- [2] Steven H. Simon. *The Oxford Solid State Basics*. OUP Oxford, 2013. ISBN: 9780199680764.
- [3] Charles Kittel. *Introduction to Solid State Physics*. Eighth Edition. Wiley, 2004. ISBN: 9780471415268.
- [4] Joseph Callaway. *Quantum Theory of the Solid State*. Second Edition. Boston, USA: Academic Press, 1991. ISBN: 978-0-12-155203-9.
- [5] Ming-Hui Lu, Liang Feng e Yan-Feng Chen. “Phononic crystals and acoustic metamaterials”. Em: *Materials Today* 12.12 (2009), pp. 34–42. ISSN: 1369-7021. DOI: [10.1016/S1369-7021\(09\)70315-3](https://doi.org/10.1016/S1369-7021(09)70315-3).
- [6] Mahmoud I. Hussein, Michael J. Leamy e Massimo Ruzzene. “Dynamics of Phononic Materials and Structures: Historical Origins, Recent Progress, and Future Outlook”. Em: *Applied Mechanics Reviews* 66.4 (mai. de 2014), p. 040802. ISSN: 0003-6900. DOI: [10.1115/1.4026911](https://doi.org/10.1115/1.4026911).
- [7] Bahaa E. A. Saleh e Malvin Carl Teich. *Fundamentals of Photonics*. Second Edition. Berlin, Heidelberg: Springer, 2006. ISBN: 9780471358329.
- [8] John D. Joannopoulos et al. *Photonic Crystals: Molding the Flow of Light*. Second Edition. New York, USA: Princeton University Press, 2008. ISBN: 9780691124568.
- [9] Maksim Skorobogatiy e Jianke Yang. *Fundamentals of Photonic Crystal Guiding*. First Edition. New York, USA: Cambridge University Press, 2008. ISBN: 978-0-521-51328-9.
- [10] Kazuaki Sakoda. *Optical Properties of Photonic Crystals*. Second Edition. John Wiley & Sons, Inc., 2004. ISBN: 9783540206828.
- [11] M. Neviere e E. Popov. *Light Propagation in Periodic Media: Differential Theory and Design*. First Edition. CRC Press, 1999. DOI: [10.1201/9781482275919](https://doi.org/10.1201/9781482275919).
- [12] A. Yariv e P. Yeh. *Optical Waves in Crystals: Propagation and Control of Laser Radiation*. Wiley classics library. Wiley-Interscience, 2003. ISBN: 9780471320814.
- [13] S. Longhi. “Quantum-optical analogies using photonic structures”. Em: *Laser & Photonics Reviews* 3.3 (2009), pp. 243–261. DOI: [10.1002/lpor.200810055](https://doi.org/10.1002/lpor.200810055).
- [14] S. Longhi. “Photonic analog of Zitterbewegung in binary waveguide arrays”. Em: *Opt. Lett.* 35.2 (jan. de 2010), pp. 235–237. DOI: [10.1364/OL.35.000235](https://doi.org/10.1364/OL.35.000235).

- [15] Emil Wolf e Leonard Mandel. *Optical Coherence and Quantum Optics*. First Edition. Cambridge University Press, 1995. ISBN: 9780521417112.
- [16] Joseph W Goodman. “Statistical optics”. Em: *New York, Wiley-Interscience, 1985, 567 p.* 1 (1985).
- [17] John M. Senior e M. Yousif Jamro. *Optical Fiber Communications Principles and Practice*. Third Edition. Essex, England: Pearson Education Limited, 2009. ISBN: 978-0-13-032681-2.
- [18] V. P. Bykov. “Spontaneous Emission in a Periodic Structure”. Em: *Soviet Journal of Experimental and Theoretical Physics* 35 (1972), pp. 269–273.
- [19] Eli Yablonovitch. “Inhibited Spontaneous Emission in Solid-State Physics and Electronics”. Em: *Phys. Rev. Lett.* 58 (20 mai. de 1987), pp. 2059–2062. DOI: [10.1103/PhysRevLett.58.2059](https://doi.org/10.1103/PhysRevLett.58.2059).
- [20] Sajeev John. “Strong localization of photons in certain disordered dielectric superlattices”. Em: *Phys. Rev. Lett.* 58 (23 mai. de 1987), pp. 2486–2489. DOI: [10.1103/PhysRevLett.58.2486](https://doi.org/10.1103/PhysRevLett.58.2486).
- [21] K. M. Leung e Y. F. Liu. “Full vector wave calculation of photonic band structures in face-centered-cubic dielectric media”. Em: *Phys. Rev. Lett.* 65 (21 nov. de 1990), pp. 2646–2649. DOI: [10.1103/PhysRevLett.65.2646](https://doi.org/10.1103/PhysRevLett.65.2646).
- [22] Ze Zhang e Sashi Satpathy. “Electromagnetic wave propagation in periodic structures: Bloch wave solution of Maxwell’s equations”. Em: *Phys. Rev. Lett.* 65 (21 nov. de 1990), pp. 2650–2653. DOI: [10.1103/PhysRevLett.65.2650](https://doi.org/10.1103/PhysRevLett.65.2650).
- [23] K. M. Ho, C. T. Chan e C. M. Soukoulis. “Existence of a photonic gap in periodic dielectric structures”. Em: *Phys. Rev. Lett.* 65 (25 dez. de 1990), pp. 3152–3155. DOI: [10.1103/PhysRevLett.65.3152](https://doi.org/10.1103/PhysRevLett.65.3152).
- [24] S. Y. Lin et al. “A three-dimensional photonic crystal operating at infrared wavelengths”. Em: *Nature* 394 (jul. de 1998), pp. 251–253. DOI: [10.1038/28343](https://doi.org/10.1038/28343).
- [25] E. Yablonovitch et al. “Donor and acceptor modes in photonic band structure”. Em: *Phys. Rev. Lett.* 67 (24 dez. de 1991), pp. 3380–3383. DOI: [10.1103/PhysRevLett.67.3380](https://doi.org/10.1103/PhysRevLett.67.3380).
- [26] Henri Benisty et al. “Recent advances toward optical devices in semiconductor-based photonic crystals”. Em: *Proceedings of the IEEE* 94.5 (2006), pp. 997–1023. DOI: [10.1109/JPROC.2006.873441](https://doi.org/10.1109/JPROC.2006.873441).
- [27] El-Hang Lee et al. “Fabrication and integration of VLSI micro/nano-photonic circuit board”. Em: *Microelectronic Engineering* 83.4 (2006). Micro- and Nano-Engineering MNE 2005, pp. 1767–1772. ISSN: 0167-9317. DOI: [10.1016/j.mee.2005.12.010](https://doi.org/10.1016/j.mee.2005.12.010).

- [28] M. François et al. “Photonic band gap material for integrated photonic application: technological challenges”. Em: *Microelectronic Engineering* 61-62 (2002). Micro- and Nano-Engineering 2001, pp. 537–544. ISSN: 0167-9317. DOI: [10.1016/S0167-9317\(02\)00526-9](https://doi.org/10.1016/S0167-9317(02)00526-9).
- [29] E. Viasnoff-Schwoob et al. “Compact wavelength monitoring by lateral outcoupling in wedged photonic crystal multimode waveguides”. Em: *Applied Physics Letters* 86.10 (mar. de 2005), p. 101107. ISSN: 0003-6951. DOI: [10.1063/1.1879105](https://doi.org/10.1063/1.1879105).
- [30] Y. Xia et al. “Monodispersed Colloidal Spheres: Old Materials with New Applications”. Em: *Advanced Materials* 12.10 (2000), pp. 693–713. DOI: [10.1002/SICI1521-4095](https://doi.org/10.1002/SICI1521-4095).
- [31] C. López. “Materials Aspects of Photonic Crystals”. Em: *Advanced Materials* 15.20 (2003), pp. 1679–1704. DOI: [10.1002/adma.200300386](https://doi.org/10.1002/adma.200300386).
- [32] Dennis W. Prather et al. “Photonic Crystal Structures and Applications: Perspective, Overview, and Development”. Em: *IEEE Journal of Selected Topics in Quantum Electronics* 12.6 (2006), pp. 1416–1437. DOI: [10.1109/JSTQE.2006.884063](https://doi.org/10.1109/JSTQE.2006.884063).
- [33] Michael Escuti e Gregory Crawford. “Holographic photonic crystals”. Em: *Optical Engineering - OPT ENG* 43 (set. de 2004), pp. 1973–1987. DOI: [10.1117/1.1773773](https://doi.org/10.1117/1.1773773).
- [34] Inc Luxtera. *Luxtera: Fiber to the chip*. 2024. URL: <https://www.luxcapital.com/companies/luxtera>.
- [35] NKT Photonics A/S. *NKT Photonics*. 2024. URL: <https://www.nktphotonics.com/products/optical-fibers-and-modules/>.
- [36] Jaime Gómez Rivas, Toni López e Mohamed S. Abdelkhalik. *Lumileds*. 2024. URL: https://spie.org/photonics-west/presentation/Integrated-metasurfaces-for-solid-state-lighting/12890-3#_=_.
- [37] David Torres et al. “OmniGuide photonic bandgap fibers for flexible delivery of CO₂ laser energy for laryngeal and airway surgery”. Em: *Photonic Therapeutics and Diagnostics*. Vol. 5686. International Society for Optics e Photonics. SPIE, 2005, pp. 310–321. DOI: [10.1117/12.590355](https://doi.org/10.1117/12.590355).
- [38] Inc OmniGuide Holdings. *OmniGuide Surgical: Advanced CO₂ Laser Systems and Fibers*. 2024. URL: <https://www.omni-guide.com/technology/co2/>.
- [39] Jian Zi et al. “Coloration strategies in peacock feathers”. Em: *Proceedings of the National Academy of Sciences* 100.22 (2003), pp. 12576–12578. DOI: [10.1073/pnas.2133313100](https://doi.org/10.1073/pnas.2133313100).
- [40] Jérémie Teyssier et al. “Photonic crystals cause active colour change in chameleons”. Em: *Nature Communications* 6 (1 2015), pp. 2041–1723. DOI: [10.1038/ncomms7368](https://doi.org/10.1038/ncomms7368).

- [41] L.P. Biró et al. “Living photonic crystals: Butterfly scales — Nanostructure and optical properties”. Em: *Materials Science and Engineering: C* 27.5 (2007). EMRS 2006 Symposium A: Current Trends in Nanoscience - from Materials to Applications, pp. 941–946. ISSN: 0928-4931. DOI: [10.1016/j.msec.2006.09.043](https://doi.org/10.1016/j.msec.2006.09.043).
- [42] Remo Proietti Zaccaria. “Butterfly wing color: A photonic crystal demonstration”. Em: *Optics and Lasers in Engineering* 76 (2016). Special Issue: Optical Methods in Nanobiotechnology, pp. 70–73. ISSN: 0143-8166. DOI: [10.1016/j.optlaseng.2015.04.008](https://doi.org/10.1016/j.optlaseng.2015.04.008).
- [43] V. L. Welch e J.-P. Vigneron. “Beyond butterflies—the diversity of biological photonic crystals”. Em: *Optical and Quantum Electronics* 39 (mar. de 2007), pp. 1572–817X. DOI: [10.1007/s11082-007-9094-4](https://doi.org/10.1007/s11082-007-9094-4).
- [44] W. Kohn. “Analytic Properties of Bloch Waves and Wannier Functions”. Em: *Phys. Rev.* 115 (4 ago. de 1959), pp. 809–821. DOI: [10.1103/PhysRev.115.809](https://doi.org/10.1103/PhysRev.115.809).
- [45] P. St. J. Russell. “Optics of Floquet-Bloch waves in dielectric gratings”. Em: *Applied Physics B* 39.4 (abr. de 1986), pp. 231–246. ISSN: 1432-0649. DOI: [10.1007/BF00697490](https://doi.org/10.1007/BF00697490).
- [46] A. A. Cottley. “Floquet’s Theorem and Band Theory in One Dimension”. Em: *American Journal of Physics* 39.10 (out. de 1971), pp. 1235–1244. ISSN: 0002-9505. DOI: [10.1119/1.1976612](https://doi.org/10.1119/1.1976612).
- [47] Su-Miau Wu e Chun-Ching Shih. “Construction of solvable Hill equations”. Em: *Phys. Rev. A* 32 (6 dez. de 1985), pp. 3736–3738. DOI: [10.1103/PhysRevA.32.3736](https://doi.org/10.1103/PhysRevA.32.3736).
- [48] Farouk Odeh e Joseph B. Keller. “Partial Differential Equations with Periodic Coefficients and Bloch Waves in Crystals”. Em: *Journal of Mathematical Physics* 5.11 (mai. de 2005), pp. 1499–1504. ISSN: 0022-2488. DOI: [10.1063/1.1931182](https://doi.org/10.1063/1.1931182).
- [49] Valery S. Shchesnovich, Anton S. Desyatnikov e Yuri S. Kivshar. “Interband resonant transitions in two-dimensional hexagonal lattices: Rabi oscillations, Zener tunnelling, and tunnelling of phase dislocations”. Em: *Opt. Express* 16.18 (set. de 2008), pp. 14076–14094. DOI: [10.1364/OE.16.014076](https://doi.org/10.1364/OE.16.014076).
- [50] Valery S. Shchesnovich e Sabino Chavez-Cerda. “Bragg-resonance-induced Rabi oscillations in photonic lattices”. Em: *Opt. Lett.* 32.13 (jul. de 2007), pp. 1920–1922. DOI: [10.1364/OL.32.001920](https://doi.org/10.1364/OL.32.001920).
- [51] Ksenia Shandarova et al. “Experimental Observation of Rabi Oscillations in Photonic Lattices”. Em: *Phys. Rev. Lett.* 102 (12 mar. de 2009), p. 123905. DOI: [10.1103/PhysRevLett.102.123905](https://doi.org/10.1103/PhysRevLett.102.123905).
- [52] K. G. Makris et al. “Optical transitions and Rabi oscillations in waveguide arrays”. Em: *Opt. Express* 16.14 (jul. de 2008), pp. 10309–10314. DOI: [10.1364/OE.16.010309](https://doi.org/10.1364/OE.16.010309).

- [53] Valery S. Shchesnovich et al. “Zener tunneling in two-dimensional photonic lattices”. Em: *Phys. Rev. E* 74 (5 nov. de 2006), p. 056602. DOI: [10.1103/PhysRevE.74.056602](https://doi.org/10.1103/PhysRevE.74.056602).
- [54] Henrike Trompeter et al. “Bloch Oscillations and Zener Tunneling in Two-Dimensional Photonic Lattices”. Em: *Phys. Rev. Lett.* 96 (5 fev. de 2006), p. 053903. DOI: [10.1103/PhysRevLett.96.053903](https://doi.org/10.1103/PhysRevLett.96.053903).
- [55] Anton S. Desyatnikov et al. “Resonant Zener tunneling in two-dimensional periodic photonic lattices”. Em: *Opt. Lett.* 32.4 (fev. de 2007), pp. 325–327. DOI: [10.1364/OL.32.000325](https://doi.org/10.1364/OL.32.000325).
- [56] Andrey A. Sukhorukov et al. “Nonlinear Bloch-Wave Interaction and Bragg Scattering in Optically Induced Lattices”. Em: *Phys. Rev. Lett.* 92 (9 mar. de 2004), p. 093901. DOI: [10.1103/PhysRevLett.92.093901](https://doi.org/10.1103/PhysRevLett.92.093901).
- [57] H. S. Eisenberg et al. “Diffraction Management”. Em: *Phys. Rev. Lett.* 85 (9 ago. de 2000), pp. 1863–1866. DOI: [10.1103/PhysRevLett.85.1863](https://doi.org/10.1103/PhysRevLett.85.1863).
- [58] John David Jackson. *Classical Electrodynamics*. Third Edition. Wiley, 1998. ISBN: 9780471309321.
- [59] Eugene Hecht. *Optics*. Fifth Edition. Pearson, 2017. ISBN: 978-1-292-09693-3.
- [60] Robert W. Boyd. *Nonlinear Optics*. Third Edition. Academic Press, 2008. ISBN: 978-0-12-369470-6.
- [61] Arthur R. McGurn e Alexei A. Maradudin. “Photonic band structures of two- and three-dimensional periodic metal or semiconductor arrays”. Em: *Phys. Rev. B* 48 (23 dez. de 1993), pp. 17576–17579.
- [62] E. R. Brown e O. B. McMahon. “Large electromagnetic stop bands in metallodielectric photonic crystals”. Em: *Applied Physics Letters* 67.15 (out. de 1995), pp. 2138–2140. ISSN: 0003-6951.
- [63] Ramamurti Shankar. *Principles of Quantum Mechanics*. Second Edition. New York, USA: Springer, 2011. ISBN: 978-0306447907.
- [64] Albert Messiah. *Quantum Mechanics*. New York, USA: Dover Publications, 2014. ISBN: 978-0486784557.
- [65] J. J. Sakurai e Jim Napolitano. *Modern Quantum Mechanics*. Third Edition. New York, USA: Cambridge University Press, 2020. ISBN: 978-1108473224.
- [66] Mary L. Boas. *Mathematical Methods in the Physical Sciences*. Third Edition. New York, USA: Wiley, 2005. ISBN: 978-0471198260.
- [67] C. Kittel. *Berkeley Physics Course: Waves, by F. S. Crawford, Jr.* Berkeley Physics Course. McGraw-Hill, 1965.

- [68] Moisés Fernandes de Souza et al. “Um breve tratado sobre a aproximação paraxial”. Em: *Revista Brasileira de Ensino de Física* 36.3 (jul. de 2014), pp. 1–13. ISSN: 1806-1117. DOI: [10.1590/S1806-11172014000300008](https://doi.org/10.1590/S1806-11172014000300008).
- [69] J.W. Goodman. *Introduction to Fourier Optics*. McGraw-Hill physical and quantum electronics series. W. H. Freeman, 2005. ISBN: 9780974707723.
- [70] Emil Wolf. *Introduction to the Theory of Coherence and Polarization of Light*. First Edition. Cambridge University Press, 2007. ISBN: 9780521822114.
- [71] Beran Mark J. e George B. Parrent Jr. *Theory of Partial Coherence*. Second Edition. Prentice-Hall, 1974. ISBN: 9780608308616.
- [72] Andrey S. Ostrovsky, Miguel Á. Olvera-Santamaría e Paulo C. Romero-Soría. “Effect of coherence and polarization on resolution of optical imaging system”. Em: *Opt. Lett.* 36.9 (mai. de 2011), pp. 1677–1679. DOI: [10.1364/OL.36.001677](https://doi.org/10.1364/OL.36.001677).
- [73] Erwan Baleine e Aristide Dogariu. “Variable coherence tomography”. Em: *Opt. Lett.* 29.11 (mai. de 2004), pp. 1233–1235. DOI: [10.1364/OL.29.001233](https://doi.org/10.1364/OL.29.001233).
- [74] P H Tomlins e R K Wang. “Theory, developments and applications of optical coherence tomography”. Em: *Journal of Physics D: Applied Physics* 38.15 (jul. de 2005), p. 2519. DOI: [10.1088/0022-3727/38/15/002](https://doi.org/10.1088/0022-3727/38/15/002).
- [75] Andreas Norrman, Sergey A. Ponomarenko e Ari T. Friberg. “Partially coherent surface plasmon polaritons”. Em: *Europhysics Letters* 116.6 (fev. de 2017), p. 64001. DOI: [10.1209/0295-5075/116/64001](https://doi.org/10.1209/0295-5075/116/64001).
- [76] Alfonso Nardi et al. “Encoding information in the mutual coherence of spatially 9arated light beams”. Em: *Opt. Lett.* 47.18 (set. de 2022), pp. 4588–4591. DOI: [10.1364/OL.463813](https://doi.org/10.1364/OL.463813).
- [77] Olga Korotkova e Greg Gbur. “Chapter Four - Applications of optical coherence theory”. Em: *A Tribute to Emil Wolf*. Ed. por Taco D. Visser. Vol. 65. Progress in Optics. Elsevier, 2020, pp. 43–104. DOI: [10.1016/bs.po.2019.11.004](https://doi.org/10.1016/bs.po.2019.11.004).
- [78] Max Born e Emil Wolf. *Principles of Optics: Electromagnetic Theory of Propagation, Interference and Diffraction of Light*. Seventh Edition. Cambridge University Press, 1999. ISBN: 0521642221.
- [79] W. Werner Lauterborn e T. Thomas Kurz. *Coherent optics: fundamentals and applications*. Second Edition. Advanced texts in physics. Berlin: Springer, 2003. ISBN: 3540439331.
- [80] William H. Press et al. *Numerical Recipes 3rd Edition: The Art of Scientific Computing*. Third Edition. Cambridge University Press, 2007. ISBN: 0521880688.
- [81] Lloyd N. Trefethen. *Spectral Methods in MATLAB*. Society for Industrial e Applied Mathematics, 2000. DOI: [10.1137/1.9780898719598](https://doi.org/10.1137/1.9780898719598).

- [82] Thiab R Taha e Mark I Ablowitz. “Analytical and numerical aspects of certain nonlinear evolution equations. II. Numerical, nonlinear Schrödinger equation”. Em: *Journal of Computational Physics* 55.2 (1984), pp. 203–230. ISSN: 0021-9991. DOI: [10.1016/0021-9991\(84\)90003-2](https://doi.org/10.1016/0021-9991(84)90003-2). URL: <https://www.sciencedirect.com/science/article/pii/0021999184900032>.
- [83] P.A. Brandão e S.B. Cavalcanti. “Bragg-induced oscillations in non-PT complex photonic lattices”. Em: *Physics Letters A* 383.22 (2019), pp. 2672–2677. ISSN: 0375-9601. DOI: [10.1016/j.physleta.2019.06.001](https://doi.org/10.1016/j.physleta.2019.06.001).
- [84] A. T. Friberg e R. J. Sudol. “Propagation parameters of gaussian Schell-model beams”. Em: *Optics Communications* 41.6 (1982), pp. 383–387. DOI: [10.1016/0030-4018\(82\)90161-4](https://doi.org/10.1016/0030-4018(82)90161-4).
- [85] “Propagation and imaging experiments with Gaussian Schell-model beams”. Em: *Optics Communications* 67.4 (1988), pp. 245–250. ISSN: 0030-4018. DOI: [10.1016/0030-4018\(88\)90143-5](https://doi.org/10.1016/0030-4018(88)90143-5).
- [86] Yangjian Cai et al. “Chapter Three - Generation of Partially Coherent Beams”. Em: ed. por Taco D. Visser. Vol. 62. Progress in Optics. Elsevier, 2017, pp. 157–223. DOI: [10.1016/bs.po.2016.11.001](https://doi.org/10.1016/bs.po.2016.11.001).
- [87] F. Gori. “Mode propagation of the field generated by Collett-Wolf Schell-model sources”. Em: *Optics Communications* 46.3 (1983), pp. 149–154. ISSN: 0030-4018. DOI: [10.1016/0030-4018\(83\)90266-3](https://doi.org/10.1016/0030-4018(83)90266-3).
- [88] J. Deschamps, D. Courjon e J. Bulabois. “Gaussian Schell-model sources: an example and some perspectives”. Em: *J. Opt. Soc. Am.* 73.3 (mar. de 1983), pp. 256–261. DOI: [10.1364/JOSA.73.000256](https://doi.org/10.1364/JOSA.73.000256).
- [89] Anthony Zee. *Quantum Field Theory in a Nutshell*. Second Edition. Princeton University Press, 2010. ISBN: 978-0691140346.
- [90] Jean Zinn-Justin. *Quantum Field Theory and Critical Phenomena*. Fourth Edition. Clarendon Press, 2002. ISBN: 978-0198509233.
- [91] Wlodek Zawadzki e Tomasz M. Rusin. “Nature of electron Zitterbewegung in crystalline solids”. Em: *Physics Letters A* 374.34 (2010), pp. 3533–3537. ISSN: 0375-9601. DOI: [10.1016/j.physleta.2010.06.028](https://doi.org/10.1016/j.physleta.2010.06.028).
- [92] W. Zawadzki e T. M. Rusin. “Nature of electron Zitterbewegung in crystalline solids”. Em: *Physics Letter A* 374 (jul. de 2010), pp. 3533–3537.
- [93] M. J. Cirino, P. A. Brandão e S. B. Cavalcanti. “Spatial coherence effects of stochastic optical beams in periodic potentials”. Em: *Phys. Rev. A* 107.3 (mar. de 2023), p. 033518.

-
- [94] P. A. Brandão, M. J. Cirino e S. B. Cavalcanti. “Bragg scattering of stochastic beams in \mathcal{PT} -symmetric photonic lattices”. Em: *Opt. Lett.* 49.3 (fev. de 2024), pp. 618–621. DOI: [10.1364/OL.512326](https://doi.org/10.1364/OL.512326). URL: <https://opg.optica.org/ol/abstract.cfm?URI=ol-49-3-618>.
- [95] Konstantinos G. Makris et al. “ \mathcal{PT} -symmetric optical lattices”. Em: *Phys. Rev. A* 81 (6 mai. de 2010), p. 063807. DOI: [10.1103/PhysRevA.81.063807](https://doi.org/10.1103/PhysRevA.81.063807).
- [96] G. Bachmann, L. Narici e E. Beckenstein. *Fourier and Wavelet Analysis*. 1^a ed. New York, USA: Springer New York, 2002. ISBN: 9780387988993.
- [97] James S. Walker. *Fast Fourier Transforms*. 2^a ed. Flórida, USA: CRC Press, 1996. ISBN: 9780849371639.

APPENDIX A – Analytical Signals

All the basic quantities in classical optics, like the electric field \mathbf{E} , magnetic field \mathbf{B} , charge ρ and current densities \mathbf{J} are real functions of position \mathbf{r} and time t . In statistical optics, one is concerned with correlations and it is very useful to represent quantities by complex functions, taking the real part to work with [15]. It is common to represent the electromagnetic field by a scalar field, especially in wave optics. This is usually called the scalar wave $u(\mathbf{r}, t) \in \mathbb{R}$, satisfying the wave equation:

$$\nabla^2 u(\mathbf{r}, t) = \frac{1}{c^2} \frac{\partial}{\partial t} u(\mathbf{r}, t), \quad (\text{A.1})$$

and the properties of such an equation give the possibility of working with a complex field $U(\mathbf{r}, t) \in \mathbb{C}$ satisfying

$$u(\mathbf{r}, t) = \text{Re} [U(\mathbf{r}, t)], \quad (\text{A.2})$$

and the complex scalar field $U(\mathbf{r}, t)$ is called the **analytical signal**.

A.1 Monochromatic Waves

A light signal can be viewed as a monochromatic one, with one single frequency component, or a polychromatic one, with a range of frequencies to be considered in the frequency space. In a fixed spatial position, a monochromatic field with frequency ν_0 can be represented as the real scalar field

$$u(t) = A \cos(2\pi\nu_0 t + \phi), \quad (\text{A.3})$$

where A is the field amplitude and ϕ the phase. One can write its analytical signal as:

$$U(t) = A e^{-i\phi} e^{-2\pi i \nu_0 t} \quad (\text{A.4})$$

where the factor $e^{-i\phi}$ it is usually called phasor [7, 59]. A similar way to represent the real signal is to rewrite the cosine as a sum of complex exponentials:

$$u(t) = \frac{A}{2} e^{-i\phi} e^{-2\pi i \nu_0 t} + \frac{A}{2} e^{i\phi} e^{2\pi i \nu_0 t}, \quad (\text{A.5})$$

hence, one can obtain the analytical signal from $u(t)$ considering only the negative frequencies (terms with a positive exponential argument) and doubling the amplitude of the remaining term.

A.2 Polychromatic Waves

A real signal $u(t)$ representing a polychromatic wave can be described in the frequency space as a continuous function $\tilde{u}(\nu)$, and the Fourier integral that represents this signal is

$$u(t) = \int_{-\infty}^{\infty} \tilde{u}(\nu) e^{-2\pi i \nu t} d\nu, \quad (\text{A.6})$$

where

$$\tilde{u}(\nu) = \int_{-\infty}^{\infty} u(t) e^{2\pi i \nu t} dt, \quad (\text{A.7})$$

and, as $u(t)$ is a real function, the complex spectral amplitudes given by $\tilde{u}(\nu)$ satisfy $\tilde{u}(-\nu) = \tilde{u}^*(\nu)$ and, thus, the negative frequency components carry no information. Thus, the analytical signal in this case is better represented as the following:

$$U(t) = 2 \int_0^{\infty} \tilde{u}(\nu) e^{-2\pi i \nu t} d\nu. \quad (\text{A.8})$$

One may ask why this is important. In the study of correlations, which are the main quantities of the study of the stochastic nature of light, cross-correlations Γ_{ij} are in the core results of the theory. The Wiener-Khintchine theorem [15, 16, 71] states that the cross-correlation can be thought of as an analytical signal of another quantity, enabling a variety of results to the second-order scalar theory of coherence framework.

APPENDIX B – Orthogonality condition of Floquet-Bloch modes in finite and discrete lattices

The objective of this appendix is to establish the orthogonality conditions for the Floquet-Bloch functions. Here, this result will be achieved through the plane wave expansion of each function, which is the most useful for this purpose [4]. As demonstrated in Chapter 4, the plane wave expansion for the n^{th} Floquet-Bloch function is given by:

$$u_n(x, k) = \frac{1}{\sqrt{2\pi}} \sum_m b_n^m(k) e^{i(k+K_m)x}; \quad (\text{B.1})$$

here, K_m represents a reciprocal lattice vector, and the $1/\sqrt{2\pi}$ factor is included to simplify the orthogonality condition.

The coefficients $b_n^m(k) = b_n(k + K_m)$, forming elements of a unitary matrix denoted as B . They serve as eigenvectors of $\hat{\Lambda}(k)$, hence $B_{mn} = b_n^m(k)$. Consequently, the following property holds:

$$B^* B = B B^* = I, \quad (\text{B.2})$$

consequently, this property yields relationships among our Fourier coefficients:

$$\sum_m [b_p^m(k)]^* b_q^m(k) = \delta_{pq} \quad (\text{B.3})$$

and

$$\sum_n [b_n^p(k)]^* b_n^q(k) = \delta_{pq}. \quad (\text{B.4})$$

Hence, we know are able to compute the orthogonality condition for an infinite lattice, considering $x \in [-\infty, \infty]$:

$$\begin{aligned} \int_{-\infty}^{\infty} u_n^*(x, k) u_m(x, q) dx &= \frac{1}{2\pi} \int_{-\infty}^{\infty} \sum_r [b_n^r(k)]^* e^{-i(k+K_r)x} \sum_s b_m^s(q) e^{i(q+K_s)x} dx \\ &= \frac{1}{2\pi} \sum_{r,s} [b_n^r(k)]^* b_m^s(q) \int_{-\infty}^{\infty} e^{-i(k+K_r)x} e^{i(q+K_s)x} dx \\ &= \frac{1}{2\pi} \sum_{r,s} [b_n^r(k)]^* b_m^s(q) \int_{-\infty}^{\infty} e^{i(q+K_s-k-K_r)x} dx \\ &= \sum_{r,s} [b_n^r(k)]^* b_m^s(q) \delta(q + K_s - k - K_r) \end{aligned} \quad (\text{B.5})$$

where we used the distribution theory result, that relates the following distributions

$$\frac{1}{2\pi} \int_{-\infty}^{\infty} e^{ikx} dx = \delta(k). \quad (\text{B.6})$$

Let us discuss the relevant terms within the summation. We assume that the wavenumbers k and q belongs to the first Brillouin zone, denoted as $k, q \in [-\pi/a, \pi/a)$, thereby $k - q$ cannot exceed $2\pi/a = |K_{\pm 1}|$. Consequently, the delta function generally equals zero except when $K_s - K_r = 0$. Hence,

$$\begin{aligned} \int_{-\infty}^{\infty} u_n^*(x, k) u_m(x, q) dx &= \sum_r [b_n^r(k)]^* b_m^r(q) \delta(q - k) \\ &= \delta_{nm} \delta(q - k), \end{aligned} \quad (\text{B.7})$$

where we utilized equation B.1. While this holds true for an infinite lattice, in our computational treatment of a finite lattice, the normalization will differ.

Let us discuss the discrete case. If we try to do the integral in a unit cell, $x \in [-a/2, a/2)$ for our 1D lattice, we obtain

$$\int_{\text{cell}} u_n^*(x, k) u_m(x, q) dx = \frac{1}{2\pi} \sum_{r,s} [b_n^r(k)]^* b_m^s(q) \int_{\text{cell}} e^{i(K_r - K_s + q - k)x} dx, \quad (\text{B.8})$$

establishing that u_n and u_m won't be orthogonal for distinct wave numbers. Therefore, we assume $k = q$, allowing the integral to be easily solved. Considering $\Omega = a$ as the length of our unit cell, we obtain:

$$\begin{aligned} \int_{\text{cell}} u_n^*(x, k) u_m(x, k) dx &= \frac{1}{2\pi} \sum_{r,s} [b_n^r(k)]^* b_m^s(k) \int_{\text{cell}} dx e^{i(K_r - K_s)x} \\ &= \frac{\Omega}{2\pi}, \end{aligned} \quad (\text{B.9})$$

where the Kronecker's delta arises from evaluating the integral:

$$\int_{\text{cell}} e^{i(K_r - K_s)x} dx = \begin{cases} 0, & r \neq s \\ \Omega, & r = s \end{cases}, \quad (\text{B.10})$$

in the case of a finite lattice, it proves beneficial to modify the factor multiplying the plane wave expansion for the Bloch modes from $1/\sqrt{2\pi}$ to $1/\sqrt{N\Omega}$, where N represents the total number of unit cells.

To rescue the integral over all the lattice [4, 95], we consider a lattice comprising $2N + 1$ unit cells. Consequently, the integral over the lattice can be expressed as a sum within each cell:

$$\begin{aligned} \int_{\text{lattice}} u_n^*(x, k) u_m(x, q) dx &= \int_{\text{lattice}} v_n^*(x, k) v_m(x, q) e^{i(q-k)x} dx \\ &= \int_{-aN}^{-a(N-1)-a/2} v_n^*(x, k) v_m(x, q) e^{i(q-k)x} dx + \dots \\ &+ \int_{-3a/2}^{-a/2} v_n^*(x, k) v_m(x, q) e^{i(q-k)x} dx \\ &+ \int_{-a/2}^{a/2} v_n^*(x, k) v_m(x, q) e^{i(q-k)x} dx \\ &+ \int_{a/2}^{3a/2} v_n^*(x, k) v_m(x, q) e^{i(q-k)x} dx \\ &+ \dots + \int_{a(N-1)+a/2}^{aN+a/2} v_n^*(x, k) v_m(x, q) e^{i(q-k)x} dx, \end{aligned} \quad (\text{B.11})$$

then, by performing a substitution of the form $x = \tilde{x} \pm \nu a$ in each integral, where ν is an integer, and considering $\Delta k = q - k$, we arrive at:

$$\begin{aligned} \int_{\text{lattice}} u_n^*(x, k) u_m(x, q) dx &= \int_{-a/2}^{a/2} v_n^*(x, k) v_m(x, k) e^{i\Delta k x} dx \left[\sum_{\nu=-N}^N e^{i(a\Delta k)\nu} \right] \\ &= D_N(a\Delta k) \int_{-a/2}^{a/2} v_n^*(x, k) v_m(x, k) e^{i\Delta k x} dx, \end{aligned} \quad (\text{B.12})$$

and the sum between brackets is the Dirichlet kernel [96]. As we take the limit $N \rightarrow \infty$, it transforms into a sum of Dirac delta functions [97]:

$$\int_{-\infty}^{\infty} u_n^*(x, k) u_m(x, q) dx = 2\pi \sum_{\nu=-\infty}^{\infty} \delta(a\Delta k - 2\pi\nu) \int_{-\pi/a}^{\pi/a} u_n^*(x, k) u_m(x, q) dx, \quad (\text{B.13})$$

and, given the restriction of k to the first Brillouin zone, the only term that remains in the sum is the one where $\nu = 0$. Consequently, we arrive at the previously established orthogonality condition:

$$\int_{-\infty}^{\infty} u_n^*(x, k) u_m(x, q) dx = \delta_{nm} \delta(k - q). \quad (\text{B.14})$$

Annex

ANNEX A – published articles

- A.1 Spatial coherence effects of stochastic optical beams in periodic potentials

Spatial coherence effects of stochastic optical beams in periodic potentials

M. J. Cirino ^{*}, P. A. Brandão [†], and S. B. Cavalcanti [‡]

Universidade Federal de Alagoas, Instituto de Física, 57072-900, Brazil



(Received 30 November 2022; accepted 10 March 2023; published 23 March 2023)

The interaction between a partially coherent field with a one-dimensional periodic photonic environment is investigated within the framework of Floquet-Bloch modes. To this end, we describe the interplay between lattice properties and field fluctuations by considering the optical beam as a linear combination of Floquet-Bloch modes, whose coefficients are described by a stationary random process. It is demonstrated that the propagation of partially coherent beams depends not only on the average of the excitation of each band but also on the correlations existent among the various bands supported by the lattice.

DOI: [10.1103/PhysRevA.107.033518](https://doi.org/10.1103/PhysRevA.107.033518)

I. INTRODUCTION

Wave propagation through periodic structures has been extensively studied in diverse physical environments such as optical lattices, waveguide arrays, and Bose-Einstein condensates, among others. Stemming from the analogy between electromagnetic waves in a periodic dielectric structure and electrons in a periodic atomic potential, work based on Floquet-Bloch (FB) optical modes has flourished since the advent of photonic crystals [1–4]. One of the most important features exhibited by wave propagation in periodic media is the existence of bands and forbidden frequency gaps for electromagnetic waves, [5,6]. Their existence in the photonic density of states is of fundamental importance as dispersion and diffraction are strongly enhanced, modifying severely the properties of light propagation. Based on these facts, theoretical and experimental research on modulated photonic lattices has been developed intensely in the last decades, revealing rich phenomena [2,7].

However, in real experiments all light sources fluctuate in the sense that the fields they generate undergo random fluctuations, and it is well known that the spatial coherence properties of a source strongly affect the spectrum of the propagating wave. By coherence here we mean a measure of correlations between the components of the fluctuating field at two or more points in the space at the same time. Coherence is a fundamental concept about the nature of light and investigating its influence upon optical systems is necessary if one is to achieve spatial coherence control, as it is required in many practical applications such as imaging [8], tomography [9], and beam propagation [10], among many others [11,12]. Therefore, owing to the fact that fluctuations are always present in real systems, one must include them in the investigation of periodic systems to find the extent that they might modify the spectrum dynamics [13]. To this

end, one may rely on the techniques of statistical optics, also known as optical coherence theory [14,15].

Based on the above discussion, in this paper we introduce a method to understand the interaction between a partially coherent field with a one-dimensional periodic photonic environment within the framework of Floquet-Bloch modes together with a space-frequency representation of stationary random processes. For comparison purposes, we apply our scheme to the propagation of a deterministic Gaussian beam as well as the propagation of partially coherent Gaussian-Schell beams [16]. We choose to work with the FB basis considering that a FB wave traveling through a periodic medium is the counterpart of a plane wave traveling through a homogeneous medium. A FB mode itself is composed of a group of plane waves. In both cases the final beam is defined as the linear combination of the FB modes, which are the eigenvalues of the paraxial equation. In the partially coherent case, each linear combination is just a member of an ensemble of possible output beam shapes. The output beam profiles are determined by the interference among multi FB modes. We shall describe the role played by band correlations and their consequences. To this end, in the next section we introduce our theory in the case of a deterministic beam and apply it to a wide Gaussian beam. In Sec. III we present the generalization of the deterministic theory to include the statistical properties of the incident beam, and describe the evolution of the Gaussian-Schell beam. In Sec. IV we conclude.

II. DETERMINISTIC THEORY

Let us begin by considering a monochromatic realization of an optical field represented by the slowly varying envelope $\psi(x, z)$ propagating along the homogeneous z direction through a periodic medium positioned along the transverse direction x . Its dynamical behavior can be well described by the normalized paraxial wave equation

$$i \frac{\partial \psi(x, z)}{\partial z} + \frac{\partial^2 \psi(x, z)}{\partial x^2} + V(x) \psi(x, z) = 0, \quad (1)$$

^{*}miqueias@fis.ufal.br

[†]paulo.brandao@fis.ufal.br

[‡]solange@fis.ufal.br

where $\psi(x, z)$ represents the normalized electric field envelope. The function $V(x + a) = V(x)$ describes the periodic lattice and is proportional to the refractive index of the material. We suppose that it has the following general form:

$$V(x) = \sum_{m=-\infty}^{\infty} V_m e^{2\pi i m x / a}, \quad (2)$$

where the parameter a is a positive number representing the lattice period and V_m represents the m th Fourier amplitude, which is a complex number, in general.

The eigenstates of the paraxial wave equation are defined as $\psi_n(x, k) = u_n(x, k) e^{i\beta_n(k)z}$, with k as the Bloch wave number corresponding to the FB mode $u_n(x, k)$, which satisfies the following equation:

$$\frac{d^2 u_n(x, k)}{dx^2} + V(x) u_n(x, k) = \beta_n(k) u_n(x, k); \quad (3)$$

here, we fix the Bloch wave number within the first Brillouin Zone (BZ), that is $k \in [-\pi/a, \pi/a]$; n is the band index; and $\beta_n(k)$ is the propagation constant of the FB wave. The FB modes are the eigenstates of the paraxial wave equation (3). In a periodic medium they play the same role as plane waves in a homogeneous medium. They are stationary states just like in the solid state, except that here in the space description they are diffractionless solutions, meaning that the intensity is independent of the propagation direction. These modes are fully determined by the structure of the lattice and remain dormant unless they become excited by the incident wave field. In a linear propagation regime, each FB mode acquires its own phase, independent of the other modes. Since these modes remain the same in spite of the different relative phases acquired during propagation, the beam may have a completely different profile at the output compared to the input profile according to the dynamics determined by the band structure, as we shall demonstrate in the following.

We begin by considering that a general solution for Eq. (1) can be written as a linear superposition of FB modes, in the sense that each mode supported by the lattice is a FB wave with its own propagation constant β_n :

$$\psi(x, z) = \sum_{n=1}^{\infty} \int_{-\pi/a}^{\pi/a} c_n(k) u_n(x, k) e^{i\beta_n(k)z} dk, \quad (4)$$

where $c_n(k)$ is the participation coefficient of band n at wave vector k . It represents the relative power within the correspondent FB mode with Bloch wave number k and band n . The envelope profile of the optical field is then determined by the interference among these modes. These coefficients are fully defined at the input plane $z = 0$, and can be calculated from

$$c_n(k) = \int_{-\infty}^{\infty} u_n^*(x, k) \psi(x, 0) dx, \quad (5)$$

after the orthogonality between FB modes $\int_{-\infty}^{\infty} u_n^*(x, k_1) u_m(x, k_2) dx = \delta_{nm} \delta(k_1 - k_2)$ was used, and $\psi(x, 0)$ describes the beam profile at $z = 0$. Depending on the variation of the beam amplitude at $z = 0$, and also on the values of the Fourier components V_m , the incident beam may excite FB modes belonging to more than one band.

Figure 1 displays the first three bands for a periodic lattice represented by the truncated expansion of Eq. (2), that is,

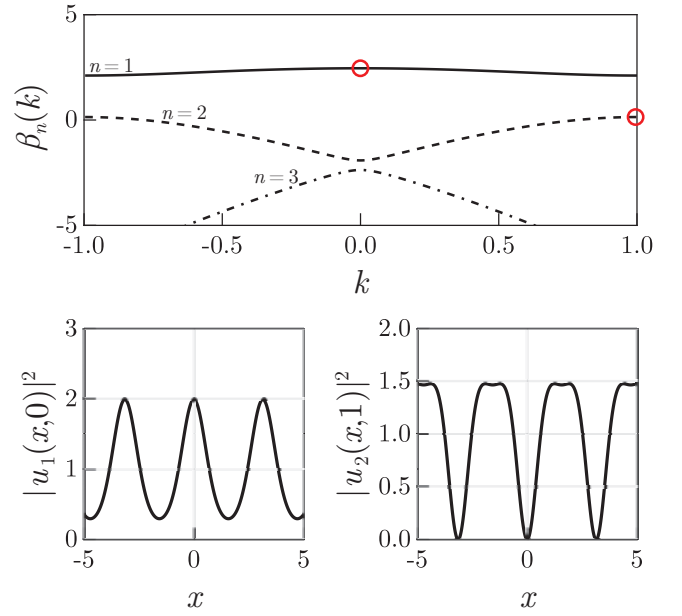


FIG. 1. (Top) Propagation constant $\beta_n(k)$ versus Bloch wave number k for modes $n = 1, 2$, and 3 and fixed potential amplitude $A = 4$. Floquet-Bloch mode amplitudes $|u_1(x, k = 0)|^2$ (bottom left) and $|u_2(x, k = 1)|^2$ (bottom right) versus lattice position x . The red circles in the top panel represent the propagation numbers for each of the FB modes represented in the bottom panels.

$V(x) = A \cos^2 x$, which is the potential used in all subsequent analysis. More specifically, $V_0 = A/2$ and $V_{\pm 1} = A/4$ and $V_m = 0$ otherwise. Along with the bands, the figure displays two FB modes corresponding to Bloch wave number $k = 0$ (bottom left) and $k = 1$ (bottom right) for $n = 1$ and $n = 2$, respectively. The zeros of FB modes at the band edges are characteristic of Hermitian lattices only [17].

Gaussian beam source

Let us now apply the formalism developed above by considering the propagation of a fully coherent Gaussian beam described by the incident field amplitude,

$$\psi(x, 0) = S_0 e^{-x^2/2\sigma^2} e^{iqx}, \quad (6)$$

where σ is the beam width, q the transverse momentum k , and S_0 the field amplitude, at $x = 0$. To gain physical insight into the contribution of the Bloch coefficients $c_n(k)$, we write the Bloch mode $u_n(x, k)$ as

$$u_n(x, k) = e^{ikx} \sum_{\alpha=-\infty}^{\infty} d_{\alpha}^{(n)}(k) e^{2\pi i \alpha x / a}, \quad (7)$$

where $d_{\alpha}^{(n)}(k)$ is the α th expansion coefficient of band n and Bloch wave number k . Next, we substitute (6) and (7) into (5) to obtain

$$c_n(k) = \sigma S_0 \sqrt{2\pi} \sum_{\alpha=-\infty}^{\infty} [d_{\alpha}^{(n)}(k)]^* e^{-(\sigma^2/2)(2\pi\alpha/a+k-q)^2}. \quad (8)$$

Since $d_{\alpha}^{(n)}(k)$ (for varying α) are the eigenvectors' coefficients of the matrix obtained after substituting (7) into (3),

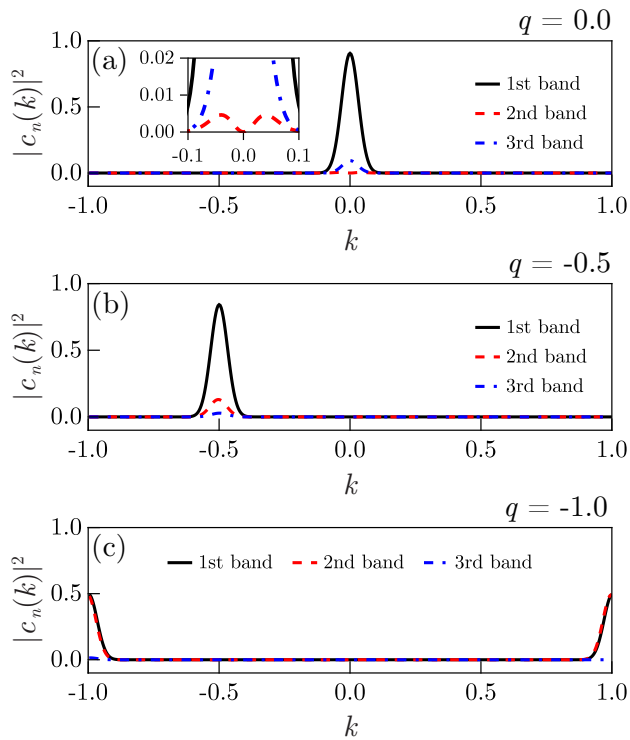


FIG. 2. Absolute squared Floquet-Bloch coefficients $|c_n(k)|^2$ versus wave number k , for fixed $A = 4.0$ input beam width $\sigma = 7\pi$ and various input wave numbers: (a) $q = 0.0$ (the inset illustrates the contribution of the second and third bands), (b) $q = -0.5$, and (c) $q = -1.0$.

Eq. (8) is more suitable from a computational point of view since one does not need to deal with the integration over the x axis, as Eq. (5) suggests. Also, for a fixed Bloch wave vector k and moderate values of A , only a few of $d_a^{(n)}(k)$ are significantly different from zero, as we show in the examples discussed below. Figure 2 illustrates the participation coefficients $|c_n(k)|^2$ (normalized by $\sigma S_0 \sqrt{2\pi}$) for the first three bands $n = 1, 2, 3$. Figure 2(a) displays the coefficient profiles for $q = 0$ (normal incidence) and indicates that most of the contribution comes from the first band, with a small fraction of the third band, and as illustrated in the inset an even smaller contribution of the second band. Part (b) is plotted for $q = -0.5$ and shows a similar behavior, with the first band exhibiting most of the contribution, but now the second band contribution grows and overcomes the contribution of the third one.

By simply changing the excitation angle, which determines the transverse momentum q of a beam, one can dynamically control its diffraction properties [18]. We turn to Fig. 2(c), the case $q = -1$, corresponding to Bragg scattering. We see that the first two bands exhibit identical contributions to the overall beam evolution. Since the beam direction is determined essentially by the direction of the group velocity $\nabla_k \beta_n(k)$, which is perpendicular to the transmission band, it is expected that in the Bragg condition the beam evolves mainly along the z direction, diffractionless as shown in Fig. 1. This claim is confirmed by Fig. 3(a), which displays the plot of $|\psi(x, z)|^2$, calculated directly from (4).

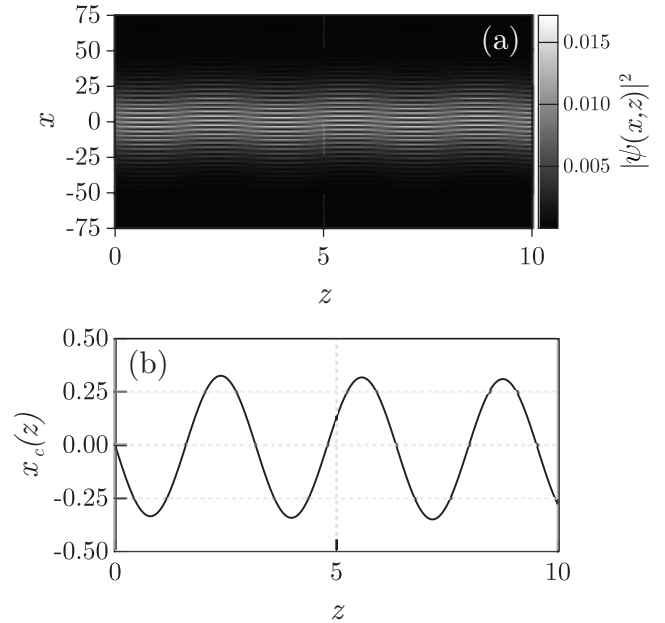


FIG. 3. (a) Beam intensity $|\psi(x, z)|^2$. (b) Beam center oscillation $x_c(z)$ versus propagation distance z for input wave number $q = -1.0$, input beam width $\sigma = 7\pi$, and potential amplitude $A = 4.0$.

After a close inspection of Fig. 3(a), one finds that the beam center oscillates during propagation along z . Let us then define the beam center as

$$x_c(z) = \frac{\int x |\psi(x, z)|^2 dx}{\int |\psi(x, z)|^2 dx}. \quad (9)$$

Figure 3(b) displays the beam center oscillations $x_c(z)$. It should be pointed out that these oscillations are not centered around $x_c = 0$. There is a slow rectilinear movement in the negative x direction superposing the oscillations. This behavior resembles the quivering of the free Dirac electron, well known by Zitterbewegung (ZB) [19]. In the context of photonic systems such oscillations have been reported in the case of waveguide arrays [20–22].

III. STOCHASTIC THEORY

Random fluctuations are inherent in all optical fields irrespective of their origin; whether spontaneous emission, temperature fluctuations, or mechanical vibrations, among many others, the fluctuations are always present. Therefore, to deal with measurable quantities in optical systems one must incorporate statistical concepts to the theory to characterize, not the field evolution in one space-time point, but the correlations between two (or more) space-time points. In second-order classical statistical optics, one characterizes the two-point correlations by using the cross-spectral density function. Under general conditions, likely to be valid in many systems of interest, the cross-spectral density of a statistical stationary source is defined as

$$W(x_1, x_2, z) = \langle \psi^*(x_1, z) \psi(x_2, z) \rangle_\omega, \quad (10)$$

where $\langle \cdot \rangle_\omega$ implies an ensemble average of monochromatic realizations of the incident optical field.

A random beam can be generated by choosing the FB functions as an orthonormal basis to obtain a linear combination that represents the beam profile inside the periodic medium, as suggested in the last section. However, now we suppose that the respective FB coefficients $c_n(k)$ are described by stationary random processes of the FB wave number so that each mode represents one configuration of the ensemble. The evolution of the overall field $\psi(x, z)$ depends not only on the average values of $c_n(k)$ but also on the correlations existent between the bands that correspond to the cross-correlations $C_{mn}(k_1, k_2) = \langle c_m^*(k_1)c_n(k_2) \rangle_\omega$. In this way, one may speak of the correlations between $c_m(k_1)$ and $c_n(k_2)$ and study their influence upon the evolution of a partially coherent beam. Previous works on the propagation of partially coherent beams in periodic structures have been published in nonlinear [23] and linear [24,25] systems. The approach taken by Hoenders and Bertolotti is very similar to ours, differing in that they assume a weakly periodic media and a nonparaxial propagation, which results in a somewhat more involved analysis of the propagation dynamics.

Thus, in the following we shall be concerned with this problem: given the initial distribution of field correlations $W(x_1, x_2, 0)$, how can one obtain the cross-spectral density at a given $z > 0$? The answer to this question lies within the correlation $C_{mn}(k_1, k_2)$ between $c_n(k_1)$ and $c_m(k_2)$ that can be directly evaluated from (5):

$$\begin{aligned} C_{mn}(k_1, k_2) &= \langle c_m^*(k_1)c_n(k_2) \rangle_\omega \\ &= \iint u_m(x_1, k_1)u_n^*(x_2, k_2)W(x_1, x_2, 0)dx_1dx_2. \end{aligned} \quad (11)$$

The coefficients $C_{mn}(k_1, k_2)$ represent a measure of the correlations between bands m and n for FB wave numbers k_1 and k_2 . Once the coefficients $C_{mn}(k_1, k_2)$ are obtained, and with the knowledge of the statistical properties at the input, the cross-spectral density $W(x_1, x_2, z)$ for $z > 0$ is readily obtained for any state of light:

$$\begin{aligned} W(x_1, x_2, z) &= \sum_{n,m=1}^{\infty} \int_{-\pi/a}^{\pi/a} dk_1 \int_{-\pi/a}^{\pi/a} dk_2 \\ &\times C_{mn}(k_1, k_2)u_m^*(x_1, k_1)u_n(x_2, k_2) \\ &\times e^{-i[\beta_m(k_1) - \beta_n(k_2)]z}. \end{aligned} \quad (12)$$

The averaged intensity is given by $S(x, z) = W(x, x, z) = \langle |\psi(x, z)|^2 \rangle$, that is,

$$\begin{aligned} S(x, z) &= \sum_{n,m=1}^{\infty} \int_{-\pi/a}^{\pi/a} dk_1 \int_{-\pi/a}^{\pi/a} dk_2 \\ &\times C_{mn}(k_1, k_2)u_m^*(x, k_1)u_n(x, k_2) \\ &\times e^{-i[\beta_m(k_1) - \beta_n(k_2)]z}. \end{aligned} \quad (13)$$

By inspection of Eq. (13), one can conclude that the spatial correlation represented by the cross-spectral function $W(x_1, x_2, z)$ does induce additional FB modes to the overall field. One may visualize the correlations through the spectral degree of coherence, a convenient quantity that measures the normalized degree of coherence between the modes, defined

here as

$$\mu_{nm}(k_1, k_2) = \frac{\langle c_n^*(k_1)c_m(k_2) \rangle}{\sqrt{\langle |c_n(k_1)|^2 \rangle \langle |c_m(k_2)|^2 \rangle}}, \quad (14)$$

which satisfies the condition $0 \leq |\mu_{nm}(k_1, k_2)| \leq 1$. When $|\mu_{nm}(k_1, k_2)| = 1$, the field is fully correlated at wave numbers (k_1, k_2) and bands (n, m) . In the opposite extreme, the field is fully uncorrelated, and in between these two extreme cases, the field is partially coherent. Next, we illustrate this theory, applying it to the specific case of Gaussian-Schell sources.

Gaussian-Schell sources

Gaussian-Schell models describe an important class of partially coherent beams that are easily created in the laboratory [26,27]. They are characterized by a spectral degree of coherence that depends only on the difference between the location of the two points, x_1 and x_2 . Considering that the field fluctuations are well described by a stationary process, one suitable model for the cross-spectral density function for this class of beams at the input is given by

$$W(x_1, x_2, 0) = S_0^2 e^{-(x_1^2+x_2^2)/2\sigma^2} e^{-(x_1-x_2)^2/2\delta^2} e^{-iq(x_1-x_2)}, \quad (15)$$

where S_0 is the field amplitude, σ is the beam width, δ is the coherence parameter ($\delta \rightarrow \infty$ describing a fully spatially coherent beam), and $-q(x_1 - x_2)$ is a phase factor related to the transverse incident wave vector q .

The FB correlation coefficients $C_{mn}(k_1, k_2)$ are written in the same form as in Eq. (8) after substituting (15) and (7) into (11) to obtain

$$\begin{aligned} C_{mn}(k_1, k_2) &= \frac{2\pi S_0^2 \delta \sigma^2}{\sqrt{\delta^2 + 2\sigma^2}} \sum_{\alpha, \beta=-\infty}^{\infty} d_\alpha^{(m)}(k_1) [d_\beta^{(n)}(k_2)]^* \\ &\times \exp \left[-\frac{\delta^2 \sigma^2 (k_1 + \frac{2\pi}{a} \alpha - q)^2}{2(\delta^2 + 2\sigma^2)} \right] \\ &\times \exp \left[-\frac{\delta^2 \sigma^2 (k_2 + \frac{2\pi}{a} \beta - q)^2}{2(\delta^2 + 2\sigma^2)} \right] \\ &\times \exp \left\{ -\frac{\sigma^4 [k_1 - k_2 + \frac{2\pi}{a} (\alpha - \beta)]^2}{2(\delta^2 + 2\sigma^2)} \right\}. \end{aligned} \quad (16)$$

Equation (16) is a generalization of the absolute square of Eq. (8). Note that by taking the limit $\delta \rightarrow \infty$, with $k_1 = k_2 = k$ and $m = n$, one retrieves Eq. (8). It is easy to see that in the special case of high coherence, $\delta \rightarrow \infty$, the coefficients $C_{mn}(k_1, k_2)$ can be written as a product between two independent functions of n (m) and k_1 (k_2), which is indicative of a full correlation between the modes. Figure 4 illustrates the mean participation coefficients $\langle |c_n(k)|^2 \rangle$ for two FB bands ($n = 1$ and 2), for several values of the coherence parameter δ , and for three incidence wave vectors $q = 0$, $q = -0.5$ and $q = -1.0$ where all the coefficients are divided by the constant factor multiplying the summation. The arrow in Fig. 4(a) indicates the growth direction of the coherence parameter, and this applies to all plots in the figure. It is clear that as the spatial coherence decreases, the contribution to the overall beam increases in the sense that many FB modes are now excited when compared to the fully coherent case. Conversely,

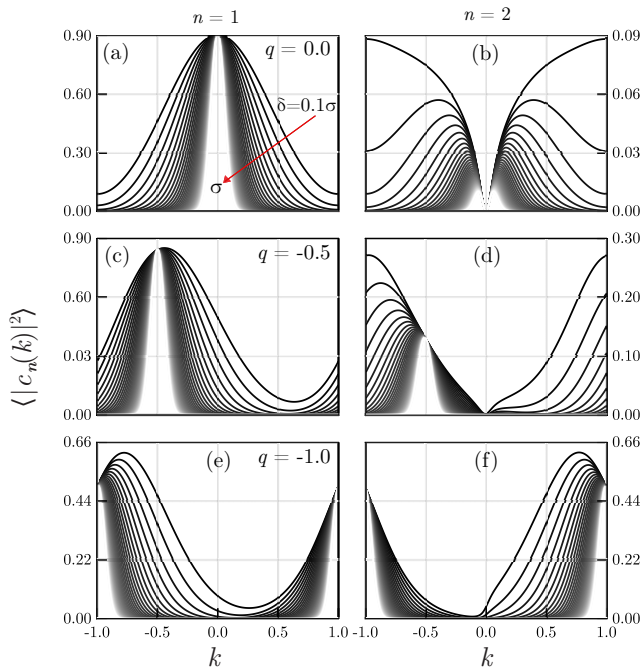


FIG. 4. Mean absolute squared of the first two FB coefficients $\langle |c_n(k)|^2 \rangle$ versus wave number k with input beam width $\sigma = 7\pi$, amplitude $A = 4.0$, and coherence parameter $\delta \in [\sigma/10, \sigma]$ for various input wave numbers: (a and b) with $q = 0.0$; (c and d) with $q = -0.5$; and (e and f) with $q = -1.0$. The arrow indicates increasing δ . The n th column corresponds to the n th mode, $n = 1, 2$.

as the spatial coherence increases, the broadening that once occupied the whole Brillouin zone becomes smaller and tends to localize along a limited band around $k = 0$, as in the fully coherent case depicted in Fig. 2. Therefore, it is clear that the lack of spatial coherence does indeed excite additional FB modes, broadening the spectrum. The extent of the broadening can be controlled by the coherence degree, a feature that is quite interesting from the point of view of applications.

The spectral degree of coherence $\mu_{nm}(k_1, k_2)$ as a function of the coherence parameter δ is displayed in Fig. 5 for some FB wave numbers k_1 and k_2 in the Brillouin zone, where we considered the correlations between the first and second bands $n = 1$ and $n = 2$. Figures 5(a) and 5(d) show an example at the same FB wave number, k . In the solid state, a transition between bands at the same k value is considered a direct transition. Otherwise, it is known as indirect. Here, we adapt this nomenclature referring to direct points $k_1 = k_2$ and indirect ones $k_1 \neq k_2$. Therefore, Figs. 5(a) and 5(d) are direct points, while Figs. 5(b) and 5(c) are indirect points. In both cases, direct or indirect, as the coherence parameter δ increases, the correlation between bands also increases, reaching the unit value asymptotically $\mu_{12} \rightarrow 1$ as $\delta \rightarrow \infty$ as expected. However, for indirect points the rate at which the coherence degree increases is much slower than the rate for direct points.

The resulting beam spectral density is plotted in Fig. 6(a) against the propagation distance z for $\delta = 0.01\sigma$. As expected, in this low-coherence regime, the influence of the coherence parameter upon the propagation causes spreading of the beam

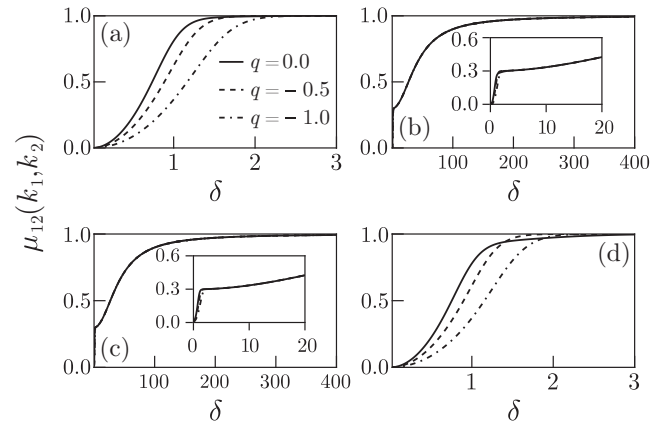


FIG. 5. Spectral degree of coherence $\mu_{12}(k_1, k_2)$ versus the coherence parameter δ for input beam width $\sigma = 7\pi$ and amplitude $A = 4.0$ at various incident angles, correspondent to $q = -1.0$ (solid line), $q = -0.5$ (dashed line), and $q = 0.0$ (dot-dashed line). Several spectral degrees of coherence between points of the Brillouin zone are displayed: (a) $k_1 = k_2 = -0.3$; (b) $k_1 = -0.2$ and $k_2 = -0.3$; (c) $k_2 = -0.3$ and $k_1 = -0.2$; and (d) $k_1 = k_2 = -0.2$.

intensity all over the BZ, resembling the case where there is no periodic lattice at all, as illustrated.

Now we turn to Fig. 6(b), where the beam center $X_c(z)$ is depicted according to the definition

$$X_c(z) = \frac{\int x S(x, z) dx}{\int S(x, z) dx}. \quad (17)$$

It can be demonstrated that Eq. (17) has the general form $X_c(z) = X_c(0) + v z + p(z)$, where $p(z)$ is a periodic

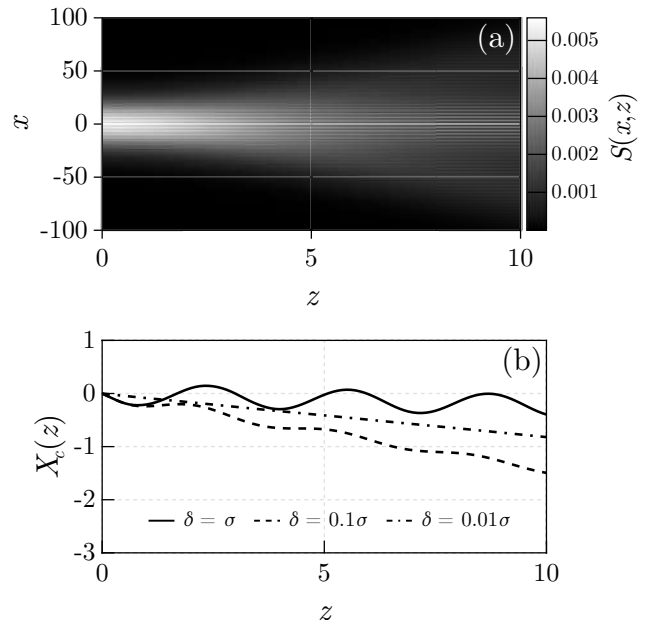


FIG. 6. (a) Beam spectral density $S(x, z)$ with coherence parameter $\delta = \sigma/100$. (b) Mean beam center oscillation $X_c(z)$ versus propagation distance z for three coherence parameters: σ , $\sigma/10$, and $\sigma/100$. For input wave number $q = -1.0$, input beam width $\sigma = 7\pi$ and potential amplitude $A = 4.0$.

function of z that depends on the correlation between bands $\langle c_n^*(k)c_m(k) \rangle$ and v denotes the linear ramp which depends on the average values $\langle |c_n(k)|^2 \rangle$ for each band n . They both also depend on the group velocity $d\beta_n(k)/dk$. The exact dependence of $X_c(z)$ on the cross-correlations $C_{mn}(k_1, k_2)$ and the group velocity $d\beta_n(k)/dk$ is so intricate that it will be investigated in more detail in a future work. Nevertheless, one finds that for an intermediate regime ($\delta = 0.1\sigma$), although the oscillations executed by the beam center undergo damping, they do not cease to exist. However, as δ decreases, the damping effect is more severe and tends to wipe them off to the extent that only the rectilinear movement is left. This is expected to occur in view of the previous discussion involving the direction of the group velocity of a Gaussian wave packet, which is determined by the band diagram illustrated at the top of Fig. 1 and by the distribution of the absolute squared Floquet-Bloch coefficients for each band, like the ones shown in Fig. 2. Here, the group velocity of the propagating beam is severely affected when additional FB modes are excited in various bands due to the low spatial coherence (see Fig. 4) of the incident beam. As a consequence, the number of modes belonging to the final superposition increases, changing substantially the correlations between the various modes. The consequence is that the averaged group velocity will not maintain periodic coherence during propagation.

IV. CONCLUSIONS

We have presented a theory of diffraction of partially coherent paraxial optical beams propagating through a

periodic medium. Within the framework of Floquet-Bloch waves, we have considered a linear combination of FB modes with random coefficients to obtain a general expression for the cross-spectral density $W(x_1, x_2, z)$ at propagation distance z . Considering as input a Gaussian-Schell beam, we have shown that weak correlations may modify severely the power distribution of the FB modes by spreading the power among additional FB wave vectors, in contrast with the fully coherent beam, whose FB power content is localized within a finite bandwidth in the neighborhood of the input wave vector. In an intermediate regime of coherence the modes tend to broaden up to the point of low coherence, where the power distribution is extended to all over the BZ and the beam profile can hardly note the grating.

A knowledge of the changes as light propagates through the transverse periodic medium in the presence, as well as in the absence, of field fluctuations is necessary to understand their influence upon light transport. These properties depend basically on the band structure. By introducing the statistical properties of the optical field in the investigation of beam propagation, one should unravel useful phenomena that will lead to remarkable techniques that manipulate light using the notion of coherence.

ACKNOWLEDGMENTS

The authors would like to thank the Brazilian Agencies FAPESP, CNPq, and CAPES for partial financial support. M.J.C. acknowledges fruitful discussions with J. C. A. Rocha throughout this work.

-
- [1] E. Yablonovitch, Inhibited Spontaneous Emission in Solid-State Physics and Electronics, *Phys. Rev. Lett.* **58**, 2059 (1987).
 - [2] S. John, Strong Localization of Photons in Certain Disordered Dielectric Superlattices, *Phys. Rev. Lett.* **58**, 2486 (1987).
 - [3] J. D. Joannopoulos, S. G. Johnson, J. N. Winn, and R. D. Meade, *Photonic Crystals Molding the Flow of Light* (Princeton Univ. Press, Princeton, 2008).
 - [4] P. S. J. Russell, Optics of Floquet-Bloch waves in dielectric gratings, *Appl. Phys. B* **39**, 231 (1986).
 - [5] K. Sakoda, *Optical Properties of Photonic Crystals*, 2nd ed., Optical Sciences (Springer, Heidelberg, 2005).
 - [6] P. Sheng, *Introduction to Wave Scattering, Localization, and Mesoscopic Phenomena*, 2nd ed. (Academic, San Diego, 2000).
 - [7] I. L. Garanovich, S. Longhi, A. A. Sukhorukov, and Y. S. Kivshar, Light propagation and localization in modulated photonic lattices and waveguides, *Phys. Rep.* **518**, 1 (2012).
 - [8] A. S. Ostrovsky, M. Á. Olvera-Santamaría, and P. C. Romero-Sorúa, Effect of coherence and polarization on resolution of optical imaging system, *Opt. Lett.* **36**, 1677 (2011).
 - [9] E. Baleine and A. Dogariu, Variable coherence tomography, *Opt. Lett.* **29**, 1233 (2004).
 - [10] A. Norrman, S. A. Ponomarenko, and A. T. Friberg, Partially coherent surface plasmon polaritons, *Europhys. Lett.* **116**, 64001 (2017).
 - [11] O. Korotkova and G. Gbur, Applications of optical coherence theory, *Prog. Opt.* **65**, 43 (2020).
 - [12] A. Nardi, S. Divitt, M. Rossi, F. Tebbenjohanns, A. Militaru, M. Frimmer, and L. Novotny, Encoding information in the mutual coherence of spatially separated light beams, *Opt. Lett.* **47**, 4588 (2022).
 - [13] E. Wolf and D. F. James, Correlation-induced spectral changes, *Rep. Prog. Phys.* **59**, 771 (1996).
 - [14] J. W. Goodman, *Statistical Optics* (Wiley, New York, 2015).
 - [15] E. Wolf, *Introduction to the Theory of Coherence and Polarization of Light* (Cambridge University, Cambridge, 2007).
 - [16] O. Korotkova, M. Salem, and E. Wolf, Beam conditions for radiation generated by an electromagnetic Gaussian Schell-model source, *Opt. Lett.* **29**, 1173 (2004).
 - [17] K. G. Makris, R. El-Ganainy, D. N. Christodoulides, and Z. H. Musslimani, Pt-symmetric optical lattices, *Phys. Rev. A* **81**, 063807 (2010).
 - [18] H. S. Eisenberg, Y. Silberberg, R. Morandotti, and J. S. Aitchison, Diffraction Management, *Phys. Rev. Lett.* **85**, 1863 (2000).
 - [19] J. J. Sakurai, *Advanced Quantum Mechanics* (Pearson, Delhi, 2006).
 - [20] V. S. Shchesnovich and S. Chávez-Cerda, Bragg-resonance-induced Rabi oscillations in photonic lattices, *Opt. Lett.* **32**, 1920 (2007).
 - [21] P. A. Brandão and S. B. Cavalcanti, Bragg-induced power oscillations in pt-symmetric periodic photonic structures, *Phys. Rev. A* **96**, 053841 (2017).

- [22] S. Longhi, Photonic analog of Zitterbewegung in binary waveguide arrays, *Opt. Lett.* **35**, 235 (2010).
- [23] H. Buljan, G. Bartal, O. Cohen, T. Schwartz, O. Manela, T. Carmon, M. Segev, J. Fleischer, and D. Christodoulides, Partially coherent waves in nonlinear periodic lattices, *Stud. Appl. Math.: Special issue: Nonlinear optics* **115**, 173 (2005).
- [24] B. J. Hoenders and M. Bertolotti, Theory of partial coherence for weakly periodic media, *J. Opt. Soc. Am. A* **22**, 2682 (2005).
- [25] P. A. Brandão and J. C. A. Rocha, Propagation of partially coherent light in non-Hermitian lattices, *Phys. Rev. A* **106**, 063503 (2022).
- [26] P. De Santis, F. Gori, G. Guattari, and C. Palma, An example of a Collett-Wolf source, *Opt. Commun.* **29**, 256 (1979).
- [27] Q. He, J. Turunen, and A. T. Friberg, Propagation and imaging experiments with Gaussian Schell-model beams, *Opt. Commun.* **67**, 245 (1988).

A.2 Bragg scattering of stochastic beams in PT-symmetric photonic lattices

Bragg scattering of stochastic beams in PT-symmetric photonic lattices

P. A. BRANDÃO,*  M. J. CIRINO, AND S. B. CAVALCANTI 

Universidade Federal de Alagoas, Instituto de Física, 57072-900, Brazil
*paulo.brandao@fis.ufal.br

Received 15 November 2023; revised 29 December 2023; accepted 30 December 2023; posted 2 January 2024; published 25 January 2024

The propagation of a Gaussian–Schell beam through a PT-symmetric optical lattice, whose index of refraction is represented by a sinusoidal type of function, is theoretically investigated. Within the framework of standard coherence theory, one is able to access and elucidate unexpected consequences of the interplay between the spatial coherence properties of the beam and the non-Hermitian nature of the photonic lattice. We describe how one may use a non-Hermitian periodic medium to enhance the spatial coherence properties of a partially coherent beam. © 2024 Optica Publishing Group

<https://doi.org/10.1364/OL.512326>

In the last decades, investigations on optical systems described by non-Hermitian Hamiltonians have revealed a great deal of exotic optical phenomena with no counterpart in a Hermitian environment, particularly those Hamiltonians which are simultaneously symmetric under both space inversion (parity P) and temporal reversal (T), i.e., the PT-symmetric Hamiltonians. Effects, such as loss-induced optical transparency [1], non-reciprocal diffraction patterns [2], power oscillations [3], and enhanced transmission [1], among many others, were discovered. The depart of the optical system from its Hermitian character can be described by a parameter which measures the ratio between the complex part and the real part of the refractive index. Once this parameter reaches a critical point [4], the PT-symmetric system undergoes a spontaneous symmetry breaking, meaning that a real eigenvalue solution of the wave equation bifurcates into a pair of conjugate complex values, i.e., the system undergoes a phase transition to the complex plane. As a consequence, some eigenmodes of the Hamiltonian will decay, while others will grow indefinitely, and this is the origin of the exotic properties they exhibit.

Considering the remarkable techniques available nowadays, the development of artificial materials specifically designed to contain spatially distributed balanced gain and loss, in a PT-symmetric arrangement, has provided the ideal conditions to investigate PT-symmetric optical materials. Considering the analogy between the optical paraxial wave equation and the Schrödinger equation, the index of refraction plays the role of the PT-symmetric potential. Therefore, the complex index of refraction abides by the relation $n(\mathbf{r}) = n^*(-\mathbf{r})$, and consequently, its real part is an even function of \mathbf{r} in contrast with the imaginary

part which is odd. Nowadays, researchers have realized that the application of the ideas of PT symmetry and exceptional points to optical systems has opened an important area of research in integrated photonics [5].

However, there is one particular important aspect of the optical fields that has to be taken into account in real physical systems: the fact that the optical field fluctuates. For a thorough realistic theoretical investigation in PT-symmetric optical systems, one should include the contribution of spatial correlations. To include randomness here, one can rely on classical optical coherence theory which is based on observable quantities, in the sense that these quantities can be measured in an experiment using ordinary optical instruments [6].

Motivated by these remarkable phenomena which have the potential to inaugurate a new era of photonic devices, we have investigated the interplay between the Bragg scattering and the PT symmetry of a partially coherent optical beam that travels through a one-dimensional periodic PT-symmetric structure. The simpler deterministic Hermitian version of this system sustains optical power oscillations, due to the coupling between the beam and the periodic structure. These oscillations occur between a particular pair of transverse modes, i.e., those related with the Bragg resonance condition [7,8]. Furthermore, it is well-known that interference effects are severely modified by the correlation properties of light. Therefore, inspired by all of these facts and guided by the standard coherence theory, in this Letter, we set out to study the Bragg diffraction of a Gaussian–Schell beam [9] propagating through a PT-symmetric sinusoidal optical lattice. We find that the peculiarities typical of PT-symmetric systems are modified by the spatial coherence properties of the beam. These, in turn, are severely modified by the PT-symmetric medium which induces correlations to incoherent beams, as we proceed to describe.

Let us begin by considering a statistically stationary scalar optical field $\psi(x, z, t)$ propagating mainly along the z -direction through a periodic medium along the transversal direction x , characterized by its cross-spectral density $W_{12}(z, \omega) = W(x_1, x_2, z, \omega)$, defined as the Fourier transform of the mutual coherence function $\Gamma(x_1, x_2, \tau) = \langle \psi^*(x_1, t) \psi(x_2, t + \tau) \rangle$. The field varies in the (x, z) plane and ω is the angular frequency. The cross-spectral density can also be directly written as a correlation function $W(x_1, x_2, z, \omega) = \langle \psi^*(x_1, z, \omega) \psi(x_2, z, \omega) \rangle_\omega$, where $\psi(x, z, \omega)$ is the space–frequency component of the analytic signal $\psi(x, z, t)$ at frequency ω and the average is taken

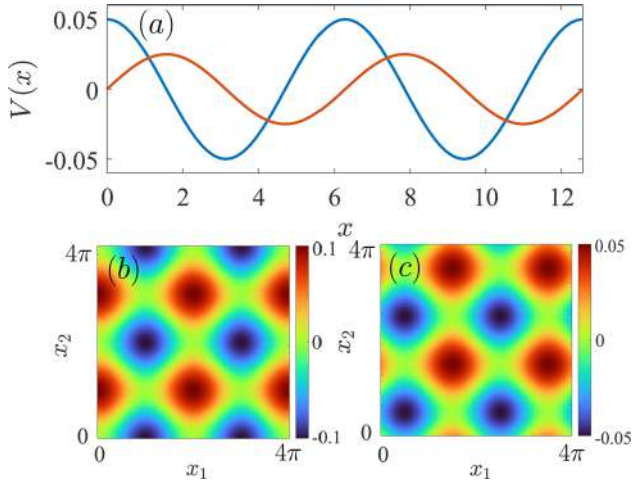


Fig. 1. (a) Real (blue) and imaginary (orange) parts of $V(x)$ whose period is 2π and assuming $V_0 = 0.05$. (b) Real and (c) imaginary parts of the effective potential $\mathcal{V}(x_1, x_2)$. The non-Hermitian lattice is characterized by $\beta = 0.5$.

over an ensemble of monochromatic realizations all having the same frequency [10]. The dependence upon ω is omitted from now on. Assuming that each element of the ensemble representing the optical field satisfies the paraxial wave equation $i\psi_z(x, z) + \psi_{xx}(x, z) + V(x)\psi(x, z) = 0$, it is easy to demonstrate that the cross-spectral density evolves according to [11]

$$i\frac{\partial W_{12}(z)}{\partial z} + \left(\frac{\partial^2}{\partial x_2^2} - \frac{\partial^2}{\partial x_1^2} \right) W_{12}(z) + \mathcal{V}_{12} W_{12}(z) = 0, \quad (1)$$

where $\mathcal{V}_{12} = V(x_2) - V(x_1)$ is the effective potential representing the transverse variations of the refractive index profile $V(x)$ relative to a substrate where the heterogeneous material is deposited. Please take note that the paraxial wave equation defined here differs from the one presented in Ref. [11].

We assume that $V(x)$ satisfies the PT -symmetry condition, i.e., $V^*(-x) = V(x)$ and write $V(x) = V_0(\cos x + i\beta \sin x)$, where V_0 and β are the real parameters. Here, β is a measure of the depart of the system from its Hermitian character. By increasing it, one enhances the imaginary part driving the spectrum of the Hamiltonian to the complex plane. In summary, while each member $\psi(x, z)$ of the ensemble evolves under the potential $V(x)$, the cross-spectral density $W_{12}(z)$ propagates through an effective potential function $\mathcal{V}(x_1, x_2)$. Figure 1 displays both potential profiles $V(x)$ and $\mathcal{V}(x_1, x_2)$. The periodic potential has a symmetry breaking point at $\beta_c = 1$. For values of $\beta < \beta_c$, the propagation constants are real (for each member of the ensemble), and the field profile remains bounded during propagation. In the case $\beta > \beta_c$, the propagation constants acquire positive and negative nonzero imaginary values and the propagation is unstable. At $\beta = \beta_c$, the field evolves under a nontrivial dynamics [12].

The simplest nontrivial model of a random optical beam is the Gaussian–Schell beam, and therefore we choose one for which the initial correlation profile is given by

$$W_{12}(0) = e^{-(x_1^2 + x_2^2)/4\sigma^2} e^{-(x_1 - x_2)^2/2\delta^2} e^{-iq(x_1 - x_2)}, \quad (2)$$

where σ is related to the initial beam width, δ is the coherence parameter, and q is the incident transverse wavevector, which must be chosen at the edge of the Brillouin zone, for

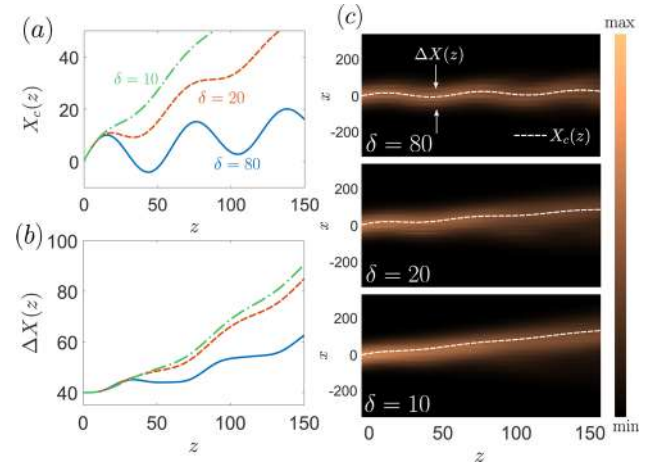


Fig. 2. Stochastic beam dynamics in a real lattice with $\beta = 0$. (a) Beam center $X_c(z)$ and (b) beam width $\Delta X(z)$ for $\delta = 80$ (blue), 20 (orange), and 10 (yellow). The plots in (c) display the spectral density $S(x, z)$ evolution in the (x, z) plane for the three values of δ . Parameters used: $\sigma = 40$, $V_0 = 0.1$, and $q = 1/2$.

the Bragg resonance to occur. The beam is fully coherent in the limit $\delta \rightarrow \infty$. The initial spectral density is described by a Gaussian function $S(x, 0) = W(x, x, 0) = e^{-x^2/2\sigma^2}$. To numerically solve Eq. (1), we write it as $\partial W_{12}(z)/\partial z = i(\nabla_{12}^2 + \mathcal{V})W_{12}(z)$, where $\nabla_{12}^2 = \partial^2/\partial x_2^2 - \partial^2/\partial x_1^2$. The formal solution to this equation is given by $W_{12}(z) = e^{i(\nabla_{12}^2 + \mathcal{V})z} W_{12}(0)$ such that $W_{12}(z + dz) = e^{i(\nabla_{12}^2 + \mathcal{V})dz} W_{12}(z)$. By using the approximated expression for the exponential, $e^{idz(\nabla_{12}^2 + \mathcal{V})} \approx e^{iVdz/2} e^{idz\nabla_{12}^2/2} e^{iVdz/2}$, one can iterate this last equation, introducing an error $O(dz^3)$ at each step. Then, the operator $e^{idz\nabla_{12}^2}$ can be applied to the resulting field by using the fast Fourier transform [13].

To characterize the optical beam propagation, we use the normalized moments Δ_r of the spectral density $S(x, z)$, defined as

$$\Delta_r(z) = \frac{1}{P(z)} \int_{-\infty}^{+\infty} x^r S(x, z) dx, \quad (3)$$

where $P(z) = \int_{-\infty}^{+\infty} S(x, z) dx$ is the transverse beam power at propagation distance z . The beam center is given by the first moment $X_c(z) = \Delta_1(z)$, and one resorts to the second moment to define the beam width as the root mean square, $\Delta X(z) = [\Delta_2(z) - \Delta_1^2(z)]^{1/2}$. The effective degree of spatial coherence μ is given by

$$\mu^2(z) = \frac{\int |W(x_1, x_2, z)|^2 dx_1 dx_2}{\left[\int S(x, z) dx \right]^2}. \quad (4)$$

It should be noted here that Eq. 4) characterizes the spatial coherence of a light beam by taking into account its intensity [14].

Now we are ready to investigate the properties of the random beam on propagation, beginning with a real lattice ($\beta = 0$). Let us turn to Fig. 2, where the evolution in space of the beam center (a) and the beam width (b) are illustrated for three values of the coherence parameter. We find that partial coherence promotes the damping of the oscillation movement, and the more incoherent, more severe the effect up to the point where the coherence becomes so low that the beam center hardly oscillates, as if

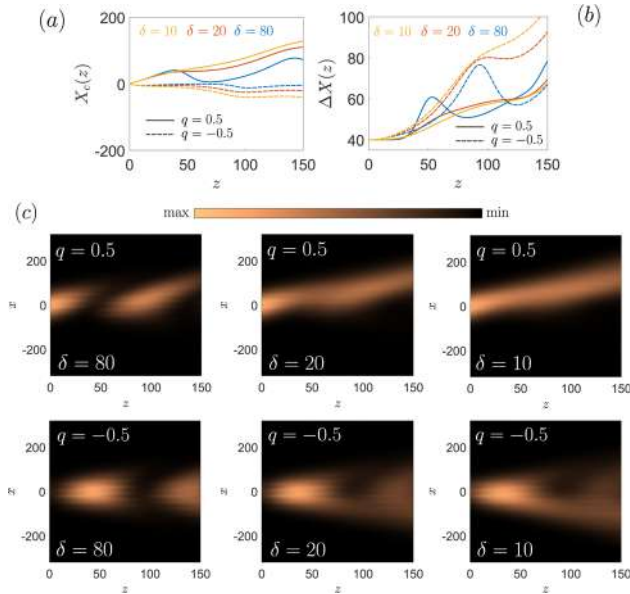


Fig. 3. Beam evolution of partially coherent light in a PT-symmetric periodic potential below the symmetry breaking point $\beta = 0.8$. (a) Beam center, (b) beam width, and (c) spectral density in the plane (x, z) . The coherence parameters are $\delta = 10$ (yellow), $\delta = 20$ (orange), and $\delta = 80$ (blue). Continuous (dashed) lines represent $q = 0.5$ ($q = -0.5$).

the lattice has been washed out. In Fig. 2(c), the spectral density is depicted in the x - y plane exhibiting the damping of the oscillations as the coherence decreases.

These findings can be elucidated by considering the excitation of an ensemble of Floquet–Bloch modes that describes the dynamics of a partially coherent beam [15]. Recent research has shown that optical beams characterized by a low spatial coherence exhibit a larger number of excited Floquet–Bloch modes when compared to fully coherent beams. This phenomenon results in a complex propagation dynamics wherein both the central position and the width of the beam undergo nontrivial changes on propagation. The observations presented in Fig. 2 are confirmed by earlier studies in the field.

We proceed by considering a complex lattice below the symmetry breaking point ($\beta < 1$) and compare the results with the Hermitian ones shown in Fig. 2. To this end, we turn to Fig. 3, which is identical to Fig. 2, with the same parameters, except for the complex lattice. Furthermore, besides the wavevector $q = 1/2$, Fig. 3 shows the dynamics for both $q = \pm 1/2$ to illustrate the non-reciprocity aspect of the dynamics. In all circumstances, the beam center, the beam width, and the spectral density exhibit complete different behaviors depending on the initial wavevector, which is a manifestation of the non-Hermitian nature of the medium. It may be noted that beams with a low degree of coherence for $q = .5$ do not exhibit the interference pattern, which is more visible in the high-degree regime. This fact is expected in the optical coherence theory [15], indicating that the decrease in spatial coherence erases the presence of the lattice, and the beam proceeds in the same direction and with steady intensity. On the other hand, for $q = -.5$, the interference pattern is still there although with its contrast distorted and reduced as the width increases. In all cases, the overall effect of a lack of spatial coherence provokes a damping of the oscillations of both the beam width.

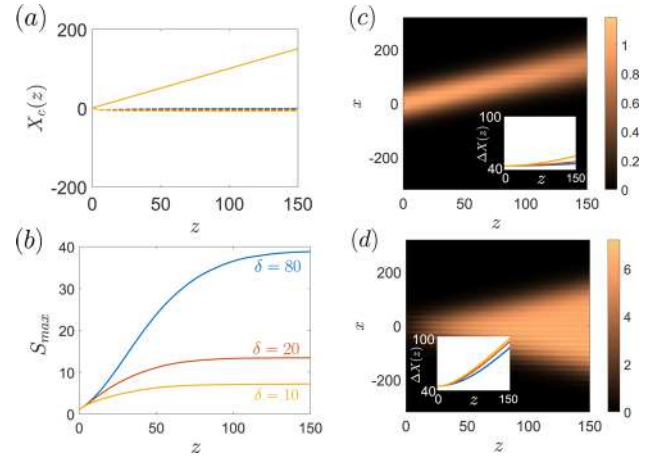


Fig. 4. Beam evolution of partially coherent light in a periodic potential at the symmetry breaking point $\beta = 1$. (a) Beam center. Continuous (dashed) lines represent $q = 0.5$ ($q = -0.5$). (b) Evolution of the spectral density for various values of the coherence parameter. (c) and (d) show the spectral density in the plane (x, z) at $q = 0.5$ and $q = -0.5$, respectively. The coherence parameters are $\delta = 10$ (yellow), $\delta = 20$ (orange), and $\delta = 80$ (blue).

Let us now compare the dynamics of the beam just described with the nontrivial dynamics exhibited at the symmetry breaking point $\beta = 1$. To this end, we turn to Fig. 4 where four panels present the evolution of (a) the beam center for $q = .5$ (continuous line) and $q = -.5$ (dashed line), (b) the maximum spectral density, and (c) and (d) the spectral density in the plane $(x - z)$ for $q = .5$ and $q = -.5$, exhibiting the non-reciprocal and nontrivial behavior. The oscillations disappear. It is clear that for $q = .5$, the beam propagates immune to diffraction, along a straight line and consequently the beam center follows this line. While for $q = -.5$, the beam experiences normal diffraction so that the beam center does not move. This result is very similar to the result obtained in the deterministic version of the Bragg diffraction in a PT-symmetric optical lattice [16], and one might conjecture at this point that the interaction with the non-Hermitian medium could possibly induce correlations into the beam on propagation.

Note that the overall behavior of the random beam at the critical point is essentially the same as that of a fully coherent beam, except for the maximum spectral density which is quite depressed in the presence of fluctuations as it is illustrated in Fig. 4(b). Consequently, the spectral density clearly exhibits the saturation of the secular Bragg scattering for wide beams, mentioned in the literature and considered as a signature of spectral singularities that arise at the symmetry breaking point [13,17]. For $\beta < \beta_c$, oscillations although damped, are still present. Increasing the complex content, they disappear accordingly until the critical point is reached where they disappear. Although there is a strong influence of the fluctuations on the value of S_{max} , both the beam center and beam width are quite robust under the lack of correlations. This robustness is attributed to the overall qualitative behavior that the random system experiments which is essentially the same as the fully coherent one. By diminishing the beam's degree of coherence, one drives the system to a deterministic behavior, and this explains why one may conjecture on the generation of spatial correlations, promoted by the non-Hermitian medium. To understand this feature, one may resort to the concept of spatial

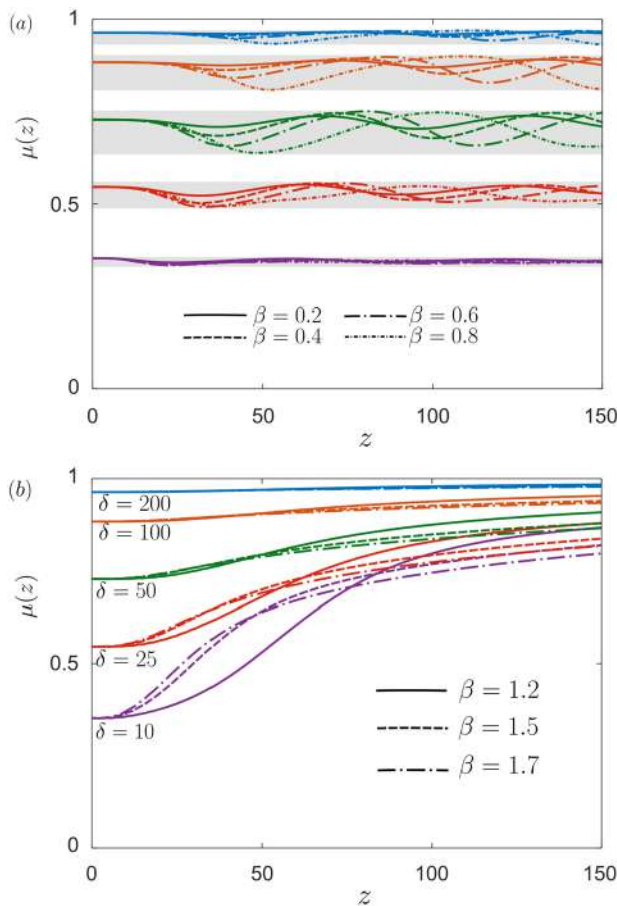


Fig. 5. Effective degree of coherence $\mu(z)$ as a function of propagated distance z for a PT -symmetric lattice (a) below and (b) above the symmetry breaking point.

degree of coherence of the input field and inspect its properties under propagation through a PT -symmetric photonic lattice, as we show in the following.

Figure 5 gives a remarkable example of the interplay between spatial correlations and non-Hermitian phenomena. Part (a) depicts the effective degree of coherence $\mu(z)$ on propagation for various values of β and δ as a function of z , below the symmetry breaking point ($0 < \beta < 1$), while part (b) exhibits the behavior above the symmetry breaking point ($\beta > 1$). In (a), the effective degree of coherence oscillates about its initial value during propagation. Additionally, we note that the amplitudes of the resulting oscillations depend on the state of coherence at the input. So, for very high or very low coherence at the input, the oscillations are quite feeble.

Past a breaking point, a quite unusual dynamics emerges, showing that the degree of coherence actually increases on propagation, more intensely for beams with a lower degree of coherence and also for values of β in the neighborhood of the

breaking point. By inspecting Fig. 5(b), one finds that a lower coherence at the input may reach a greater value of the degree of coherence when β is smaller. Thus, an initial degree with $\delta = 10$ and $\beta = 1.2$ reaches a higher value than an initial degree with $\delta = 25$ and $\beta = 1.5$. Thus, an optimal combination of these parameters may be used to control the spatial correlations of these partially coherent beams. A similar unusual phenomenon where correlations are generated by non-Hermiticity has been recently reported in a waveguide system, with loss only [18].

In summary, we have investigated the interplay between the PT symmetry and spatial coherence in the Bragg scattering. The overall effect of decreasing the spatial coherence is to promote a damping in the oscillations executed by the beam center and the beam width. Below the symmetry breaking point, the degree of coherence is more affected in a regime where spatial coherence is neither too high nor too low. Above the breaking point, the effective degree of coherence increases more intensely for beams with low spatial coherence. Thus, one concludes that the complex medium generates spatial correlations to the initial beam. By introducing fluctuations, one is adding an important asset to unravel new techniques in the control of the flow of light, via the manipulation of the beam coherence properties.

Funding. Fundação de Amparo à Pesquisa do Estado de Alagoas; Conselho Nacional de Desenvolvimento Científico e Tecnológico; Coordenação de Aperfeiçoamento de Pessoal de Nível Superior.

Disclosures. The authors declare no conflict of interest.

Data availability. Data underlying the results presented in this paper are not publicly available at this time but may be obtained from the authors upon reasonable request.

REFERENCES

1. A. Guo, G. Salamo, D. Duchesne, *et al.*, *Phys. Rev. Lett.* **103**, 093902 (2009).
2. K. G. Makris, R. El-Ganainy, D. N. Christodoulides, *et al.*, *Phys. Rev. Lett.* **100**, 103904 (2008).
3. M. C. Zheng, D. N. Christodoulides, R. Fleischmann, *et al.*, *Phys. Rev. A* **82**, 010103 (2010).
4. W. Heiss, *J. Phys. A: Math. Theor.* **45**, 444016 (2012).
5. Ş. K. Özdemir, S. Rotter, F. Nori, *et al.*, *Nat. Mater.* **18**, 783 (2019).
6. E. Wolf, *Introduction to the Theory of Coherence and Polarization of Light* (Cambridge University Press, 2007).
7. V. S. Shchesnovich and S. Chávez-Cerda, *Opt. Lett.* **32**, 1920 (2007).
8. P. A. Brandão and S. B. Cavalcanti, *Phys. Rev. A* **96**, 053841 (2017).
9. Q. He, J. Turunen, and A. T. Friberg, *Opt. Commun.* **67**, 245 (1988).
10. E. Wolf, *J. Opt. Soc. Am.* **72**, 343 (1982).
11. P. A. Brandão and J. C. A. Rocha, *Phys. Rev. A* **106**, 063503 (2022).
12. S. Longhi, *Phys. Rev. A* **81**, 022102 (2010).
13. J. Javanainen and J. Ruostekoski, *J. Phys. A: Math. Gen.* **39**, L179 (2006).
14. P. Vahimaa and J. Tervo, *J. Opt. A: Pure Appl. Opt.* **6**, S41 (2004).
15. M. J. Cirino, P. A. Brandão, and S. B. Cavalcanti, *Phys. Rev. A* **107**, 033518 (2023).
16. P. A. Brandão and S. B. Cavalcanti, *Phys. Rev. A* **100**, 043822 (2019).
17. E.-M. Graefe and H. Jones, *Phys. Rev. A* **84**, 013818 (2011).
18. P. A. Brandão, *Phys. Rev. A* **108**, 023522 (2023).